

Università degli Studi di Napoli Federico II

Dottorato di Ricerca in Ingegneria Strutturale, Geotecnica
e Rischio Sismico - XXXIV ciclo



Tesi per il titolo di Philosophiæ Doctor (Ph.D.)

Performance-based wind risk assessment: computational tools for a building-component oriented vulnerability approach

di
Francesco Pandolfi

Tutor: Prof. Ing. Iunio Iervolino

Co-tutor: Dr. Ing. Georgios Baltzopoulos



Scuola Politecnica e delle Scienze di Base

Dipartimento di Strutture per l'Ingegneria e l'Architettura - Via Claudio 21 (Napoli, Italia)

*Ad Anna Mucci,
potente battito d'ali di farfalla.*

Capuano: 'A tien 'na cos 'a raccuntà? Forz, curagg! 'A tien o no 'na cos 'a raccuntà? E muovt, scém. 'A tien 'na cos 'a raccuntà? Tien 'o curagg d' 'o ddicer. E t vuò movr o no? 'A tien 'na cos 'a raccuntà? Scém.

Schisa: Sì. Sì!

Capuano: E dimmell.

È stata la Mano di Dio,
di Paolo Sorrentino

Performance-based wind risk assessment: computational tools for a building-component oriented vulnerability approach.

Ph.D. thesis presented for the fulfillment of the degree of Doctor of Philosophy in Ingegneria Strutturale, Geotecnica e Rischio Sismico

by
Francesco Pandolfi

March 2022



Approved as to style and content by

Prof. Eng. Iunio Iervolino, Advisor

Dr. Eng. Georgios Baltzopoulos, Co-advisor



University of Naples Federico II
Ph.D. Program in Ingegneria Strutturale, Geotecnica e Rischio
Sismico - XXXIV cycle - Coordinator: Prof. Iunio Iervolino
www.dist.unina.it/dottorati-diricerca/dottorati

Candidate's declaration

I hereby declare that this thesis submitted to obtain the academic degree of Philosophiæ Doctor (Ph.D.) in Ingegneria Strutturale, Geotecnica e Rischio Sismico is my own unaided work, that I have not used other than the sources indicated, and that all direct and indirect sources are acknowledged as references.

Napoli, March 10, 2022

Francesco Pandolfi

Abstract

The impact of extreme winds on industrial assets and the built environment is gaining increasing attention from stakeholders, including the corporate insurance industry. This has led to a progressively more in-depth study of building vulnerability and fragility to wind. Wind vulnerability models are used in probabilistic risk assessment, to relate a loss metric to an intensity measure of the natural event, in this case usually a gust or mean wind speed. In fact, vulnerability models can be integrated with wind hazard to provide an assessment of future losses due to extreme wind. Wind hazard on the other hand, can be quantified by associating a probability to the exceedance of each intensity level within a time interval which has been the objective of world- and regional-scale wind hazard studies.

One approach often adopted for the probabilistic description of building vulnerability to wind, is the use of fragility functions, which provide the conditional probability that selected building components will exceed certain damage states, given wind intensity. In fact, in wind engineering literature, it is more common to find structural system- or component-level fragility functions, rather than wind vulnerability models for an entire building.

In this context, models for assessing the vulnerability and fragility of structures to wind and their historical evolution over the last 50 years were investigated. On this basis it was possible to identify the fundamental characteristics in the assessment of the vulnerability of structures to wind. Among these, the importance of the relationships between the failures of different components of the structure emerged. Loss assessment based on component fragility requires some logical combination rules that define the building's damage state given the damage state of each component, and the availability of a consequence model that provides the losses associated to each damage state.

In state-of-the-art risk calculations, which are based on numerical simulation of a structure's behavior during extreme wind scenarios, the interaction of component damage is intertwined with the computational procedure. Since simulation-based approaches are usually computationally demanding

and case-specific, an approach for the composition of a fragility function for the entire structure, using available component fragilities, is developed and discussed in this thesis. This procedure also involves the development of a database containing a large number of recent and past vulnerability studies. The heterogeneity of models found in the literature also promoted a search for vulnerability function conversion methods.

All these features have been integrated in the *ExtReMe wind risk assessment prototype Software, ERMES*, an ad-hoc developed wind risk assessment tool for insurance applications, based on in-built or user-defined wind hazard data. Collecting a wide assortment of available wind vulnerability models and fragility functions, this software implements also the previously introduced alternative method for building-specific risk assessment based on existing component-level fragility functions and on a number of simplifying assumptions for their interactions.

The applicability of ERMES's output has been validated and, despite the simplifying assumptions, the procedure can yield evaluations that are comparable to those obtained via more rigorous building-level simulation-based methods, at least in the considered examples. The advantage of this approach lies in the fact that a database of building component fragility curves can be put to use for the development of new wind vulnerability models to cover building typologies not yet adequately covered by existing works and whose rigorous development is usually beyond the budget of portfolio-related industrial applications.

Keywords: Extreme wind, Probabilistic risk assessment, Component wind fragility, Vulnerability model, Wind-induced losses, Computer-aided risk assessment.

Sommario

L'impatto dei venti estremi sugli asset industriali e sulle costruzioni sta guadagnando una crescente attenzione da parte degli stakeholder, compreso il settore assicurativo. Ciò ha portato ad un crescente sempre più approfondito studio della vulnerabilità e della fragilità degli edifici al vento. In particolare, i modelli di vulnerabilità sono utilizzati nella valutazione probabilistica del rischio, per mettere in relazione una metrica di perdita con una misura di intensità dell'evento naturale, in questo caso solitamente una raffica o una velocità media del vento. Di fatto, questi modelli, integrati con la pericolosità del vento, restituiscono una misura delle perdite future dovute a fenomeni eolici estremi. La pericolosità del vento è solitamente quantificata attraverso la probabilità di superamento di ogni suo livello di intensità, in un dato intervallo di tempo e ciò è alla base degli esistenti studi sulla pericolosità del vento, su scala mondiale e regionale.

Un approccio spesso adottato per la descrizione probabilistica della vulnerabilità degli edifici al vento, è l'uso di funzioni di fragilità, i quali forniscono la probabilità che componenti selezionati dell'edificio superino determinati stati di danno, condizionatamente all'intensità del fenomeno. Nell'ambito dell'ingegneria del vento, è infatti più comune trovare funzioni di fragilità, sia a livello di sistema strutturale che di componente, piuttosto che modelli di vulnerabilità per edificio.

In questo contesto, sono dunque stati approfonditi i modelli per la valutazione della vulnerabilità e la fragilità delle strutture al vento e la loro evoluzione storica negli ultimi 50 anni. Tale studio ha condotto all'identificazione delle caratteristiche salienti che entrano in gioco nella valutazione affidabile della vulnerabilità delle strutture al vento. Tra queste, è emersa l'importanza delle relazioni tra i guasti dei diversi componenti della struttura. La valutazione delle perdite basata sulla fragilità dei componenti richiede, quindi, regole di combinazione logica che definiscano lo stato di danno dell'edificio dato lo stato di danno di ogni componente, oltre alla disponibilità di un modello di conseguenze che fornisca le perdite associate a ogni stato di danno.

Nelle analisi di rischio considerate ad oggi le più raffinate che si basano

sulla simulazione numerica del comportamento di una struttura durante scenari di vento estremi, l'interazione del danno dei componenti è legata alla procedura di calcolo. Dato che tali approcci risultano computazionalmente onerosi e struttura-specifici, in questa tesi viene sviluppato e discusso un approccio semplificato per la composizione di una funzione di fragilità di intera struttura, attraverso le fragilità dei componenti disponibili. Tale procedura è stata quindi integrata con la raccolta di un gran numero di funzioni di vulnerabilità, recenti e passate, raccolte all'interno di un unico database. L'eterogeneità dei risultati raccolti ha inoltre promosso la ricerca di metodi di conversione delle funzioni di vulnerabilità.

Tutte questi prodotti sono quindi stati integrati nel software *ExtReMe wind risk assEStment, ERMES*, che rappresenta uno strumento per la valutazione speditiva del rischio eolico, sviluppato ad-hoc per applicazioni assicurative e basato su dati di pericolosità del vento incorporati o definiti dall'utente. Costruito sull'ampio assortimento di modelli di vulnerabilità al vento disponibili, raccolti all'interno del suo database, questo software implementa il metodo precedentemente introdotto per la valutazione speditiva del rischio di edificio, basato su funzioni di fragilità esistenti di componenti e su una serie di ipotesi semplificative per la definizione delle loro interazioni.

L'applicabilità di ERMES è stata in alcuni casi validata in alcuni esempi e, nonostante le ipotesi semplificative, la procedura produce risultati paragonabili a quelli ottenuti tramite metodi più rigorosi, basati sulla simulazione a livello di edificio. Il vantaggio di ciò risiede nel fatto che il database di curve di fragilità di componenti edilizi può essere utilizzato per il rapido sviluppo di nuove funzioni di vulnerabilità al vento, per tipologie edilizie non specificamente studiate, il cui sviluppo rigoroso richiederebbe un budget superiore a quello che solitamente è a disposizione per applicazioni su portafogli industriali.

Parole chiave: Vento estremo, Valutazione probabilistica del rischio, Fragilità dei componenti del vento, Modello di vulnerabilità, Perdite indotte dal vento, Valutazione del rischio assistita dal computer.

Acknowledgements

First and foremost I am extremely grateful to my supervisor, Prof. Iunio Iervolino for his invaluable advice, continuous support, and patience during my PhD study. His immense knowledge and plentiful experience have encouraged me in all the time of my academic research. I would also like to thank Dr. Georgios Baltzopoulos for the support and advice during my study. My gratitude extends to the University of Naples Federico II for the opportunity to undertake my studies at the Department of Structures for Engineering and Architecture.

I would like to thank fellow engineers Dr. Fabio Petruzzelli and Roberto Liardo of AXA XL, for their invaluable input during our collaboration on this project.

I would like to express my gratitude to the reviewers of this thesis, Massimiliano Burlando (University of Genoa) and Francesco Ricciardelli (University of Campania, Luigi Vanvitelli) for their valuable comments that helped improve the quality of my thesis.

I would like to thank the members of the Department of Civil, Chemical, and Environmental Engineering of University of Genoa and of ANIV-G, the Italian Association for Wind Engineering (Young), that have made my time spent in Genoa highly educational and inspiring.

I would also like to gratefully acknowledge Dr. Christine D. Standohar-Alfano and Prof. John W. van de Lindt for providing me with wind hazard data that were instrumental for the development of my research.

I would like to thank my friends Dr. Mabel Orlacchio, Dr. Pasquale Cito, Dr. Gaetano Cantisani, and Dr. Roberto Baraschino, for the few but essential moments of joy during the years spent together.

Finally, I would like to express my gratitude to my family in Naples but also in Amalfi, to all my friends, and to Giovanna, my greatest and inextinguishable source of happiness. Without you, this milestone would not have been achievable.

Last but not least, I want to thank me. I want to thank me for believing in me. I want to thank me for doing all this hard work. I want to thank me for having no days off. I want to thank me for never quitting. I want to

thank me for always being a giver. And trying to give more than I receive. I want to thank me for trying to do more right than wrong. I want to thank me for just being me at all times. Francesco you are...

Contents

I Wind risk assessment	25
1 Introduction	27
1.1 Performance-based wind engineering	29
1.2 Proposed PBWE approach	35
1.3 ExtReMe wind risk assessment Software	39
1.4 Thesis organization	40
II Hazard	43
2 Wind	45
2.1 Taxonomy of extreme wind	48
2.1.1 Local winds	49
3 Wind speed as intensity measure	51
3.1 Mean wind speed	53
3.1.1 Mean wind speed profile in tropical cyclones	59
3.1.2 Mean wind speed profile in thunderstorms	60
3.2 Wind turbulence	61
3.2.1 Power spectral density	63
3.3 Gust wind speed	64

3.4	IM conversion	67
3.4.1	ESDU gust factor method	68
3.4.2	Modified ESDU method from WMO	70
4	Extreme wind hazard	73
4.1	Hazard maps	74
4.1.1	Tropical cyclone hazard maps	76
4.1.2	Tornado hazard maps	78
III	Vulnerability & Loss	83
5	Wind vulnerability	85
5.1	Approaches for estimation of vulnerability functions	87
5.1.1	Past-loss data approach	88
5.1.2	Heuristic approaches	95
5.1.3	Engineering-based approach	97
5.1.4	Comparison between approaches of vulnerability assessment	106
6	Wind fragility	109
6.1	Building fragility composition	110
6.1.1	Illustrative application	115
6.2	Building component fragility composition	118
6.2.1	Roof covering fragility composition	121
6.3	Damage matrix	126
6.3.1	Hazus-based damage matrix	127
6.3.2	Roof sheathing fragility composition	131
7	Loss	135
7.1	Building direct losses	136

IV Software & Conclusion	137
8 ERMES - ExtReMe wind risk assESSment software	139
8.1 Flow chart	140
8.2 Hazard module	142
8.3 Vulnerability module	146
8.4 Loss module	148
9 Final remarks	153
Appendices	159
A Database	159
A.1 Taxonomy	160
A.2 Fragility curves	165
A.2.1 Building fragility curves	165
A.2.2 Components fragility curves	186
A.2.3 Element fragility curves	205
A.3 Vulnerability curves	213
A.3.1 Building vulnerability curves	213
A.3.2 Component vulnerability curves	240

List of Figures

1.1	Historical tracks and intensity of all tropical storms according to Saffir-Simpson hurricane intensity scale (adapted from https://earthobservatory.nasa.gov/images/7079/historic-tropical-cyclone-tracks).	29
1.2	Vulnerability curves for the residential building class proposed by different authors ([74] on the left and [87] on the right).	30
1.3	Ciampoli et al. schematic identification of exchange and environment zones (adapted from [12]).	32
1.4	PBWE flowchart (adapted from [12]).	33
1.5	Miami (US) hurricane hazard curve according to [89] data.	36
1.6	Residential building fragility curves according to [18]. . .	36
1.7	Building main components.	37
1.8	Industrial building damage matrix (adapted from [18]). . .	38
1.9	ERMESS interface and its main inputs/outputs.	41
2.1	Mean vertical profiles scheme of atmospheric temperature over the ground.	46
2.2	<i>Mono-cellular</i> circulation scheme.	47
2.3	<i>Tri-cellular</i> circulation scheme.	47

3.1	Representation of wind velocity according to Equation 3.1.	52
3.2	Representation of wind speed characteristics for different site conditions.	53
3.3	Representation of mean wind profile according to logarithmic and power laws ($z_0 = 0.02\text{ m}$, $z_r = 50\text{ m}$, $z_h = 0\text{ m}$).	56
3.4	Schematic representation of mean wind profile variation with orography.	57
3.5	Roughness length map for Marchetti viaduct site in Ivrea, Italy (adapted from [76]).	59
3.6	Speed-up factor for different wind directions (Hainan Island, China; adapted from [84]).	60
3.7	Horizontal downburst mean wind speed profile according to Equation 3.11 ($r/R = 1.1212$).	61
3.8	Van der Hoven Power Spectral Density (PSD) spectrum. . .	63
3.9	Wind speed record (adapted from [38]).	65
3.10	Probability density functions of wind speed and its maximum value.	67
3.11	Gust factor as function of I_u and τ , for $l_u/\bar{U} = 10\text{ s}$ and $T = 3600\text{ s}$ (adapted from [44]).	68
3.12	ESDU G_T function.	71
4.1	Feature layers for wind hazard maps development.	75
4.2	Digital elevation model from the National Oceanic and Atmospheric Administration, NOAA (https://www.ngdc.noaa.gov/mgg/global/) [5].	75
4.3	Global roughness length map based on the Land Use and Land Cover data (adapted from [84]).	76
4.4	GAR tropical cyclone hazard map (250 years return period). .	77
4.5	US tornado paths from NOAA Storm Prediction Center database (adapted from [82]).	79
4.6	Standohar-Alfano and van de Lindt EF0 tornadoes hazard map.	80

4.7 Huntsville, AL (US), tornado hazard curves according to Standohar-Alfano and van de Lindt hazard maps [82] and Masoomi and van de Lindt fit [60].	80
5.1 Damage ratio versus wind speed data (adapted from [94]).	86
5.2 Regression of MDR against wind speed (adapted from [50].)	86
5.3 Vulnerability approaches relationships.	88
5.4 Vulnerability curve according to [27, 72].	90
5.5 Vulnerability data for different building typology (adapted from [56]).	91
5.6 Vulnerability data for different building components (adapted from [78]).	92
5.7 Hurricane vulnerability curve scheme according to [50].	93
5.8 Parameters of CAPRA built-in vulnerability functions.	96
5.9 Wind damage process (adapted from [87]).	101
5.10 Fault tree scheme for roof covering damage (adapted from [87]).	102
5.11 Vulnerability curve percentiles (adapted from [91]).	103
5.12 HAZUS hurricane damage estimation algorithm (adapted from [91]).	105
5.13 Flying debris model (adapted from [102]).	106
5.14 Vulnerability curves for a roofs for a given direction of the wind, a dominant opening, and different configurations of cyclone washer for the connection (adapted from [52]).	107
6.1 Damage matrix for residential building (adapted from [18]).	112
6.2 Industrial building (G.1) component fragility curves (adapted from [18]).	116
6.3 Industrial building fragility curves comparison.	119
6.4 Windows fragility curves for different values of wind direction and spatial density of buildings (adapted from [102]).	121
6.5 Single tile fragility curves for different values of external pressure coefficient, C_p (adapted from [102]).	122

6.6	Expected percentage of failed roof tiles for different values of wind direction and spatial density of buildings (adapted from [102]).	123
6.7	Cumulative number of measurement points as function of external pressure coefficient for parallel-to-ridge wind direction (adapted from [102]).	124
6.8	Result comparison ($C_A = 0.6$, $C_p = -0.25$ and parallel-to-ridge wind direction).	124
6.9	Result comparison ($C_A = 0.3$, $C_p = -0.25$ and parallel-to-ridge wind direction).	125
6.10	HAZUS-compatible roof covering fragility curves from composition approach ($C_p = -0.25$, $C_A = 0.1$, and parallel-to-ridge wind direction).	126
6.11	Complementary fragility curves for structure type 2, exposure C and 8d nail (adapted from [55]).	128
6.12	Roof sheathing fragility curves for residential building (one Story, 6d roof sheathing nails, strapped roof trusses, gable roof, no garage, unreinforced masonry walls, $z_0 = 0.03$ m - adapted from [18]).	130
6.13	Roof sheathing panels failure probability (all directions wind; structure type 1; exposure B; 8d nails - adapted from [55]) .	131
6.14	Gust pressure scheme for structure Type 1 (exposure B; 8d nails - adapted from [55]).	132
6.15	Results comparison (all directions wind; structure type 1; exposure B; 8d nails).	134
8.1	ERMESS main interface and modules.	141
8.2	Hazard module flow chart.	143
8.3	Vulnerability and exposure modules flow chart.	144
8.4	Hazard module interface.	147
8.5	Vulnerability module interface.	149
8.6	Exposure module interface.	150

List of Tables

1.1	Expected damage ratios for five residential building damage states.	39
3.1	Mean wind profile parameters provided by Tamura [83] according to Equation 3.6 and 3.7.	56
3.2	Roughness classification according to WMO [38].	58
3.3	Expected peak factors in synoptic wind events (adapted from [43]).	66
4.1	Enhanced Fujita scale intensity level	78
5.1	Building characteristics of CAPRA curves	96
5.2	Comparison of the features of vulnerability methodologies .	108
6.1	Numerical damage matrix from residential building (Figure 6.1), excluding missile impacts on the walls.	113
6.2	Numerical damage matrix for the first three industrial building damage states, according to [18]	117
7.1	Example of expected damage ratios value for five commercial building damage states.	136

Part I

Wind risk assessment

Chapter **1**

Introduction

Risk analysis consists of a probabilistic assessment of potential economic losses resulting from natural hazards. As such, it is of key importance for stakeholders, including the corporate insurance industry that usually determines insurance premiums based on the results from such analyses.

This thesis focuses on risk analysis in the context of building vulnerability to wind-induced actions, and is conducted in the context of the 2020-2022 research agreement between the *Department of Structures for Engineering and Architecture (DIST)* of *University of Naples Federico II* and the insurance company specialised in the management of complex risks *AXA-XL*.

Indeed, wind-related hazard is one of the key source of natural disaster risk. According to the 2019 Global Natural Disaster Assessment Report [3] that analyses Global Disaster Database (EM-DAT¹), China's disaster data and data collected from the insurance industry, major natural disasters affected a total of 90.638 million people in 2019; 34.53% of them were affected by storms, 32.7% by floods, 31.16% by droughts and less than 2%

¹EM-DAT is an emergency database created by the World Health Organization (WHO) and the Belgian Centre for Epidemiological and Disaster Research to collect the major natural disaster data

by other types of disasters. In terms of worldwide direct economic losses \$121.856 Billion were reported: 47.53% caused by storms [3]. It is therefore not surprising that wind-related hazard is receiving increasing attention in recent years [96], also in light of the population growth in extreme wind-prone area [55]. Except for tornadoes, historically extreme winds are not considered a life-safety issue because of the opportunity for prior warnings to the population [58] through weather forecasts. This characteristic is not found, for example, in the case of earthquakes or wildfires that have played a leading part in risk analysis over the years.

Extreme wind hazards are generally categorised according to causative meteorological phenomena (e.g., cyclones, tornadoes, and downburst) [86] but international effort on risk reduction has been greatly focused on tropical cyclones [86]. Only in recent years other phenomena are receiving great attention as remarked by the *THUNDERR project* (<http://www.thunderr.eu/>) of the University of Genoa, awarded with the Advanced Grant 2016 by the European Research Council. This project, headed by Giovanni Solari first and now by his research group, aims to investigate extreme winds related to thunderstorms, starting from the modelling of atmospheric phenomena up to wind action and its impact on society and the economy [77].

Furthermore, hazard is only one of the components in risk assessment according to the international reference for disaster risk reduction: the Sendai Framework [89]. In fact, within this framework, risk has three main components: hazard, vulnerability, and exposure. Hazard refers to the hazardous phenomenon in itself and represents the frequency with which a site, in a certain period of time, experiences a certain phenomenon; e.g., a certain wind speed. Usually, this data is obtained from an historical database of hazardous events occurring in different locations with heterogeneous intensities; e.g., the worldwide historical tracks and intensities map in Figure 1.1 of tropical cyclones occurred up to 2006 and collected by international agencies. Vulnerability refers to the susceptibility of economic assets or people to damages suffered as a consequence of the phenomenon (Figure 1.2); e.g., the probability distribution of economic losses, given wind intensity [94]. Finally, exposure defines the value of the asset or people exposed to the

risk.

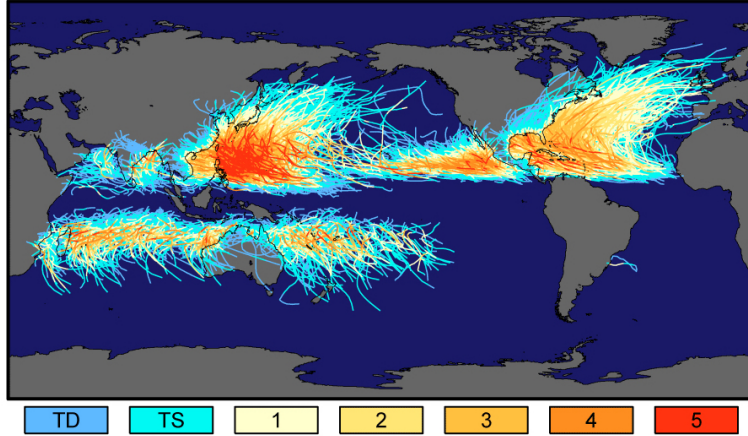


Figure 1.1: Historical tracks and intensity of all tropical storms according to Saffir-Simpson hurricane intensity scale (adapted from <https://eathobservatory.nasa.gov/images/7079/historic-tropical-cyclone-tracks>).

The most advanced risk analysis approaches to earthquake and wind hazard, are based on this three-component framework: *Performance-Based Earthquake Engineering* [17] and *Performance-Based Wind Engineering* [67], respectively. The latter provides the basis of this study and is introduced in the next section together with its evolution, from the definition in 2004 up to the present day.

1.1 Performance-based wind engineering

Nowadays, the design of buildings exposed to extreme winds (such as those exposed to hurricanes in the US) has reached high levels of life safety. These buildings have large safety margins against structural collapse, especially thanks to increased knowledge of the phenomenon and corresponding improvements in the definition of structural loads. On the other hand, there

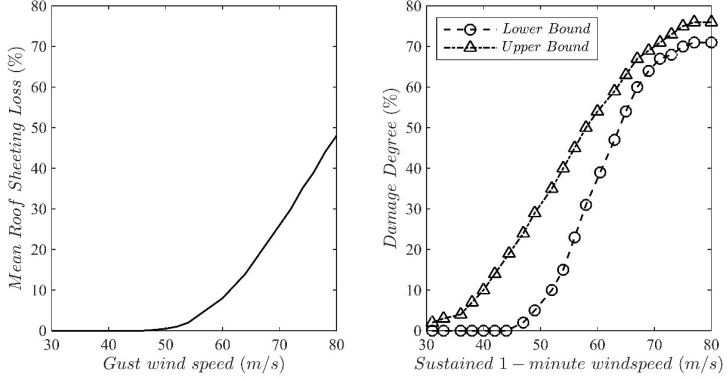


Figure 1.2: Vulnerability curves for the residential building class proposed by different authors ([74] on the left and [87] on the right).

is still much to understand when it comes to estimate and forecast direct and indirect economic losses [55] due to extreme winds. This led to the development of a new approach that deviates from the widely used *Load and Resistance Factor Design (LRFD)* with a shift to the more modern concept of *Performance-Based Design (PBD)*.

PBD procedures assess buildings' performance on the basis of quantitative targets defined on *Decision Variables (DVs)*, i.e., variables of interest to stakeholders. Although several authors over the years have tried to perform probabilistic structural performance evaluation using different approaches (e.g., [50, 87]), some consensus is being observed in recent years in Performance-Based Wind Engineering (PBWE). Its pioneering definition appeared in the work of Paulotto et al. in 2004 [67]. In their work, the authors presented an attempt to extend the approach proposed by the Pacific Earthquake Engineering Research Center (PEER) for Performance-Based Earthquake Engineering [36] to the case of PBWE, with a focus on the performance of tall buildings.

This approach was carried on and further developed by some other authors in the following years. In 2009, van de Lindt and Dao applied the

PBWE approach to wood-frame buildings in the United States [58]. The authors, given the lack of such a model in this country [21], implemented a procedure to study the fragility of buildings looking at four levels of performance: *occupant comfort*, *continued occupancy*, *life safety* and *structural instability*.

However, a more in-depth formalization of the probabilistic procedure for the application of PBWE came with the overview work of Ciampoli et al. in 2011 [12]. The authors, according to the PEER approach, define the risk of a structure to wind as the probability of exceeding a certain level of a relevant *DV* (e.g., economic loss resulting from a windstorm) as:

$$\begin{aligned}
P(DV > dv) = G_{DV}(dv) = \\
\int_{DM} \int_{EDP} \int_{IM} \int_{\{IP\}} \int_{\{SP\}} G_{DV|DM}(dv|dm) \cdot f_{DM|EDP}(dm|edp) \cdot \\
f_{EDP|IM,\{IP\},\{SP\}}(edp|im, \{ip\}, \{sp\}) \cdot f_{\{IP\}|IM,\{SP\}}(\{ip\}|im, \{sp\}) \cdot \\
f_{IM}(im) \cdot f_{\{SP\}}(\{sp\}) \cdot d(dm) \cdot d(edp) \cdot d(im) \cdot d(ip) \cdot d(sp) \quad (1.1)
\end{aligned}$$

where $G(\bullet)$ represents the *complementary cumulative distribution function (CCDF)* and $f(\bullet)$ the *probability density function (PDF)*; DM (can be a vector) represents a *Damage Measure* to quantify the structural damage (e.g., damage to a portion of building wall); EDP (can be a vector) is a relevant *Engineer Demand Parameter* that defines the response of the structure (e.g., inter-storey drift, acceleration, displacement etc.); IM is the *Intensity Measure* of the natural hazard (e.g., wind speed); $\{SP\}$ is a vector of *Structural Parameters* characterizing the structure itself (e.g., mechanical and material proprieties); $\{IP\}$ is a vector of *Interaction Parameters* and allow to take into account the interaction between the structure and the environment (e.g., *aerodynamic coefficient* and *Strouhal number*). To clarify the development of Equation 1.1, it is important to outline that the authors assume IM and SP to be uncorrelated and not affected by the uncertainty of the IP parameters.

Compared to the PEER approach, Ciampoli's formalization allows to

introduce sources of uncertainty that are essential in wind risk assessment. In fact, the authors explicit the sources of uncertainty in the so-called *exchange zone*, i.e., the region around the structure where the effect of the interaction between the structure and the wind field cannot be disregarded, by the definition of the *IP* and *SP* vectors. Sources of uncertainty in the *environment*, i.e., the region around the structure where the wind field is not affected by the presence of the structure itself, are taken into account in the *IM* vector definition. Figure 1.3 shows a schematic identification of these zones.

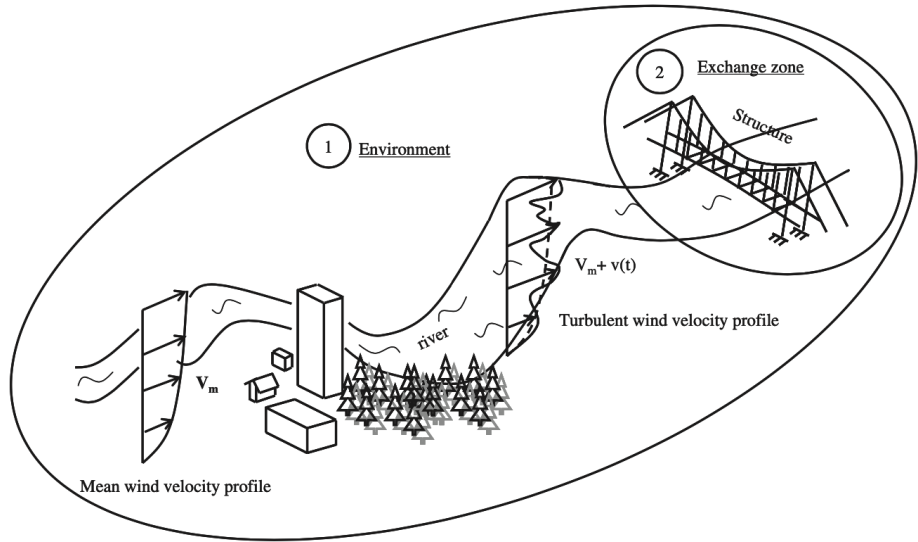


Figure 1.3: Ciampoli et al. schematic identification of exchange and environment zones (adapted from [12]).

The strength of this approach lies in its propensity to separate the components of the risk assessment in different analyses, as shown by Figure 1.4:

- *Hazard analysis* defines $f_{IM}(im)$ once the location of the structure is known.

- *Structural characterization* of the structure, i.e. its design, defines $f_{\{SP\}}(\{sp\})$.
- *Aerodynamic analysis* is needed to study the interaction between wind field and structure, if any. Usually, $f_{\{IP\}|IM,\{SP\}}(\{ip\}|im, \{sp\})$ is provided by *wind tunnel test* or *Computational Fluid Dynamics (CFD)* analyses.
- *Structural analysis* defines the structural response to the wind action as $f_{EDP|IM,\{IP\},\{SP\}}(edp|im, \{ip\}, \{sp\})$.
- *Damage analysis* develops the probability density function $f_{DM|EDP}(dm|edp)$.
- *Loss analysis* defines $G_{DV|DM}(dv|dm)$.

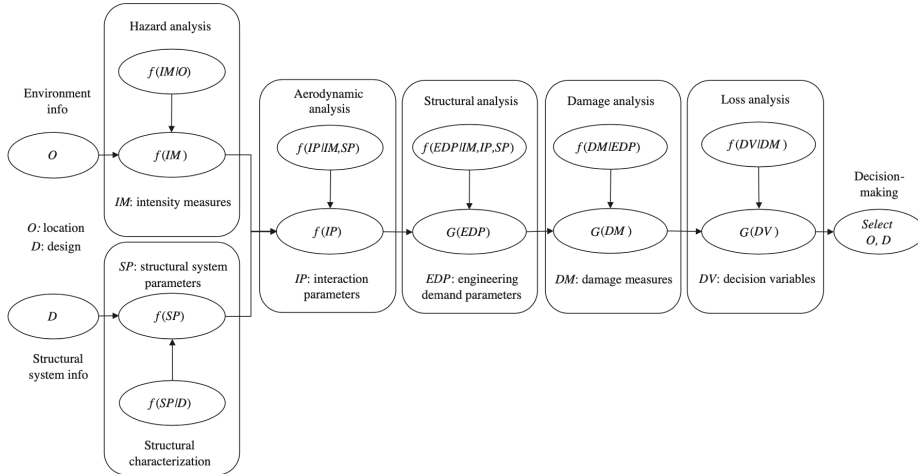


Figure 1.4: PBWE flowchart (adapted from [12]).

Assuming EDP as a measure of structural damage (i.e., $EDP \equiv DM$) and defining the *Limit States (LSS)* as a measure of the whole structural

performance (e.g., no damage, minor damage, or severe damage), the authors offer the following reduced-form risk formalization:

$$\begin{aligned}
G_{LS}(ls) &= \int_{EDP} \int_{IM} \int_{\{IP\}} \int_{\{SP\}} G_{LS|EDP}(ls|edp) \cdot \\
&f_{EDP|IM,\{IP\},\{SP\}}(edp|im, \{ip\}, \{SP\}) \cdot f_{\{IP\}|IM,\{SP\}}(\{ip\}|im, \{sp\}) \cdot \\
&f_{IM}(im) \cdot f_{\{SP\}}(\{sp\}) \cdot d(edp) \cdot d(im) \cdot d\{ip\} \cdot d\{sp\} \quad (1.2)
\end{aligned}$$

In more recent years (2019-2021), Ouyang and Spence [65, 63, 64] have further developed the PBWE framework, focusing on some aspects that had been less investigated in previous studies: wind direction, progressive damage to the building envelope, and water ingress due to concurrent rainfall. The authors formalize the risk in terms of *mean annual rate*, λ , of exceeding a *DV* threshold, dv :

$$\begin{aligned}
\lambda_{dv} = & \\
&\int_{EDP} \int_{R_T} \int_{\alpha} \int_{IM} G_{DV|EDP}(dv|edp) \cdot |dG_{EDP|R_T,A,IM}(edp|r_T, \alpha, im)| \cdot \\
&|dG_{R_T|A,IM}(r_T|\alpha, im)| \cdot |dG_{A|IM}(\alpha|im)| \cdot |d\lambda_{im}| \quad (1.3)
\end{aligned}$$

with R_T the maximum intensity of the concurrent rain event, A the direction of the wind, and IM the maximum mean wind speed at the building top. Also in this case the formulation allows separating the risk assessment in an hazard analysis to evaluate $G_{R_T|A,IM}(r_T|\alpha, im)$, $G_{A|IM}(\alpha|im)$ and λ_{im} , and in a loss analysis to define $G_{DV|EDP}(dv|edp)$. However, to evaluate $G(EDP|R_T, \alpha, IM)$, they define a more generic *response analysis* in which an aerodynamic analysis is implicit.

The strength of the PBWE approach lies in its intrinsic ability to disentangle the different risk components. This allows to move away from the predominant study of cyclonic events, in favour of different typologies of extreme wind events scarcely investigated in the literature, as evidenced by today PBWE studies on *Bora* [19] and *non-stationary winds* (e.g., downburst and tornadoes) [53].

1.2 Proposed PBWE approach

This thesis is also based on an adaptation of the approach proposed by the Pacific Earthquake Engineering Research Center (PEER) for Performance-Based Earthquake Engineering [36] to Performance-Based Wind Engineering (PBWE). The author, according to this assumption, defines the risk of a structure to extreme wind phenomena as the mean annual rate of exceedance of a loss threshold, λ_l :

$$\lambda_l = \int_{IM} P[L > l|im] \cdot |d\lambda_{im}| \quad (1.4)$$

with $|d\lambda_{im}| = |d\lambda_{im}/d(im)| \cdot d(im)$ the absolute value of the derivative of the *hazard curve* (the meaning of which will be discussed in more detail later) multiplied by $d(im)$ [46].

Defining the *Damage State (DS)* of the structure as a quantitative measure of its overall damage, by iterative application of *total probability theorem*, one obtains:

$$\begin{aligned} \lambda_l = \int_{IM} \int_{DS} \int_{\{EDP\}} G_{L|DS}(l|ds) \cdot f_{DS|\{EDP\}}(ds|\{edp\}) \cdot \\ f_{\{EDP\}|IM}(\{edp\}|im) \cdot d(ds) \cdot d\{\text{edp}\} \cdot |d\lambda_{im}| \quad (1.5) \end{aligned}$$

under the assumption of loss dependent only on the whole structure damage ($G_{L|DS,\{EDP\},IM}(l|ds, \{edp\}, im) = G_{L|DS}(l|ds)$) and the damage state dependent only on the response of structure components ($f_{DS|\{EDP\},IM}(ds|\{edp\}, im) = f_{DS|\{EDP\}}(ds|\{edp\})$).

This formalization of the risk highlights its main components. The term $|d\lambda_{im}|$ represents a measure of the hazard. In fact, this information is derived through the hazard curve that returns the annual exceedance rate of a given intensity measure, λ_{im} (Figure 1.5).

The propensity of a structure to suffer damage, given the intensity of the phenomenon, is accounted as its vulnerability. This information is usually provided in terms of losses or in a probabilistic way by vulnerability (Figure 1.2) or fragility curves (Figure 1.6). In Equation 1.5, vulnerability

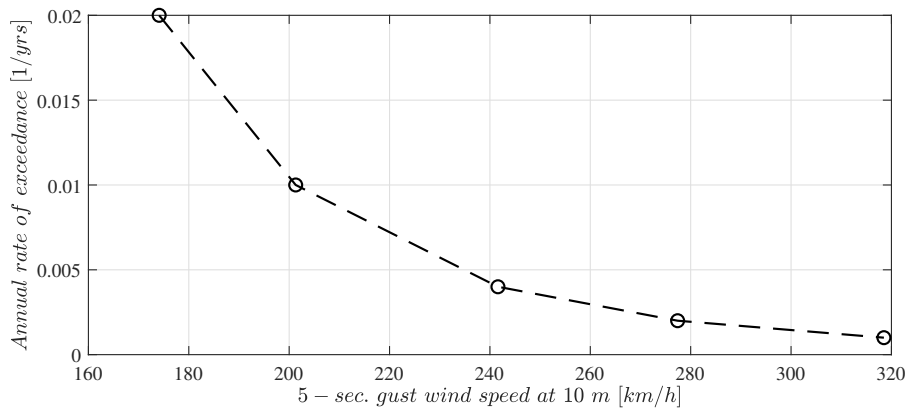


Figure 1.5: Miami (US) hurricane hazard curve according to [89] data.

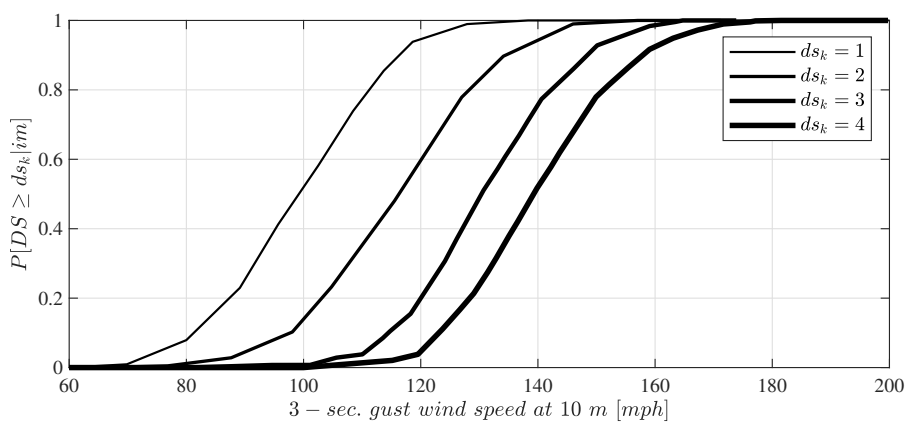


Figure 1.6: Residential building fragility curves according to [18].

is represented by the probability of an overall damage of the structure, DS , given a vector of EDP , and the probability of the latter given the intensity of the phenomenon, IM . In the proposed approach, the engineering response parameter vector $\{EDP\}$ is defined as the collection of damage measures of the most vulnerable components of the whole structure to wind. According to the existing literature (e.g., [69, 87, 34]), available data, and the author' judgement, these components pertain to its envelope. According to this assumption, the author defines four most vulnerable classes of envelope building components (Figure 1.7), hereinafter *main components*: *roof covering (RC)*, *roof structure (RS)*, *envelope openings (EO)* and *envelope walls (EW)*. Then, $f_{\{EDP\}|IM}(\{edp\}|im) \cdot d\{edp\}$ is addressed as the *joint probability* of the main component damage measures (or states).

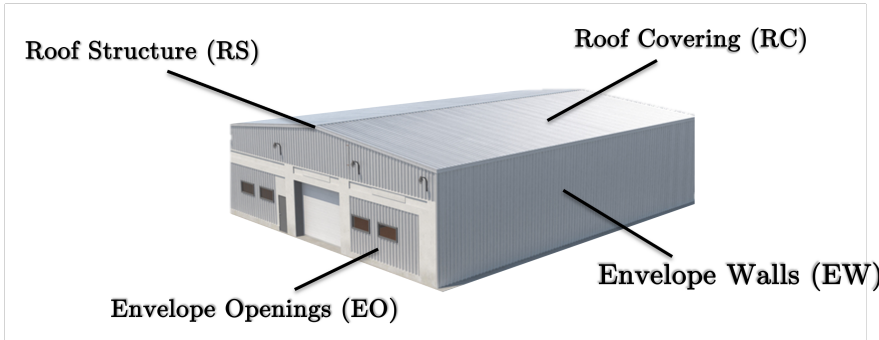


Figure 1.7: Building main components.

The link between the engineering response parameters and the building damage states is provided in a deterministic way by the definition of the *damage matrix* that associates a secondary measure of damage to that of the whole structure. Although its definition has been provided over the years by several authors (e.g., [33, 40]), the most comprehensive and detailed collection of such wind-related matrices is currently provided by the *HAZUS-MH 2.1 project* [90, 91, 18] of the *Federal Emergency Management Agency (FEMA)*. It provides matrices for different building types as the one in Figure 1.8 in which the building is considered in a specific DS if any

of the corresponding shaded building component damage measures occur.

Damage State	Qualitative Damage Description	Roof Cover Failure	Door Failures	Roof Deck Failures	Missile Impacts on Walls	Joist Failures	Wall Failures
0	No Damage or Very Minor Damage Little or no visible damage from the outside. No failed doors or roof deck. Minimal loss of roof cover, with no or very limited water penetration.	≤2%	No	No	No	No	No
1	Minor Damage Maximum of one failed door. Moderate roof cover loss that can be covered to prevent additional water entering the building. Marks or dents on walls requiring painting or patching for repair.	>2% to ≤15%	1 door	No	Typically <5 impacts	No	No
2	Moderate Damage Major roof cover damage, moderate window breakage. Minor roof sheathing failure. Some resulting damage to interior of building from water.	>15% to ≤50%	2 to ≤ the greater of 15% & 3	1 or 2 panels	Typically 5 to 10 impacts	No	No
3	Severe Damage Major window damage or roof sheathing loss. Major roof cover loss. Extensive damage to interior from water. Limited, local joist failures. Failure of one wall.	>50%	> the greater of 15% & 3 to ≤50%	3 to ≤25%	Typically 10 to 20 impacts	1 joist to ≤25%	1 wall

Figure 1.8: Industrial building damage matrix (adapted from [18]).

Finally, $G_{L|DS}(l|ds)$ refers to exposure, defined as a structure loss measure conditioned to DS . Often this information is provided in terms of an *expected value* as in the case of Table 1.1 in which the calibrated ad-hoc expected *Damage Ratio* (i.e., ratio of the value of the damage and value of the building), DR , for five residential building damage states is tabulated.

To develop a more general discussion, the introduced formalization of the risk in Equation 1.5 has been developed in continuous terms for DS , $\{EDP\}$, and IM . Although considering a continuous IM is generally quite intuitive, the same cannot be said for DS and $\{EDP\}$, given their proposed definitions. Therefore, given a finite number of damage states for the whole structure, n_{ds} , and for the main components, it is possible to reformulate

Table 1.1: Expected damage ratios for five residential building damage states.

DS	E[DR]
0	0.00
1	0.25
2	0.50
3	0.70
4	1.00

the measure of the risk as:

$$\lambda_l = \int_{IM} \sum_{j=1}^{n_{ds}} \sum_{m=1}^{n_{\{edp\}}} G_{L|DS}(l|ds_j) \cdot P[DS = ds_j | \{EDP\} = \{edp\}_m] \cdot P[\{EDP\} = \{edp\}_m | im] \cdot |d\lambda_{im}| \quad (1.6)$$

with $n_{\{edp\}}$ the number of possible realizations of the vector of engineering demand parameters, $\{edp\}$, defined by the building component damage states. The following parts of this thesis will address in detail the definition of each of the elements of this equation.

1.3 ExtReMe wind risk assESSment Software

Built on the basis of the proposed PBWE approach developed in the previous section is the *ExtReMe wind risk assESSment (prototype) Software, ERMESS*. This software is one of the main results of a three-year research agreement between the University of Naples Federico II and the insurance company AXA-XL which is specialized in the management of complex risks. ERMESS is a wind risk assessment tool for insurance applications with a focus on industrial facilities, that integrates a wide set of wind vulnerability and fragility functions. The interface of the software reflects the framework of the PBWE approach pointing out the main components of the risk as

displayed by Figure 1.9. Each one of the three *main modules*, hazard, vulnerability, and exposure, are in turn composed by *sub-modules* that allow internal specific operations, e.g., *IM* conversion or fragility composition.

The interface also displays the input and output of the risk analysis. Therefore, after the user definition of the site characteristics (geographical coordinates and ground roughness) and the type of hazardous event (tropical cyclone or tornado), the *hazard module* allows the definition of the hazard curve (or the single intensity measure in case of scenario analysis). This definition can be performed via direct user input or by build-in hazard maps. Then, the *intensity measure conversion sub-module* allows the conversion, if needed, of *IM*(s) to the reference value of *3-second gust at 10 m* (more details are provided in the following sections).

The *Vulnerability module* allows the user to choose between three different risk assessment approaches and to select/define the building characteristics according to an ad-hoc developed taxonomy, via the *taxonomy sub-module*. The first, *vulnerability approach*, requires the direct definition of the building vulnerability function. The second involves the definition of fragility functions for the entire building, i.e., *the building fragility approach*, while the third one is a simplified approach developed for composing building fragility. This *building fragility composition approach* relies on the definition of main components fragilities and the definition of a *damage matrix*. In all cases, the user is allowed to use his own functions rather than the built-in functions included within the *ERMESS database*. This database collects both literature and study results from the last 50 years and curves developed by the author.

Finally, the *exposure module* allows the definition of the risk measure according to the chosen vulnerability approach.

1.4 Thesis organization

This section describes the organization of the thesis following this Part I in which it has been described the state-of-the-art of performance-based wind engineering risk assessment (Section 1.1), the approach proposed by the

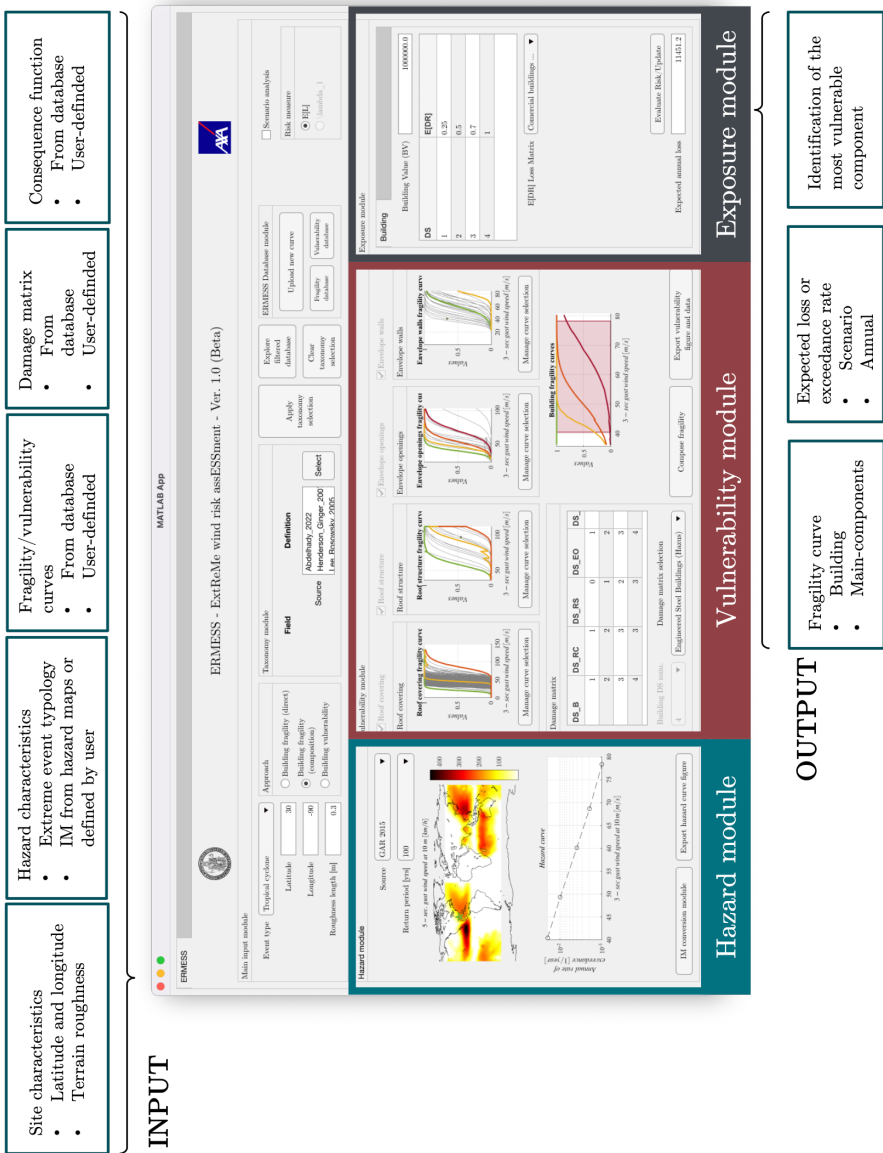


Figure 1.9: ERMES interface and its main inputs/outputs.

author for it (Section 1.2), and the introduction to the software dedicated to its automation, ERMESS (Section 1.3).

Part II discusses the wind-related hazards. Chapter 2 and 3 describe the characteristics of wind phenomena, the description of the intensity measure, and conversion methods. Chapter 4 specifically focuses on wind hazards and existing hazard maps.

Part III describes vulnerability and losses. While Chapter 5 recalls the three main state-of-the-art approaches to estimate the vulnerability of structures to extreme wind events, Chapter 6 focuses on the fragility curves and describes the proposed methodologies to compose building and component fragility functions. Chapter 7 analyses the direct loss assessment.

Part IV describes ERMESS in all its modules and sub-modules, according to the user interface (Chapter 8), and the future developments and critical issues of the proposed risk assessment approach and software (Chapter 9).

Finally Appendix A describes the database developed to date curve-by-curve after its taxonomy introduction.

Part II

Hazard

Chapter 2

Wind

Holmes, in his book [43], defines wind as:

"...air movement relative to the earth, driven by several different forces, especially pressure differences in the atmosphere, which are themselves produced by differential solar heating of different parts of the Earth's surface, and forces generated by the rotation of the earth."

Affected by solar radiation, the ground and the atmosphere return some energy in the form of thermal radiation. The lower atmospheric layer retains most of this heat and, on average, the thermal radiation decreases as the altitude increases, according to the *International Standard* piece wise linear profile *IS* in Figure 2.1 [15]. However, the energy received and returned to the atmosphere is a function of the incidence angle of the sun's rays on the earth's surface. Therefore, the average temperature profile as a function of altitude in the equatorial zone (*Tropical Maximum*, *TM*, in Figure 2.1) is characterized by greater temperatures than the *IS*. This results in the formation of a low pressure zone near the equatorial zone. Conversely, a high pressure zone is formed in polar zones where the average *Arctic Minimum* temperature profile, *AM*, moves to the left of *IS*. In the absence of other influencing factors, in each hemisphere, air circulates as a *single*

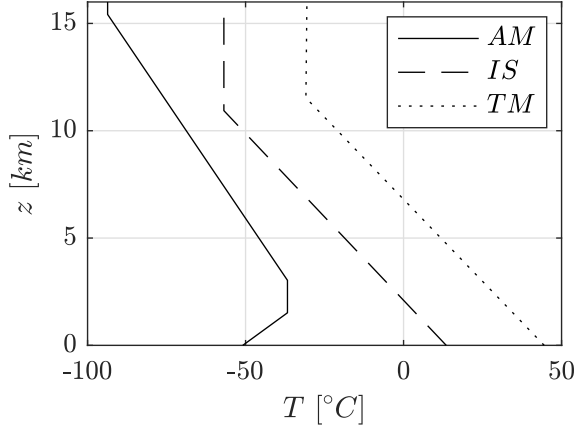


Figure 2.1: Mean vertical profiles scheme of atmospheric temperature over the ground.

convention cell running from the pole to the equator according to Figure 2.2 scheme.

However, the irregular presence of oceans and continents causes the formation of the *sub-tropical high-pressure* and the *sub-polar low-pressure belts*. This phenomenon leads, in each hemisphere, to the *tri-cellular circulation scheme* shown in Figure 2.3.

The winds generated by this circulation are *trade winds*, *westerlies* or *easterlies*, depending on the latitude at which they occur. Developing in monthly time scale intervals, they constitute the *primary circulation*. Acting on a *global scale*, the primary circulation determines climate around the Earth, but has a low impact on buildings due to its low wind speeds (4-5 m/s) [15].

On the other hand, the so-called *secondary circulation* arises from localized low or high pressure zones due to heating or cooling of limited parts of the low atmosphere. Its characteristic phenomena develop in time intervals varying from days to weeks and have a size that reaches a few thousand kilometres at most. These phenomena, e.g., cyclones, anticyclones and monsoons, are responsible for local climate and have a high impact

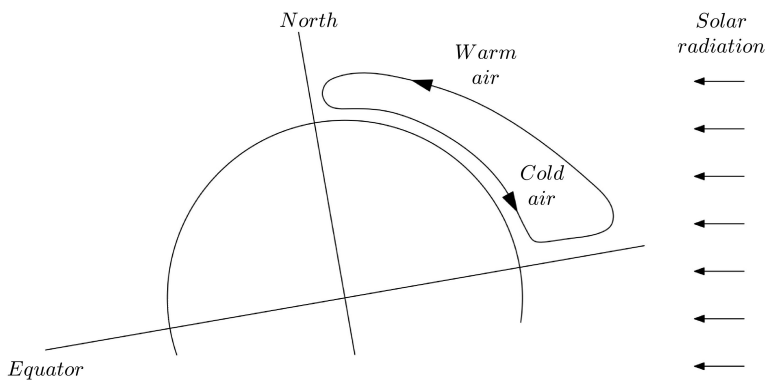


Figure 2.2: Mono-cellular circulation scheme.

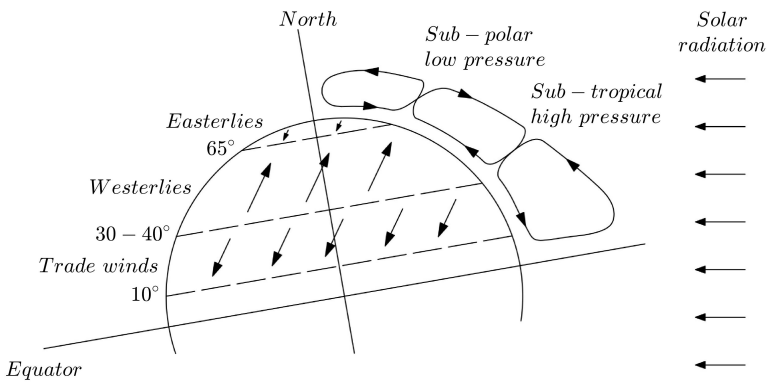


Figure 2.3: Tri-cellular circulation scheme.

on buildings due to their high wind speeds. Embedded in the secondary circulation, *local winds* are more localised phenomena, characterised by the strongest wind speeds. In the next section, the characteristics of secondary circulation phenomena, widely accepted as the main source of wind-related damage to buildings, will be discussed.

2.1 Taxonomy of extreme wind

According to the previous discussion, the atmospheric circulation is categorised as primary or secondary. While the primary circulation determines the Earth's climate and has a low impact on buildings for its low wind speeds, the secondary circulation phenomena are responsible for the local climate and have a high impact on buildings given their high wind speed. Embedded in the secondary circulation, local winds can be distinguished according to the condition under which they are generated: atmospheric or geographical. This section briefly describes what are acknowledged to be the secondary circulation phenomena of primary interest in wind engineering.

The most destructive wind-related phenomenon is globally accepted to be the **cyclone**. It is represented by winds blowing around a low pressure centre, in a direction parallel to the concentric isobars. This circulation results counterclockwise in the northern hemisphere and clockwise in the southern. They are classified depending on the latitude at which they originate in tropical or **extra-tropical cyclones**. The latter originate from the clash between cold and warm air masses coming from the sub-polar and sub-tropical belts (Figure 2.3). They develop especially in winter at latitudes ranging between 40 and 60 degrees and represent one of the main causes of wind-related damage to structures in north-western Europe [43]. Given their great extension (up to 1000 km), they take several days to expire.

Differently, **tropical cyclones** originate in the oceans at latitudes ranging between 5 and 30 degrees, in late summer and autumn. They need a sea temperature of about 26 Celsius degrees to sustain themselves and rapidly

expire at the approach to the mainland (or cooler seas). Tropical cyclones cannot be generated in the so-called *equatorial calm belt* (latitudes between -5 and 5 degrees) and do not achieve their maximum power unless they reach a latitude of at least 10 degrees. Their maximum power is developed for latitudes between 20 and 30 degrees [43]. Although less extended than extra-tropical, tropical cyclones show higher wind speeds and are called differently depending on the area in which they develop: *hurricanes* in the Americas, *typhoons* in East Asia, and *cyclones* in Indian Ocean and Australia.

On the other hand, **anti-cyclones** are winds blowing around high pressure centre and their circulation is clockwise in the northern hemisphere and counterclockwise in the southern. However, these phenomena are of limited interest in wind engineering since they develop typically calm weather and low wind speed. The same cannot be said instead for the **monsoons**, i.e., strong air movements caused by the temperature gradient between Indian Ocean and Asia continent.

2.1.1 Local winds

Without affecting its main characteristics, local winds usually develop in the domain of secondary circulation. These phenomena, although occurring at *local scale* (few kilometres) in short time spans (few hours), develop very high wind speeds. Indeed, often they set the historical maximum wind speeds in territories such as the United States, Australia, and South Africa. Moreover, they represent the main source of strong winds in the equatorial calm belt, although their magnitudes are not very high. It is common to distinguish local winds between phenomena caused by specific geographical conditions and those caused by specific atmospheric conditions [15]. The former include **breezes**, characterized by a daily periodicity, moderate speeds, generally observed in coastal areas and along slopes in hilly or mountainous areas, but also **föhn**, i.e., wind rising when a considerable mass of air, passing a relief, cools down and descends along a slope, heating up in an adiabatic way. Another example of local winds developed by specific geographical conditions is provided by **catabatic winds** (e.g., the

Bora), originated from overcoming of a relief by a mass of cold air. Due to the effect of gravity, this mass descends and reaches speeds of 150-200 km/h [15].

Originated by the collision of warm and cold air masses, a first example of local winds developed by specific atmospheric conditions is provided by **frontal winds**. However, phenomena that have gained a rising interest from the academic community in the last decades, due to their strength, are downbursts and tornadoes. **Downbursts** are descending convective currents that develop in very small time intervals (5-10 minutes) and produce strong winds speeds in the order of 100 km/h along their path. Typically, their damage footprint is 2-3 km wide and 10-15 km long [43] and, depending on their size, are classified as *macrobursts* and *microbursts* [86].

Tornadoes are funnel-shaped vertical vortexes that usually impact large continental plains in countries such as US, Argentina, Russia and South Africa. They represent the most powerful wind-related phenomena [43] since are able to travel up to 50 km developing wind speeds varying from 300 to 700 km/h. Fortunately, they have a very low probability of occurrence and a small extension, in the order of 100 meters [15].

Chapter **3**

Wind speed as intensity measure

When the wind blows over the Earth's surface, a frictional force is generated that contrasts the movement of the air up to a certain height, stronger at lower latitudes [83]. The effects of this force extend over a region up to a certain *gradient height*, z_g , above the surface, known as the *atmospheric boundary layer (ABL)*. The extent of the ABL reaches 1 km for very large wind phenomena such as extra-tropical cyclones and decreases for more localized events (e.g., few hundred meters in thunderstorms) [43]. Above the gradient height, where the effects of this friction force became negligible, it is possible to refer to *friction free wind (FFW)* or *free atmosphere*. In the ABL, the frictional force increases from a zero value at z_g to a maximum value at the ground. It usually results in an increasing profile with height of the intensity measure of interest in wind engineering: the wind speed. In fact, wind engineering is usual to quantify wind loads on a structure through *dynamic pressures* defined on the basis of wind speed. Figure 3.1 shows the common practice of considering the instantaneous wind speed, $U(t)$, as the sum of an average component, the *mean wind speed* \bar{U} in a direction, say x, and a fluctuating component in the three orthogonal directions, x, y and,

z , the *wind turbulence* $u(t)$:

$$U(t) = \bar{U} + u(t) \quad (3.1)$$

Wind engineering usually models \bar{U} as slowly-varying in time and space

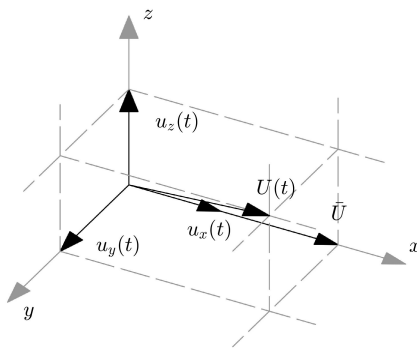


Figure 3.1: Representation of wind velocity according to Equation 3.1.

and $u(t)$ rapidly-varying in time and space [76]. The turbulence is normally dealt with as a *random stationary Gaussian process* and described by statistical descriptors like the *turbulence intensity* and the *gust factor* (Section 3.2 clarifies these concepts). The mean wind speed \bar{U} , is defined as the average value of $U(t)$ over an *averaging time*, T , usually ranging from 10 minutes to 1 hour. In this interval, it is usual to assume the mean wind speed as time-independent. This allows to represent it in a deterministic way, as a function of the height, according to different profile laws and site conditions (Figure 3.2).

A key assumption of this consolidated approach lies in the assumption of a stationary wind flow in strong wind conditions. Due to this, the choice of T plays an important role in the definition of a steady mean wind speed. It needs to be small enough to allow the observation of short and considerable

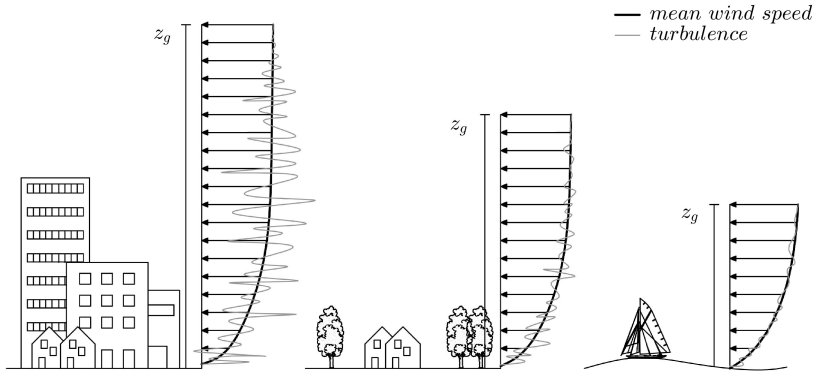


Figure 3.2: Representation of wind speed characteristics for different site conditions.

fluctuations in wind speed, but at the same time long enough to ensure the study of a stationary process. For instance, the *World Meteorological Organization (WMO)* standard for estimating the mean wind speed is $T = 10$ minutes (i.e., 10-min) [38].

These aspects became thus critical in the definition of the wind speed and therefore of the intensity measure in risk analysis. In fact, typically the *IM* provides the averaging period, the reference height, and its mean or gust characteristic; e.g., *3-sec gust wind speed at 10 m*. The following sections address these aspects and others, such as the environmental conditions of a site of interest (e.g., roughness and topography).

3.1 Mean wind speed

The most accurate expression of the mean wind speed profile in *neutral stability conditions* for the ABL is the *logarithmic law* [43]. The starting postulate for its definition concerns the definition of the *wind shear*, i.e.,

the rate of \bar{U} with height, as a function of three parameters: the *height above the ground*, z , the *surface shear stress*, τ_0 , and the *air density*, ρ_a . Neglecting in the ABL some negligible forces (e.g., the Coriolis's force), it is possible to define the *non-dimensional wind shear* as:

$$\frac{d\bar{U}}{dz} \cdot z \cdot \sqrt{\frac{\rho_a}{\tau_0}} \quad (3.2)$$

in which $\sqrt{\rho_a/\tau_0}$ is also known as *friction velocity*, u_* . Defining the quantity in Equation 3.2 as a constant, say $1/k$ ($k \approx 0.4$ is the *von Karman's constant*), its integration returns:

$$\bar{U}(z) = \frac{u_*}{k} \cdot (\log_e z - \log_e z_0) = \frac{u_*}{k} \cdot \log_e \left(\frac{z}{z_0} \right) \quad (3.3)$$

with z_0 the *roughness length*, a measure of the roughness of the ground surface. A measure of the ground roughness is also provided by the *surface drag coefficient*, κ , defined as:

$$\kappa = \frac{\tau_0}{\rho_a \cdot \bar{U}_{10}^2} = \frac{u_*^2}{\bar{U}_{10}^2} \quad (3.4)$$

with \bar{U}_{10} the mean wind speed at 10 m. Although Equation 3.3 represent a well-known formulation of the logarithmic law, in very rough surfaces such as urban areas and forests, the height z is replaced by the *effective height*, $z - z_h$, with z_h the *zero-plane displacement height* (e.g., the measure of the mean roof height in an urban environment):

$$\bar{U}(z) = \frac{u_*}{k} \cdot \log_e \left(\frac{z - z_h}{z_0} \right) \quad (3.5)$$

A common use of the logarithmic law allows to define the mean wind speeds at a generic height, by knowing its value at a given height z_1 , through:

$$\frac{\bar{U}(z)}{\bar{U}(z_1)} = \frac{\log_e \left[\left(\frac{z - z_h}{z_0} \right) \right]}{\log_e \left[\left(\frac{z_1 - z_h}{z_0} \right) \right]} \quad (3.6)$$

However, the logarithmic law has some limitations such as the inability to define the mean wind speed for $z < z_h$. To avoid some of these limitations, wind engineering often prefers the use of the *power law*. This law is a simplified empirical formulation with no theoretical basis, that defines the mean wind profile according to the following formulation:

$$\bar{U}(z) = \bar{U}_{z_r} \cdot \left(\frac{z - z_h}{z_r} \right)^\alpha \quad (3.7)$$

In this formulation, z_r is the *reference height* defined as the height at which the logarithmic and power laws match (e.g., the half of the height over which this match is required [43]), \bar{U}_{z_r} is the mean wind speed at this height, and α is the *power law index* expressed as a function of the ground roughness:

$$\alpha = \frac{1}{\log_e \left(\frac{z_r}{z_0} \right)} \quad (3.8)$$

Figure 3.3 shows the agreement between the logarithmic and power laws that justifies the extensive use of the latter for engineering purposes.

Another consolidate formulation is provided in a semi-empirical way by Deaves and Harris (1981) [16]:

$$\bar{U}(z) = \frac{u_*}{k} \cdot \left[\log_e \left(\frac{z - z_h}{z_0} \right) + 5.75 \cdot \left(\frac{z - z_h}{z_g} \right) - 1.875 \cdot \left(\frac{z - z_h}{z_g} \right)^2 - 1.33 \cdot \left(\frac{z - z_h}{z_g} \right)^3 + 0.25 \cdot \left(\frac{z - z_h}{z_g} \right)^4 \right] \quad (3.9)$$

Although this model is used today in the *Australian and New Zealand code for structural design for wind actions* [81], most of the worldwide standards employ power or logarithmic laws.

The previous discussion points out how the definition of the site characteristics plays a crucial role in the calculation of the mean wind profile (Figure 3.2). Different authors have studied and defined roughness values for different site conditions. A first example is provided in Table 3.1 collecting the Tamura [83] recommendations on the parameters to be used in

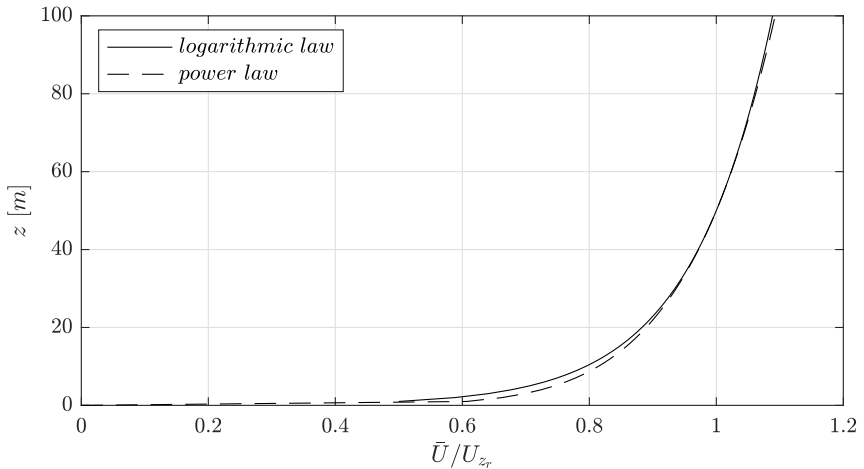


Figure 3.3: Representation of mean wind profile according to logarithmic and power laws ($z_0 = 0.02 \text{ m}$, $z_r = 50 \text{ m}$, $z_h = 0 \text{ m}$).

Table 3.1: Mean wind profile parameters provided by Tamura [83] according to Equation 3.6 and 3.7.

Site condition	$z_0 \text{ [m]}$	$\alpha \text{ [-]}$	$z_h \text{ [m]}$
Sea	0.000-0.003	0.10 - 0.13	0
Open flat terrain	0.003 - 0.2	0.14 - 0.2	0.1
Suburban area	0.2 - 1	0.2 - 0.25	5
City	1-2	0.25 - 0.30	10
Large city center	2 - 4	0.30 - 0.50	20

Equation 3.6 and 3.7 for five different site conditions. However, a more specific and extensive WMO study [38] on roughness length and drag coefficient for wider surface categories is summarised in Table 3.2.

A second fundamental site characteristic involved in the definition of the mean wind profile is the orography of the surrounding terrain. Acceleration, deceleration, and flow separation phenomena cause inevitable variations in wind speed profiles compared to those assessed on flat terrain as shown schematically by Figure 3.4. For this reason, a *topographical multiplier* is usually involved in the definition of such a profile, e.g., the ratio between the wind speed at a given height and the same assessed on a flat ground upwind.

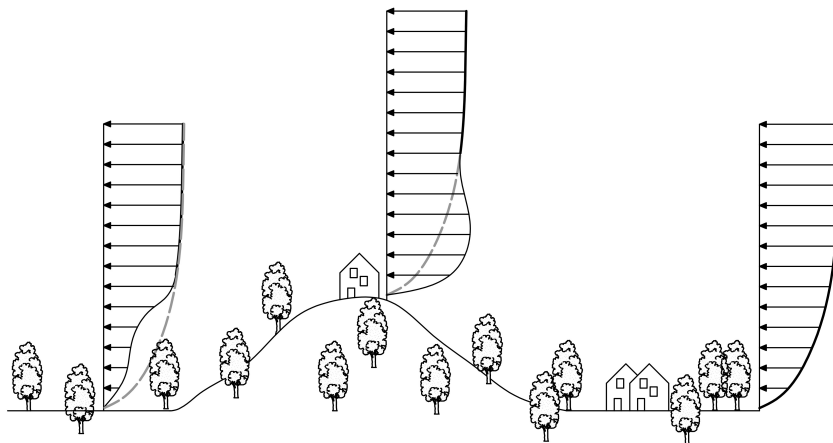


Figure 3.4: Schematic representation of mean wind profile variation with orography.

Moreover, sites of interest in wind engineering are usually immersed in a non-homogeneous three-dimensional environment, both in terms of roughness and orography. Figure 3.5 shows how a viaduct in Ivrea, Italy, is surrounded by heterogeneous roughness surfaces. The complex orography can lead instead to local *speed-up effects* whose assessment is carried out

Table 3.2: Roughness classification according to WMO [38].

Site condition	Description	z_0 [m]	κ [-]
Sea	Open sea conditions for all wind speeds, exposed tidal flats, featureless desert, and tarmac	0.0002 - 0.005	0.001 - 0.003
Smooth	Featureless land with negligible vegetation such as wide beaches and cays, exposed reefs	0.005 – 0.03	0.003 – 0.005
Open	Nearshore water for winds $> 30m/s$, level country with low grass, some isolated trees, airport surrounds	0.03 – 0.10	0.005 – 0.008
Roughly Open	Low crops, few trees, occasional bushes	0.10 – 0.25	0.008 – 0.012
Rough	Lightly wooded country, high crops, centres of small towns	0.25 – 0.5	0.012 – 0.019
Very Rough	Mangrove forests, palm plantations, metropolitan areas	0.5 – 1.0	0.019 – 0.032
Closed	Mature regular rainforests, inner city buildings	1.0 – 2.0	0.032 – 0.065
Skimming	Mixture of large high and low-rise buildings, irregular large forests with many clearings	> 2.0	> 0.065

through complex analyses, e.g., wind tunnel tests or CFD (Figure 3.6). Since the wind is characterized by directionality, this parameter becomes fundamental in the definition of the wind speed profile and then in the action on the structure.

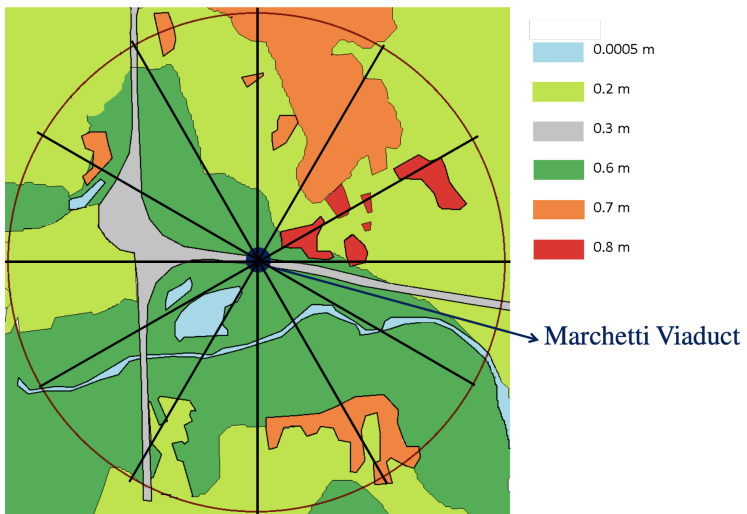


Figure 3.5: Roughness length map for Marchetti viaduct site in Ivrea, Italy (adapted from [76]).

3.1.1 Mean wind speed profile in tropical cyclones

The mean near-surface (60-200 m) wind speed in tropical cyclone conditions is well approximated by a logarithmic law profile [73]. Although studies such as that of Giant et al. in 2007 argue that there is no significant difference between the profiles in the *outer vortex* and the *eye-wall* regions [83], the logarithmic approximation is more consolidated for the former. Some studies have attempted to describe a specific profile in the eye-wall region such as the one by Francklin et al. in 2003 [25] that define the

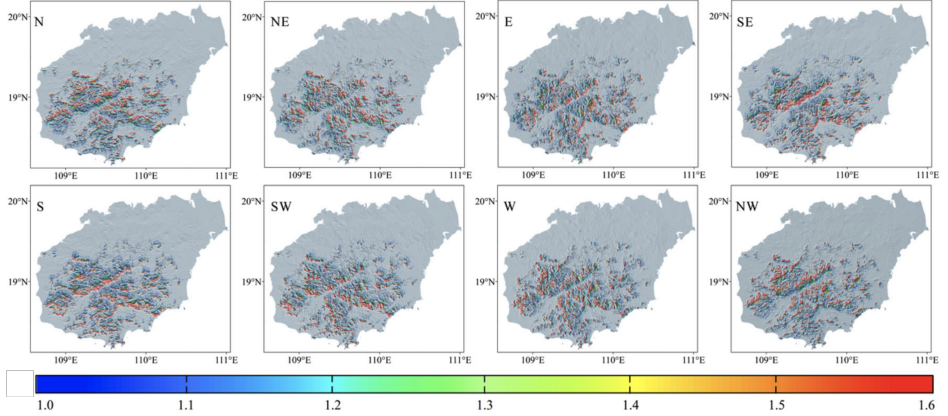


Figure 3.6: Speed-up factor for different wind directions (Hainan Island, China; adapted from [84]).

average wind speed profile in this region as:

$$\bar{U}(z) = \begin{cases} \bar{U}_{10} \cdot \frac{\log_e(\frac{z}{0.0001})}{\log_e(\frac{10}{0.0001})} & \text{for } z < 300 \text{ m} \\ \bar{U}_{300} & \text{for } z \geq 300 \text{ m} \end{cases} \quad (3.10)$$

3.1.2 Mean wind speed profile in thunderstorms

One of the most common extreme wind phenomena produced by a thunderstorm is the downburst. Since this phenomenon is characterized by a duration much shorter than one hour (in the order of a few minutes), the definitions of averaging times T generally used for long events are not appropriate in this case. Furthermore, the event is not stationary and the profiles based on this assumption seem to be worthless (e.g., logarithmic law). However, Holmes defines an averaging time of about 30-60 seconds as adequate to study this event as quasi-stationary [43].

Neglecting the movement of the downburst, a model for its typical *nose-shape* mean wind speed profile (Figure 3.7) was proposed in 1988 by Os-

eguera and Bowles [62]:

$$\bar{U}(z) = \frac{\varphi \cdot R^2}{2 \cdot r} \cdot \left[1 - e^{-\left(\frac{r}{R}\right)^2} \right] \cdot \left[e^{-\left(\frac{z}{z^*}\right)} - e^{-\left(\frac{z}{\varepsilon}\right)} \right] \quad (3.11)$$

with r the distance from the centre of the downburst; R the characteristic radius of downburst; z^* the characteristic height out of ABL; ε the characteristic height in the ABL and φ a scaling factor with a dimension of $[1/\text{time}]$.

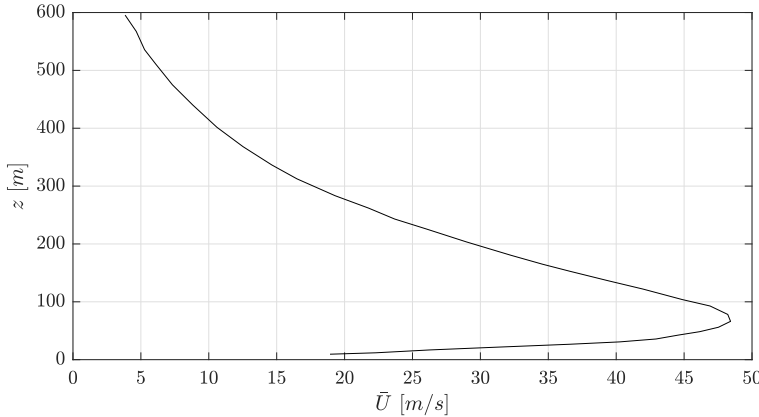


Figure 3.7: Horizontal downburst mean wind speed profile according to Equation 3.11 ($r/R = 1.1212$).

3.2 Wind turbulence

Using a common notation, the fluctuating component $u(t)$ used in Equation 3.1 is usually referred only to the *longitudinal component of the turbulence* ($u_x(t)$ in Figure 3.1), i.e., in the mean wind speed direction. The *lateral* ($u_y(t)$) and *vertical* ($u_z(t)$) components are usually referred as $v(t)$ and $w(t)$, respectively. In the following discussion it will use these notations.

The *gustiness* in the wind speed, i.e., the turbulence features, is due to the generation of vortexes and eddies in the air flow. Given the random nature of this phenomenon, its study is carried out using statistical methods. The independence and randomness of eddies' size and strength support the study of the turbulence components as a random stationary Gaussian processes [38]. Then, at a given height, in the mean wind speed direction, it results:

$$f_u(u_0) = \frac{1}{\sigma_u \cdot \sqrt{2 \cdot \pi}} \cdot e^{-\frac{1}{2} \cdot \left(\frac{u_0 - \bar{U}}{\sigma_u}\right)^2} \quad (3.12)$$

σ_u is the standard deviation of wind speed in the same direction:

$$\sigma_u = \sqrt{\frac{1}{T} \cdot \int_0^T [U(t) - \bar{U}]^2 \cdot dt} \quad (3.13)$$

Two groups of synthetic parameters are used to describe the turbulence: the *turbulence intensities* and *integral length scales*. While the latter, given their link with the auto-correlation function, provide an average size measure of eddies, the former represent the ratio between the standard deviation and \bar{U} (i.e., the *coefficient of variation*):

$$I_u = \frac{\sigma_u}{\bar{U}} ; I_v = \frac{\sigma_v}{\bar{U}} ; I_w = \frac{\sigma_w}{\bar{U}} \quad (3.14)$$

Near the ground, a common wind engineering simplification for large synoptic events is $\sigma_u = 2.5 \cdot u_*$. Under this assumption and according to a logarithmic law profile (Equation 3.5), the longitudinal turbulence intensity results:

$$I_u(z) = \frac{2.5 \cdot u_*}{\frac{u_*}{k} \cdot \log_e \left(\frac{z-z_h}{z_0} \right)} \approx \frac{1}{\log_e \left(\frac{z-z_h}{z_0} \right)} \quad (3.15)$$

According to this equation, the turbulence shows a decreasing intensity with height. The turbulence intensity in the remaining directions, assuming $\sigma_v = 2.2 \cdot u_*$ and $\sigma_w = (1.3 \text{ or } 1.4) \cdot u_*$ [43], results:

$$I_v(z) \approx \frac{0.88}{\log_e \left(\frac{z-z_h}{z_0} \right)} ; I_w(z) \approx \frac{0.55}{\log_e \left(\frac{z-z_h}{z_0} \right)} \quad (3.16)$$

3.2.1 Power spectral density

The probability density function in Equation 3.12 provides information about the magnitude of wind speed in the mean wind speed direction at a given height, without any description of how fast (or slow) it varies with time. To this aim, the energy distribution of wind speed with frequency n is provided by the *power spectral density function* (or *power spectrum*) (*PSD*) $S_u(n)$. It is defined so that the contribution of the variance σ_u^2 in the frequency range $n + dn$ is equal to $S_u(n) \cdot dn$. Given this definition, it results:

$$\sigma_u^2 = \int_0^{+\infty} S_u(n) \cdot dn \quad (3.17)$$

The most famous PSD in wind engineering has been provided by van der Hoven in 1957 for a wide range of frequencies (Figure 3.8). The left

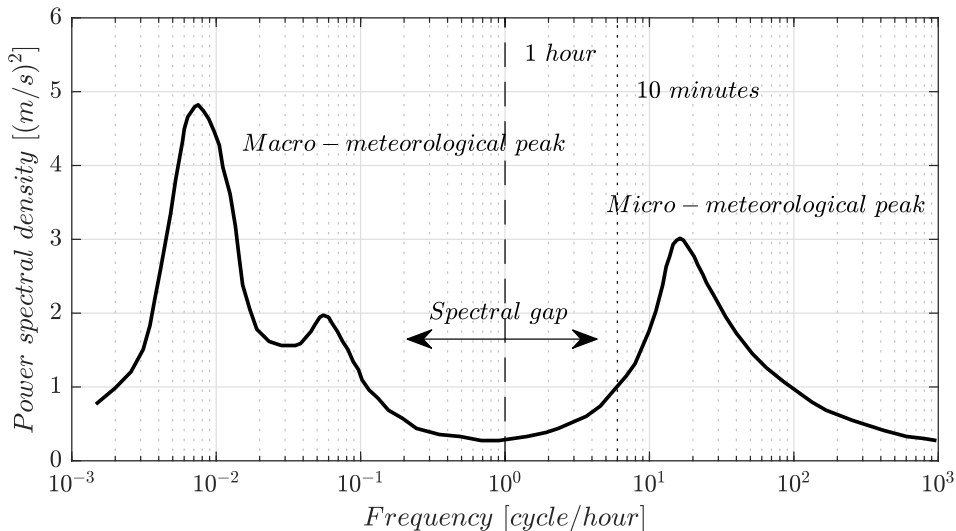


Figure 3.8: Van der Hoven Power Spectral Density (PSD) spectrum.

peak of this power spectrum in the low frequency range (about 4 days) represents the *macro-meteorological peak* related to the large-scale movement

of air associated to global circulation. The right peak of this spectrum in the high frequency range (about 1 minute) is the *micro-meteorological peak* and is related to the variation in wind speed due to local effects like orography, roughness, and then to the turbulence. The space between the two peaks, from 1 hour to 10 minutes, is addressed as the *spectral gap* and represents the lower energy zone, i.e., the frequency range characterized by the lowest variability. For this reason, as anticipated, the mean wind speed usually refers to an averaging time between 1 hour to 10 minutes since samples averaged over such periods are characterized by a relatively sharp probability density function (e.g., compared to $T < 1\text{-min}$).

Different authors have mathematically formalized the *micro-meteorological spectrum*. In 1968, Harris [39] defines a non-dimensional von Karman-type [49] spectrum, given the definition of the integral length scale l_u , as:

$$\frac{n \cdot S_u(n)}{\sigma_u^2} = \frac{4 \cdot \left(\frac{n \cdot l_u}{U}\right)}{\left[1 + 70.8 \cdot \left(\frac{n \cdot l_u}{U}\right)^2\right]^{\frac{5}{6}}} \quad (3.18)$$

Moreover, given the importance of the vertical turbulence component for horizontal-developed structures like bridges, Busch and Panofsky in 1968 [10] proposed the following power spectrum formalization:

$$\frac{n \cdot S_w(n)}{\sigma_w^2} = \frac{2.15 \cdot \left(\frac{n \cdot z}{U}\right)}{1 + 11.16 \cdot \left(\frac{n \cdot z}{U}\right)^{\frac{5}{3}}} \quad (3.19)$$

3.3 Gust wind speed

The most part of worldwide standards and codes (e.g., [7, 81]) use a *gust (or peak) wind speed*, \hat{U} , instead of a mean value, for the purpose of structure wind design. \hat{U} is defined as the maximum value, in T , of wind speed averaged over a shorter (than T) time interval τ . Figure 3.9, representing a 10 minutes wind speed history recorded (at given height) by a sonic anemometer in Western Australia, is illustrative of this concept. The thin

curve is built by averaging the sonic 10 Hz data over 1 second intervals (i.e., represents the mean wind speeds for $T = 1\text{-sec}$). The circles represent mean wind speeds for $T = 3\text{-sec}$. Then, while the thick horizontal bars show the $T = 1\text{-min}$ mean wind speeds, the thin horizontal refers to $T = 10\text{-min}$. Given the previous definition, the *1-min gust wind speed* is the maximum value between the thick horizontal bars, i.e., the one between 100 and 150 seconds. It is significant to underline that, for what observed in the previous

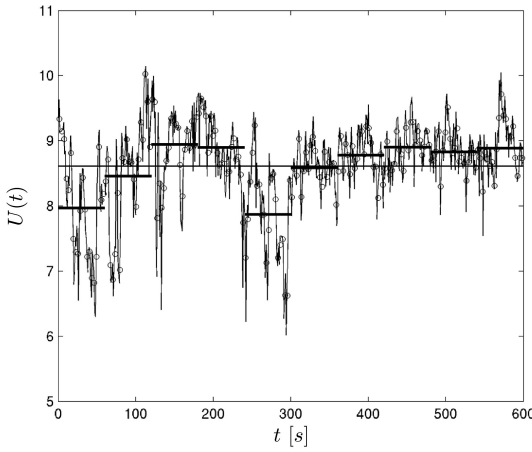


Figure 3.9: Wind speed record (adapted from [38]).

sections, although it is possible to extract a mean wind speed for each of these intervals, the smaller the T the greater the variance.

Given the nature of the wind speed as a random process, the τ gust in the time interval T can be studied as a random variable. The expected longitudinal gust wind speed, at given height, is typically modelled as:

$$\hat{U} = \bar{U} + g \cdot \sigma_u \quad (3.20)$$

with g the *peak factor* [38, 43, 15, 83]. Thus, the increase of τ gust wind speed with respect to the T mean value, is represented through an amplification factor proportional to σ_u . g is a function of T and τ and then

its definitions need the specification of both these values, as illustrated by Table 3.3.

Table 3.3: Expected peak factors in synoptic wind events (adapted from [43]).

τ [s]	T [s]	g [-]
3	3600	3.0
3	600	2.5
1	3600	3.4
1	600	2.9
0.2	3600	3.8
0.2	600	3.4

In order to emphasize the dependence of the averaging times, a more detailed formalization of Equation 3.20 (for a given height) is:

$$\hat{U}_\tau = \bar{U}_T + g_{\tau,T} \cdot \sigma_{u,T} \quad (3.21)$$

According to a Gaussian probability distribution of wind speed, $U(t)$, and a narrow and sharped probability distribution of its maximum, $\max[U(t)]$, Figure 3.10 outlines the definition in Equation 3.21 of gust wind speed as the expected value of maximum wind speed.

The longitudinal gust velocity of the wind is often expressed in a different way, through the definition of the *gust factor*, $G_{\tau,T}$, i.e., the ratio between gust and mean wind speeds:

$$\hat{U}_\tau = \bar{U}_T \cdot G_{\tau,T} \quad (3.22)$$

Given the Equation 3.14 and 3.21 it is possible to define the relationship between gust and peak factors:

$$G_{\tau,T} = \frac{\hat{U}_\tau}{\bar{U}_T} = \frac{\bar{U}_T + g_{\tau,T} \cdot \sigma_{u,T}}{\bar{U}_T} = 1 + g_{\tau,T} \cdot I_u \quad (3.23)$$

The gust factor allows to define the mean wind speed by the knowledge of gust wind speed and vice versa. Until the first years of '90, the 1960

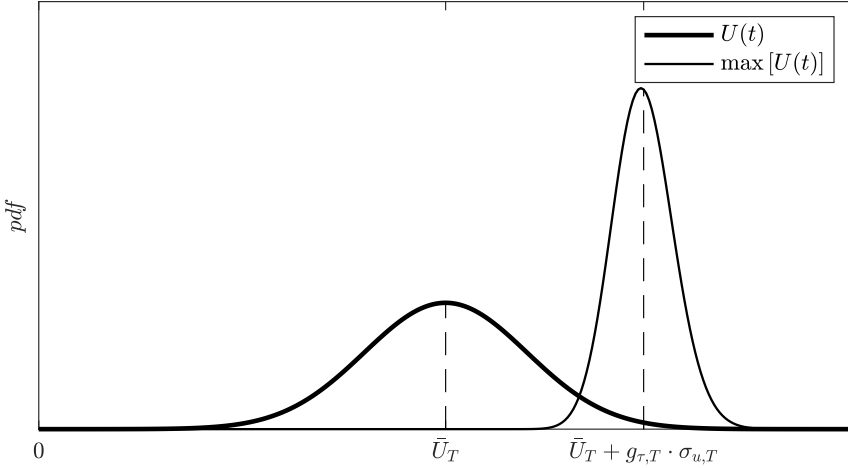


Figure 3.10: Probability density functions of wind speed and its maximum value.

Durst's curve [20] was considered an universal gust factor curve relating G to τ . Since Durst did not address site characteristics, this aspect has been deepened in the last decade by authors such as Harper et al. in 2010 [38] and Holmes et al. in 2014 [44] which have shown its influence on the gust factor definition, as displayed by Figure 3.11. It is shown the influence of I_u in the definition of the gust factor and how the Durst curve is consistent only for a value of about $I_u = 0.165$.

3.4 IM conversion

One of the results presented by this doctoral thesis is the developed database of fragility and vulnerability curves of structures to extreme winds reported in Appendix A and whose strength will be addressed in the following chapters. In addition to their heterogeneity in terms of building typology, occupancy, and site conditions, the collected data (mainly concerning tropical cyclone phenomena) deal with various definitions of intensity measures. In fact, although all the data concern a wind speed measure, they are collected

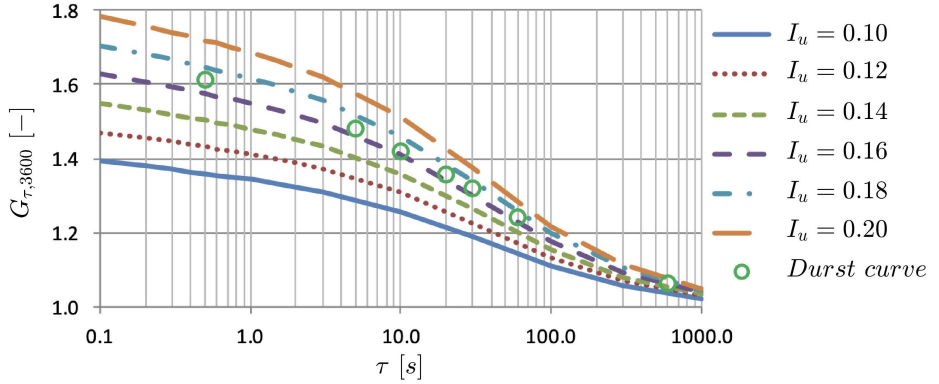


Figure 3.11: Gust factor as function of I_u and τ , for $l_u/\bar{U} = 10$ s and $T = 3600$ s (adapted from [44]).

on global scale from the last 70 years. In these years, reference standards and codes worldwide have experienced changes in design wind speed definition (e.g., gradient, mean, or gust wind speed) in accordance with the growing knowledge of the phenomenon. Since it is not unusual for scientific literature to refer to national practices in the early stages of research, this difference is reflected in the IM specification within the database. This aspect, as seen in the previous chapter, greatly influences the wind speed magnitude and therefore the data homogenization has become a key issue of this study.

In the next sections, methods for wind speed conversion between different averaging times in tropical and extra-tropical cyclone conditions will be addressed.

3.4.1 ESDU gust factor method

Engineering Sciences Data Unit (ESDU) is an engineering advisory organization that offers support at various levels in the field of engineering, from aerospace to structural engineering. Their approach to intensity measure conversion is a reference in wind engineering as shown by the re-examination

study on the gust factor of Vikery and Skerlj of 2003 [92]. In their study, the authors have examined the gust factors from real data and compared them with that provided by the ESDU theoretically-based model. Their results suggest that the gust factor for tropical cyclone conditions can be provided by models developed by the Engineering Sciences Data Unit in '80 for standard boundary layer flow conditions.

The hypothesis at the base of the ESDU approach lies in the assumption of hurricane wind flow near the ground (up to 50-100 m) described by the standard boundary layer theory. Under this assumption and considering a logarithmic profile for the 1-hour (3600 s) mean wind speed, i.e., $\bar{U}_{3600}(z) = 2.5 \cdot u_* \cdot \log_e(z/z_0)$, the peak wind speed is described by the following formulation (according to Equation 3.23):

$$\hat{U}_\tau(z) = \bar{U}_{3600}(z) \cdot [1 + g_{\tau,3600}(z) \cdot I_u(z)] \quad (3.24)$$

with the terms in the square bracket representing the theoretical magnitude of the gust factor. Furthermore, the theoretical value of the longitudinal standard deviation is:

$$\sigma_u(z) = \frac{u_* \cdot 7.5 \cdot \eta \cdot \left[0.538 + 0.09 \cdot \log_e\left(\frac{z}{z_0}\right) \right]^{\eta^{16}}}{1 + 0.156 \cdot \log_e\left(\frac{u_*}{f z_0}\right)} \quad (3.25)$$

with f the *Coriolis parameter* and $\eta = 1 - 6 \cdot f \cdot z/u_*$ the *height scaling parameter*. The peak factor is defined as:

$$g_{\tau,3600}(z) = \left[\sqrt{2 \cdot \log_e(T \cdot v)} + \frac{0.557}{\sqrt{2 \cdot \log_e(T \cdot v)}} \right] \cdot \frac{\sigma_{u,\tau}(z)}{\sigma_u(z)} \quad (3.26)$$

where v is defined as the *cycling rate* and $\sigma_{u,\tau}(z)$ is the standard deviation of the wind speed filtered via a low pass filter with a cutoff frequency of $1/\tau$. These are respectively:

$$v = \frac{0.007 + 0.213 \cdot \left[\frac{T_u}{\tau} \right]^{0.654}}{T} \quad (3.27)$$

$$\sigma_{u,\tau}(z) = \sigma_u(z) \cdot \left[1 - 0.193 \left(\frac{T_u}{\tau} + 0.1 \right)^{-0.68} \right] \quad (3.28)$$

with T_u the *integral scale time parameter* defined as $T_u = 3.13 \cdot z^{0.2}$.

By knowing $\hat{U}_\tau(z)$, τ , z , z_0 , and f , an iterative approach the previous equations return the value of the frictional velocity u_* . Once known this velocity, the same equations can be used to obtain a peak wind speed for different averaging times.

3.4.2 Modified ESDU method from WMO

A method that does not involve an iterative approach has been proposed by the WMO [38]. This approach assumes the longitudinal turbulence intensity as Equation 3.15. Given the definition of z_0 , Equation 3.24 3.26 3.27 3.28 return the gust factor $G_{\tau,3600}$.

This factor can be used to define a gust factor for a T different from 3600 s, through the *ESDU G_T function* defined as:

$$G_T = \frac{G_{\tau,T}}{G_{\tau,3600}} \quad (3.29)$$

This function, provided graphically by the WMO is approximated by the following formulation (Figure 3.12):

$$G_T = 0.2193 \cdot \log_e[\log_{10}(T)] + 0.7242 \quad (3.30)$$

(Some approximations do not ensure that $G_{\tau,T} \geq 1$ for $\tau = T$.)

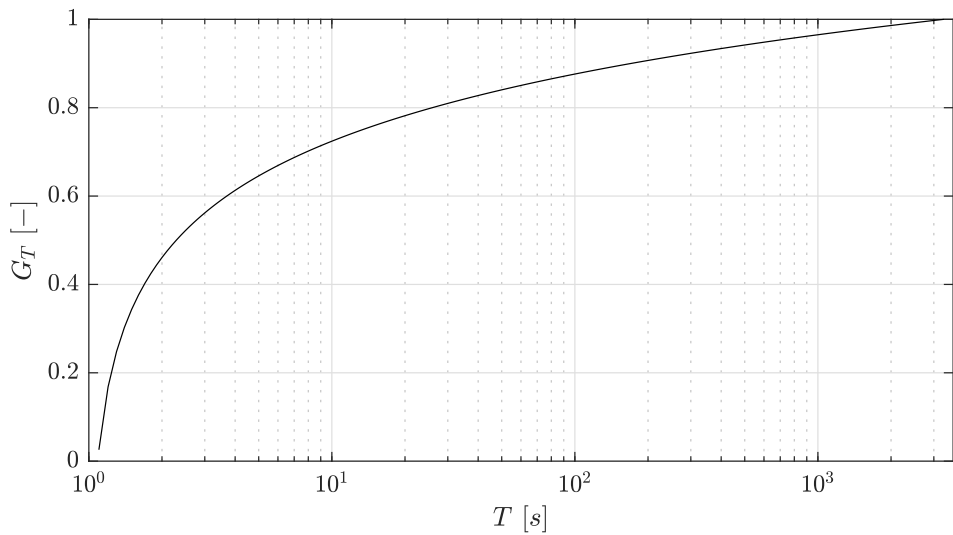


Figure 3.12: ESDU G_T function.

Chapter 4

Extreme wind hazard

The first step in extreme wind risk analysis of a structure is the study of the wind hazard, i.e., calculating the probability of exceeding a certain wind intensity at the site of interest, in a given time interval. Hazard is represented by the $|d\lambda_{im}|$ term in the reference PBWE approach adopted here in Section 1.2, defined as the absolute value of the derivative of the hazard curve multiplied by $d(im)$ [46]:

$$|d\lambda_{im}| = \left| \frac{d\lambda_{im}}{d(im)} \right| \cdot d(im) \quad (4.1)$$

Extreme wind hazard is usually provided through hazard curves defining, for each realization of the intensity measure IM , its *annual rate of exceedance*, λ_{im} [1/yr] (Figure 1.5). It is possible to demonstrate that, for high IM values ($\geq 30 - 35$ [m/s] gust wind speed), the number of observed annual exceedances is low and Poisson distributed [66]. In fact, λ_{im} is low enough to be approximately equal, numerically, with the annual probability of exceedance of the given intensity measure threshold, $G_{IM}(im)$, and it is also, by definition, the inverse of the *return period*, R , [35]; e.g., a $R = 100$ [yr] wind speed has a probability of exceedance of $1/100 = 0.01$ in one year ($\lambda_{im} = 0.01$).

Given the difference in the occurrence frequency and characteristics of different typologies of extreme wind phenomena, hazard curves should be developed separately for each one and then combined [43]. Assuming their independence in terms of the annual exceedence in each year, for a common intensity measure definition results:

$$P[IM > im] = G_{IM}(im) = \prod_{i=1}^n G_{IM}(im)_i \quad (4.2)$$

with i the index for each of the n different extreme wind phenomena (e.g., tornado, tropical cyclone, and downburst).

4.1 Hazard maps

Usually, hazard curves are provided on a regional and global scale via *hazard maps*. Defining geo-referenced intensity measures for different return periods (e.g., tropical cyclone gust wind speed for five return periods), they allow the hazard curve to be derived for a generic coordinate on the map.

The most reliable wind hazard maps are developed taking into account the following key features, reviewed in the previous sections, watched as layers in the definition of the intensity measure (Figure 4.1):

- Database
- Orography
- Roughness

Given the statistical nature of the intensity measure, a *complete and exhaustive* catalogue of extreme wind events is essential. For this reason, simulation techniques calibrated on currently available databases (e.g., Figure 1.1) are often used, especially to obtain data about rarer events.

Furthermore, it was deepened in Section 3 how orography represents an essential factor in the definition of wind speed. For this reason, *digital elevation models (DEMs)* are employed to study the geo-referenced features of the terrain (Figure 4.2).

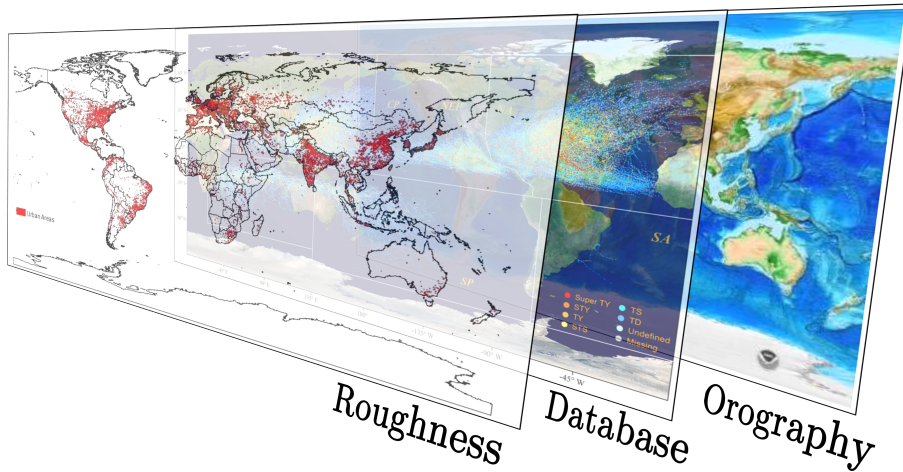


Figure 4.1: Feature layers for wind hazard maps development.

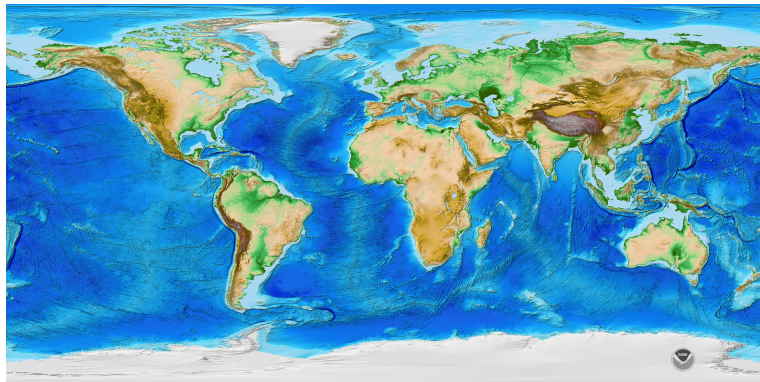


Figure 4.2: Digital elevation model from the National Oceanic and Atmospheric Administration, NOAA (<https://www.ngdc.noaa.gov/mgg/global/>) [5].

Finally, given the influence of roughness on the definition of wind speed, its characteristic values are often extracted from the study of land use, whether natural (e.g., woods) or influenced by humans (e.g., cities). Georeferenced land use data allow the definition of roughness length in each analyzed location as shown in Figure 4.3.

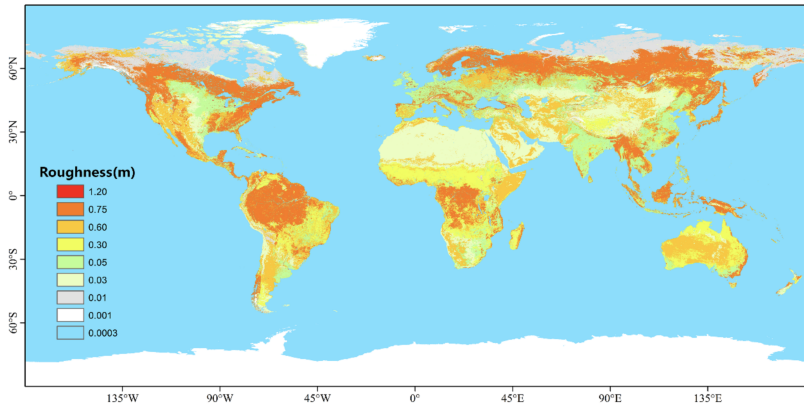


Figure 4.3: Global roughness length map based on the Land Use and Land Cover data (adapted from [84]).

4.1.1 Tropical cyclone hazard maps

At the global scale, freely available tropical cyclone wind hazard maps have been developed in the context of the *United Nation International Strategy for Disaster Reduction (UNISDR) Global Assessment Report (GAR) on Disaster Risk Reduction of 2013* [88, 13]. The supporting PREVIEW Global Risk Data Platform (<https://preview.grid.unep.ch/>) provides these hazard maps for five return periods (up to $R = 1000$ years) with a spatial resolution of 1 minute (Figure 4.4). In accordance with the previous section, these maps take into account the key aspects of database, orography, and roughness. In fact, GAR maps are built on historical data collected at the global scale from various meteorological agencies and grouped in the *National Oceanic and Atmospheric Administration (NOAA) International*

Best Track Archive for Climate Stewardship (IBTrACS) database [51]. For each return period, these maps provide a 5-sec gust wind speeds at 10 m, through a simulation-based technique. The aspects of topography and terrain roughness in the definition of wind speeds have been taken into account through the use of 1-minute resolution *National Oceanic and Atmospheric Administration (NOAA) DEM* [5] and information on land use (e.g., [9]), respectively.

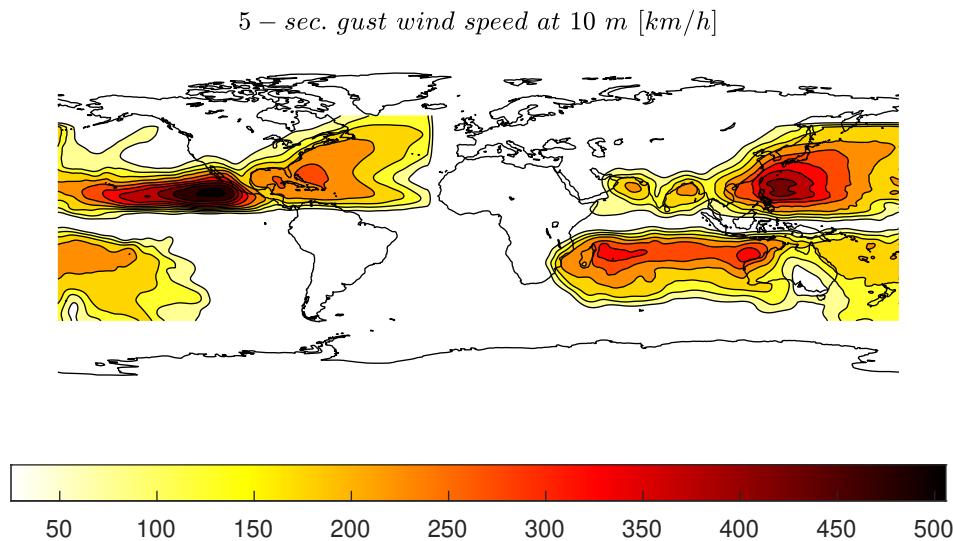


Figure 4.4: GAR tropical cyclone hazard map (250 years return period).

Given the definition of an hazard map for 50, 100, 250, 500, and 1000 years return periods, it is straightforward the definition of the hazard curve for a site affected by tropical cyclone risk, as previously discussed. In addition to wind speed, hazard modelling of tropical cyclones in a more extensive risk analysis should include related phenomena such as storm surge and precipitation [11]. However, for the moment there are no current studies that analyse this aspect at global scale [96].

4.1.2 Tornado hazard maps

Due to a low probability of occurrence, compared to cyclone-, tornado-related risk analyses have been scarcely investigated in the past and are still today at an embryonic state. The few existing studies at regional scale (there are no global scale studies) are mainly based on insurance companies claims data and therefore not freely available [96].

Although tornadoes theoretically occur all over the world, an overwhelming number of them occur in the United States (US) [30]. This reason has driven the development of studies mainly in this region.

The availability of the *NOAA Storm Prediction Center database* (about 60000 events since 1953) has pushed attempts to develop (simulation-based) tornado hazard maps at different scales (e.g., [23, 82]) for the intensity levels of *Enhanced Fujita scale (EF-scale)* [98]: from EF0 to EF5. The EF-scale take its basis in the *Fujita scale (F-scale)* [28] developed in 1973 and based on the observed damage due to the tornadoes. Given the F-scale limitations (e.g., its subjective nature) in the years some attempts have been made to improve it (e.g., [48, 47], trying to preserve its baseline. Among these, EF-scale has been defined based on 8 *degrees of damage (DODs)* that 28 *damage indicators (DIs)* - buildings, structures, but also trees - suffer from tornado extreme winds. Thus, EF-scale presented in Table 4.1 is a set of 3-sec gust wind speed range estimates (not measurements) based on the observed damage.

Table 4.1: Enhanced Fujita scale intensity level

EF	Damage description	3-s gust wind speed at 10 m [m/s]
0	Light	29-38
1	Moderate	39-49
2	Considerable	50-60
3	Severe	61-74
4	Devastating	75-89
5	Incredible	≥ 90

For each grade of the EF-scale, Christine D. Standohar-Alfano and John W. van de Lindt [82] developed US hazard maps based on the NOAA Storm Prediction Center database, covering events from 1950 to 2011. Although some of the data were excluded given the creation of a reference scale only in the 1970s, about 40000 events were considered over a span of time of about 40 years (Figure 4.5).

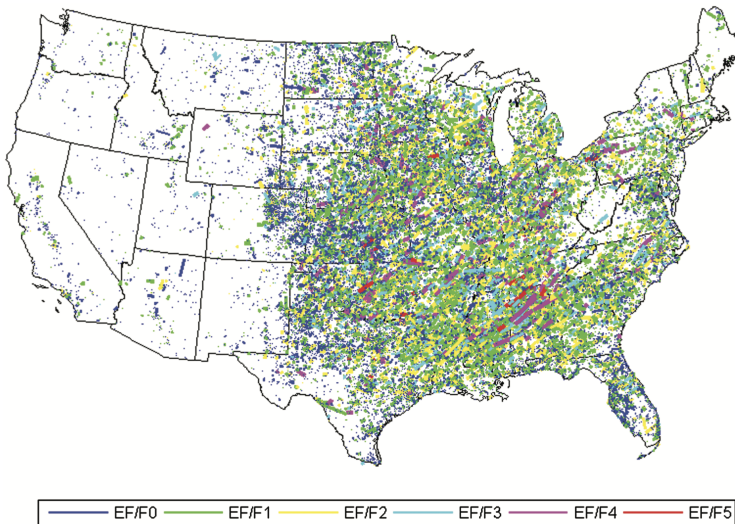


Figure 4.5: US tornado paths from NOAA Storm Prediction Center database (adapted from [82]).

Developed for different spatial resolutions (2, 1, and 0.5 degrees), these maps define the annual probability of experiencing an EF0–EF5 wind speed at any point in the continental United States (Figure 4.6). Although these maps do not consider features of topography and roughness, they take into account another important feature of tornadoes: the magnitude variability of wind speed within an event of a certain degree.

Since these maps are developed for intensity measure intervals, in Figure 4.7 it is possible to observe how the obtained hazard curve (black dashed line) is a step curve. However, in a following study [60], van de Lindt and

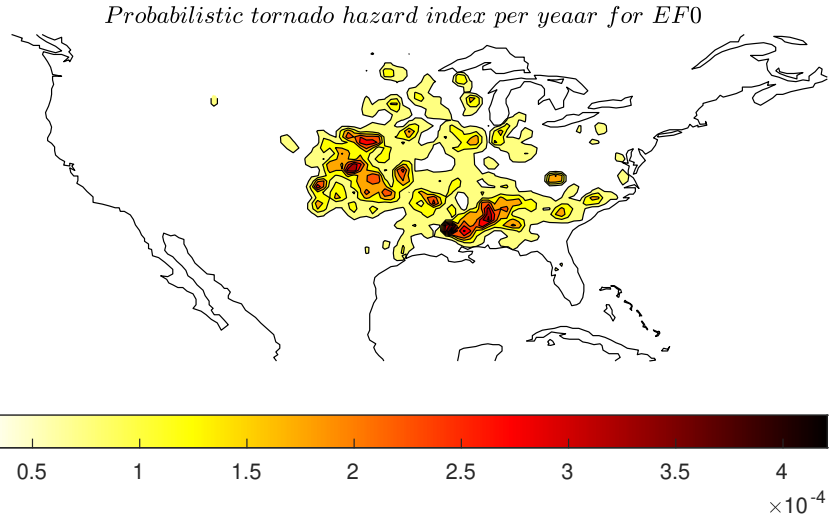


Figure 4.6: Standohar-Alfano and van de Lindt EF0 tornadoes hazard map.

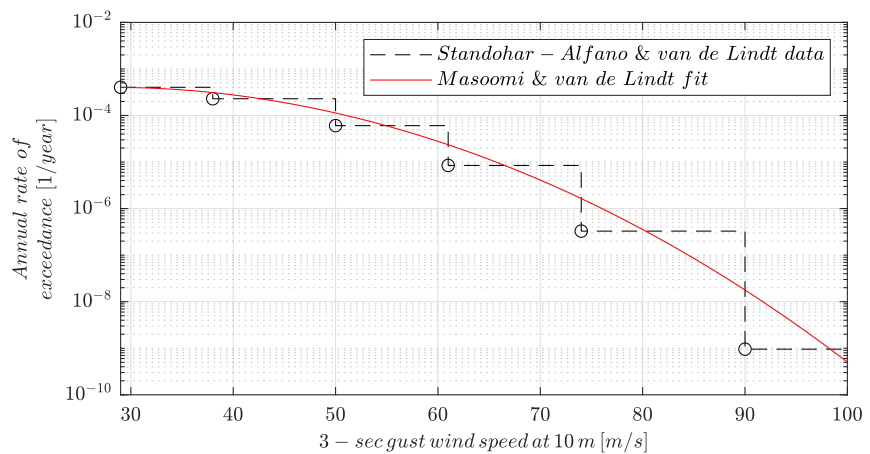


Figure 4.7: Huntsville, AL (US), tornado hazard curves according to Standohar-Alfano and van de Lindt hazard maps [82] and Masoomi and van de Lindt fit [60].

Masoomi proposed a second-order exponential function to fit the data in log-log space (red solid line in Figure 4.7), according to the following formulation (for IM ≥ 22 m/s):

$$\log_e(G_{IM}(im)_{Tornado}) = \alpha \cdot e^{\beta \cdot \log_e(im)} + \gamma \cdot e^{\delta \cdot \log_e(im)} \quad (4.3)$$

with α , β , γ , and δ fitting parameters.

Part III

Vulnerability & Loss

Chapter **5**

Wind vulnerability

Building vulnerability to wind constitutes an important part of natural catastrophe modelling. Initially introduced as a risk assessment tool by the insurance industry in the 1960s, *vulnerability functions* (or *curves*) have been subject to considerable development since then. Wind vulnerability of a building or component is usually represented by a loss measure as a function of the intensity of the hazardous phenomenon.

A common way to express losses, L , is through the *Damage Ratio*, DR (Figure 5.1), defined as the ratio between a damage measure (repair cost or total damage cost) and the value (initial cost, current value, or an insured value) of the exposed asset.

Vulnerability is usually treated in a probabilistic manner. Figure 5.2 shows a vulnerability curve as regression of the *Mean Damage Ratio*, MDR , against wind speed, provided by Khanduri and Morrow in 2002 [50]. In a simple risk calculation involving the expected value of losses given the occurrence of the hazardous event E , vulnerability can be expressed in probabilistic terms as the expected loss given a measure of wind hazard, $E[L|im]$, :

$$E[L|E] = \int_{IM} E[L|im] \cdot f_{IM}(im) \cdot d(im). \quad (5.1)$$

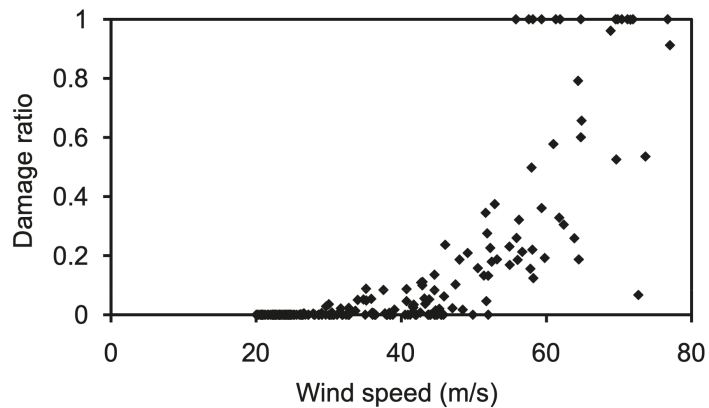


Figure 5.1: Damage ratio versus wind speed data (adapted from [94]).

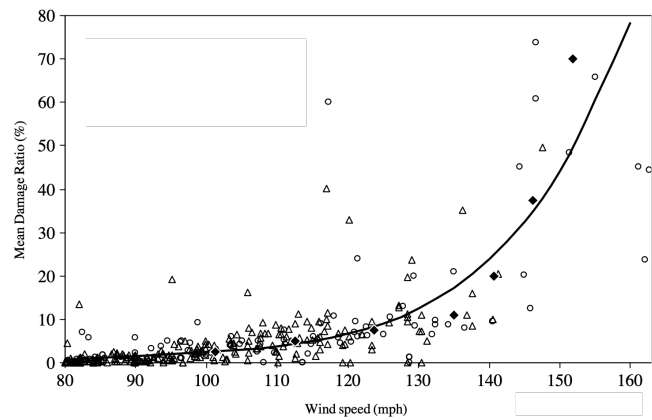


Figure 5.2: Regression of MDR against wind speed (adapted from [50].)

However, in more advanced and modern performance-based approaches such as the one adopted here in Section 1.2, vulnerability is usually expressed as the propensity to exceed a damaged state, given an intensity measure of the extreme wind phenomenon, through the definition of an engineering demand parameter vector (Equation 1.5).

In addition to the heterogeneity in the definition of vulnerability measures, the previous discussion has also highlighted the variability associated with the choice of IM. Existing vulnerability functions are usually implicitly linked to the assumptions for which they have been developed (e.g., roughness, topography, height, extreme wind phenomenon). This lack of homogeneity creates obstacles for the overall applicability and exportability of wind vulnerability curves. For this reason, since the 1960s, wind vulnerability models appearing in the literature have evolved increasingly more complex and refined, with the aim of removing these wider applicability constraints from new vulnerability functions and enabling analysts to export existing models for use under different site and wind action conditions.

5.1 Approaches for estimation of vulnerability functions

In the last 50 years, several authors have studied and developed vulnerability functions of structures to extreme winds. This section aims to present the results of a state-of-the-art study in this field. On the basis of this study, it has been possible to understand the strengths and weaknesses of different literature approaches and choose the most appropriate for the proposed risk analysis.

Literature approaches for vulnerability assessment have experienced considerable evolution over the years and can be placed in three macro-categories. The first approach consists in the development of building vulnerabilities based on loss data by means of regression against loss data (Figure 5.2). The second category models vulnerability mainly on the basis of expert opinion, while the third comprises approaches that are based

on the engineering assessment of the physical damage sustained by the building components. This approach often includes advanced simulation of wind-environment-building interactions and the resulting damages are converted to monetary losses by applying cost-estimating and actuarial principles (Figure 1.2). Although it is not always possible to observe a clear separation between approaches (Figure 5.3) e.g., early engineering-based methods were also integrated with expert judgement, in the following sections they are discussed individually, organized according to this broad category subdivision:

- **Past-loss data** methods that are based on loss data from past disasters (and, in some cases, expert judgment).
- **Heuristic** methods.
- **Engineering-based** methods based on engineering practice and concepts (component-based and simulation-based).

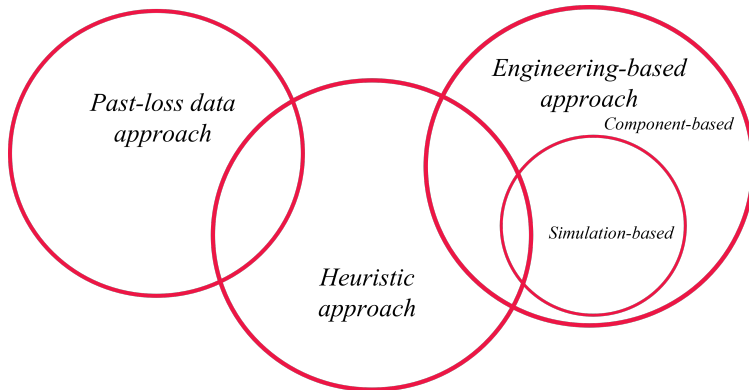


Figure 5.3: Vulnerability approaches relationships.

5.1.1 Past-loss data approach

From the 1960s to the 1990s, models for building wind vulnerability were mainly derived empirically, based on loss data available to insurance com-

panies. In fact, past-loss data come typically from insurance claims information and contain repair or replacement costs. Being able to attribute a hazard value (wind speed) to each claim, a regression of damage against IM can be performed to develop vulnerability curves.

However, this implies that vulnerabilities built on past events are exportable to future ones. This assumption can be put into question, because local building practices and construction materials used, which play a significant role in the vulnerability assessment of structures, may change with time. In fact, it is not unusual for such changes to come about in the aftermath of some destructive and/or rare event.

Additionally, at an early stage insurance-claim data were readily available only on a regional scale for aggregate sets of building (*portfolios*). At the same time, early vulnerability assessments were mostly performed at a large scale, without explicit distinction for building typology. For these reasons, there have been attempts to disaggregate the data prior to performing regression analysis, thus increasing the resolution of loss projection. To this aim, in some cases the expert judgement was integrated in the approach and a sub-category of models emerged.

However, despite their limitations, these models can still be appealing because they are based on actual loss data and therefore take into account all sources of uncertainty that more detailed models have difficulty in modelling.

Historical overview

The earliest studies of structures' vulnerability to wind were developed in the US. One of the first was the one by the Hendrick and Friedman in 1966 [42]. In this study, the authors fit a power law relating the number of claims and losses per claim to wind speed, without distinguishing between different building occupancies or typologies. In the following years, as more claims became available, different vulnerability curves were been fit by the same authors to loss data [45] according to the following formulations:

$$DR(U) = c \cdot U^k ; \quad DR(U) = c \cdot (U - d)^2 \quad (5.2)$$

where k , c , and d are regression coefficients fit against the data and U represents wind speed.

An updated model was proposed by D. G. Friedman in 1975 [26], which provided the basis for the first hurricane catastrophe models (e.g., [14]) [72]. In the following 1984 study [27], Friedman proposed a power law vulnerability curve relating the average paid claims as a percentage of insured building value, as function of peak gust wind speed (Figure 5.4).

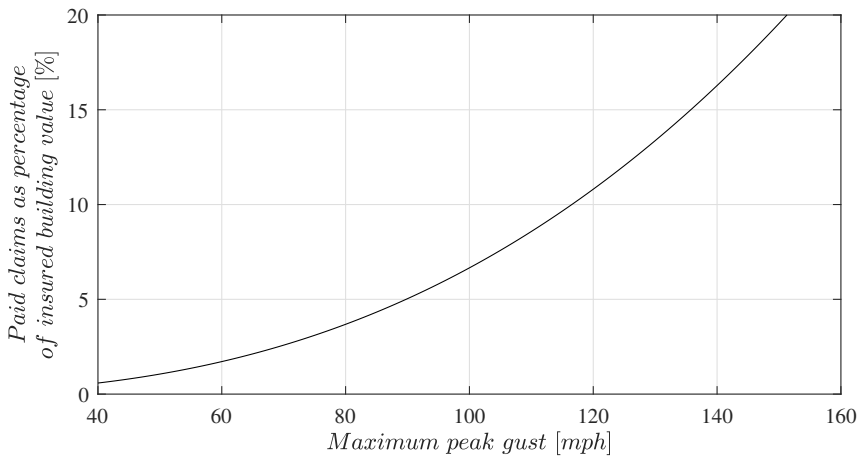


Figure 5.4: Vulnerability curve according to [27, 72].

By the end of the 1980s, there was significant accumulated material in the literature and practical experience in catastrophe modelling in the United States. This motivated insurers to rely on their own vulnerability models and a multitude of in-house vulnerability curves were developed using each insurance company's past-loss records. However, such proprietary models remain publicly unavailable due to confidentiality issues.

Disaggregation

Although early vulnerability models were based on regression of past-loss data, and were applicable to regional building stocks in their entirety, subse-

quent studies focused on individual building types. Leicester and Reardon opted to disaggregate structural damage in the aftermath of cyclone Tracy (1974, Australia) data per building type [56]. These authors studied the performance of typical Australian buildings in the city of Darwin through quantitative damage surveys. After the estimation of local wind speeds, they defined a damage repair index for each building typology (e.g., the ratio of repair cost over the initial cost of the building for one-story buildings) and observed how more recent buildings, with engineered wind-resisting structural elements, were less damaged compared to the older ones. Even if these vulnerability data (Figure 5.5) were not enough for extracting conclusions with some generality, they provide one of the first useful frameworks for assessing the effect of extreme wind speed on buildings.

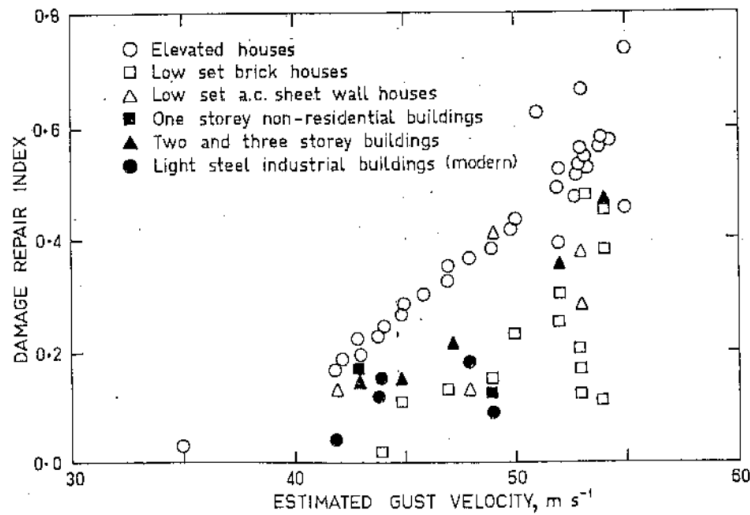


Figure 5.5: Vulnerability data for different building typology (adapted from [56]).

In the meantime, this sort of loss-data disaggregation has been also pursued by other authors, such as Sparks who in 1994 [78] separated claims data per building component: roof envelope, lateral outer shell (wall envelope) and external facilities (Figure 5.6). By dividing the component cost

by the total insured value, it was possible to determine the loss ratio (i.e., the damage ratio) for each component of the building.

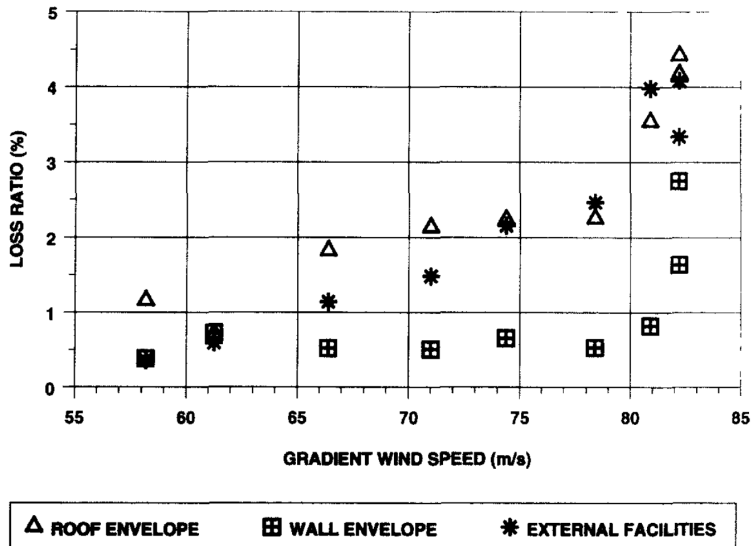


Figure 5.6: Vulnerability data for different building components (adapted from [78]).

Exportability

Some authors have studied the previously mentioned issue of exportability of past-loss data vulnerability curves developed for specific regions to other regions. Khanduri and Morrow in 2002 [50] developed a methodology that involves the application of engineering principles, judgment, and logical assumptions for such an export.

The methodology defines the aggregated hurricane vulnerability curve (i.e., C_g or MDR as a function of wind speed U) as the weighted sum of the contributing ones of specific building classes (C_i in Figure 5.7), according

to the following equation:

$$\frac{\sum_{i=1}^n MDR(U)_i \cdot w_i}{\sum_{i=1}^n w_i} = MDR(U) \quad (5.3)$$

with w_i the weight corresponding to the percentage of this specific building class in the given region, and n the number of different building classes taken into account (in order to simplify the discussion, in the following it will be omitted the dependence of MDR on U). The exporting method is based on the following assumptions:

- a set of disaggregated vulnerability curves, previously developed for a given region or country is already available representing the benchmark curves;
- the ratios of vulnerability functions for different building classes are the same in different regions or countries.

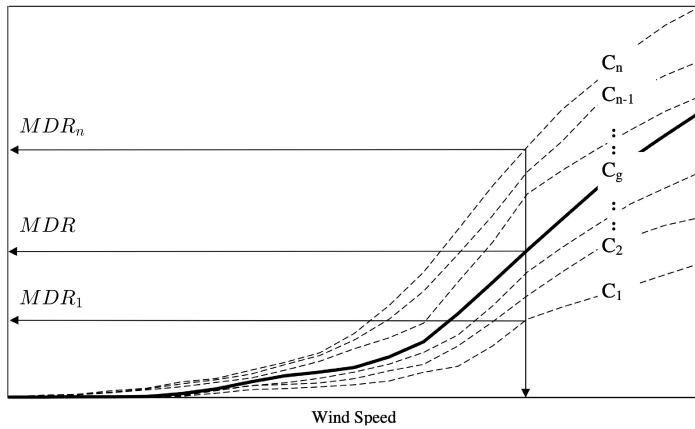


Figure 5.7: Hurricane vulnerability curve scheme according to [50].

The first assumption allows to define in a known region the benchmark ratios, k_i , between the generic i -th $MDRs$ and a reference curve MDR_r ;

i.e., $k_i = MDR_i/MDR_r$. The second allows to export these ratios to a different region, assuming they remain constant. From Equation 5.3, for the different country, results:

$$k_1 \cdot MDR_r \cdot w_1 + \dots + MDR_r \cdot w_r + \dots + k_n \cdot MDR_r \cdot w_n = MDR \cdot \sum_{i=1}^n w_i \quad (5.4)$$

Then,

$$MDR_r = \frac{MDR \cdot \sum_{i=1}^n w_i}{\sum_{i=1}^n k_i \cdot w_i} \quad (5.5)$$

Once the reference curve for the different region is known, this computation is developed for each wind speed and a vulnerability curve for an unknown class is provided. In order to take into account the differences in two different regions, the results are usually revisited on the basis of available loss data or wind engineering judgment.

Advantages and disadvantages of past-loss data vulnerability models

In addition to the inherent simplicity of the approach, inasmuch losses are provided directly as a function of wind intensity, empirical vulnerability curves based on past-loss data have the advantage of incorporating all forms of uncertainty. In fact, since they are based on real data, the size and completeness of the underlying dataset translates into greater reliability of the regression parameters obtained. This explains the perceived reliability of such models in the US where hurricane damage is a recurring phenomenon in some specific areas, that typically share building construction standards and practices with other regions, and an extensive amount of insurance loss data has been accumulated in recent years [94].

However, the challenges in exporting these models to risk analysis of building stocks or regions other than those for which they were developed and their low resolution are their main drawbacks. Regarding the former, this issue can be exacerbated by differences in construction practices and standards between worldwide regions. Low resolution, on the other hand,

is often due to the nature of the insurance claims themselves, which often contain no details on actual building response to extreme winds. Furthermore, empirical vulnerability curves might introduce some bias at low wind speeds, because insurers tend not to report claims below some lower-bound limit. Lastly, it is hard to reliably quantify the wind speeds that produced damage in the claim data and this adds an important source of uncertainty to the past-loss data models.

5.1.2 Heuristic approaches

Heuristic approaches base the assessment of building vulnerability to wind on expert judgment and experience (e.g., [99]). In most cases, expert judgement is involved in the definition of the wind speed that causes a certain degree of damage to a structure or the probability of damage conditional on wind intensity. One of the first authors which developed such a heuristic model was Hart. In his study [40], he proposed a *damage probability matrix* collecting expert opinions on estimates of the potential damage that a structure sustains, according to the intensity of the impacting tornado. Later, other authors used such an approach to various related different purposes, such as the development of wind risk mitigation strategies (US Federal Emergency Management Agency - FEMA) for typical Australian residential building stock [97].

Another work that has received attention in recent years is that of CAPRA (Probabilistic Risk Assessment) Platform led by the World Bank, the United Nations' Office for Disaster Risk Reduction (UNISDR), and the Interamerican Development Bank [70]. This project aims to improve disaster risk management in the Central America region. It is integrated with the software interface ERN-Vulnerability which contains a library of different curves calibrated by expert judgement, concerning three main building components: roof type, envelope and number of stories, according to Table 5.1. Hurricane vulnerability curves are developed through the definition of 3 parameters according to the following relation:

$$MDR(U) = \max[MDR(U)] \cdot \left[1 - 0.5^{\left(\frac{U}{U_\gamma}\right)^\rho} \right] \quad (5.6)$$

with U being the 5-sec gust wind speed (in km/h), U_γ the wind speed causing half of the maximum damage (i.e., a scale parameter) and ρ is a shape parameter (i.e., the slope of the curve at U_γ) (Figure 5.8). In this case $MDR(U)$ is defined as the repair building cost divided by the total building cost. ERN-Vulnerability also provides an estimate of the uncertainty for each wind speed via a *Beta distribution*.

Table 5.1: Building characteristics of CAPRA curves

Roof type	Envelope walls	Stories
Concrete, ligh, or heavy	Mansony or felxible	1-5

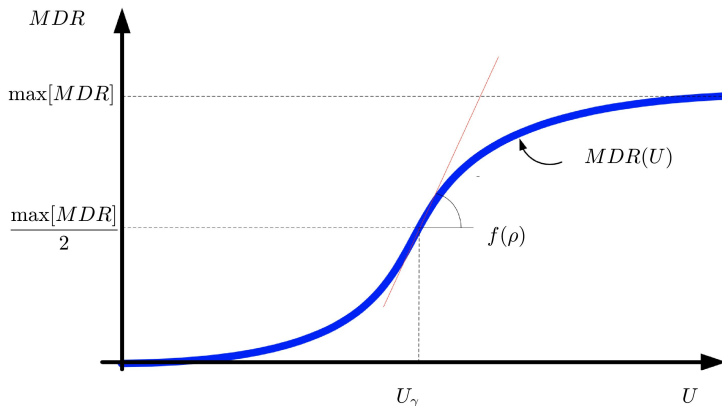


Figure 5.8: Parameters of CAPRA built-in vulnerability functions.

Advantages and disadvantages of heuristic wind vulnerability models

Clearly, the heuristic approach is called to fill the gap in cases where empirical methods lack data or more complex engineering approaches (next

section) cannot be (or have not yet been) developed. Although these models allow for a quick definition of vulnerability and some uncertainty management as seen in the case of CAPRA, they are strongly affected by the subjectivity of individual judgment. Since these methods depend almost exclusively on the experience of the engineer or other expert, this often leads to the models unable to capture small variations in structures that are quite similar (e.g., occupancy).

5.1.3 Engineering-based approach

The engineering-based approach can be considered as a natural evolution of the heuristic one. In this approach the modelling of structural response to wind, with the objective of predicting damage and vulnerability, is achieved by applying mathematical tools of structural engineering practice. Thus, the performance of both primary and secondary structural elements can be evaluated once capacities and loads are assigned to them. This level of detail in the analysis results in commensurate levels of detail in the output, that cannot be achieved using the methods introduced previously. In this case, better knowledge of structural detailing and layout can be translated into a more reliable loss assessment.

Although this approach does employ expert judgement at times and still requires validation, same as with heuristic methods, said expert judgement is not directed at the definition of overall damage but rather in the study of individual component responses and how those propagate to the rest of the structure. Only at the end, by assembling and combining the failures of the various components, a measure of damage to the entire structure is obtained.

While the first engineering-based methods had a more deterministic point of view, it was later recognised, by several authors, that a more rigorous probabilistic treatment was necessary. While Sciaudone et al. presented the basic outline of a probabilistic framework in 1997 [75], a few years later, in 2002, Unanwa et al. presented a more detailed study [94] that incorporated the consequence of one component's failure on the probability of failure of other components via a fault tree scheme and an expert

judgment [87].

Although these methods did not consider all the parameters involved as random variables and required a lot of input from expert judgement due to the lack of reliable data, they represented a major step forward that prepared the way for the PBWE framework discussed in Section 1.1.

The latest developments of the aforementioned *component-based* methods are to be found in the literature concerned with *simulation-based* methods, which are some of the most advanced engineering-based vulnerability models in use today. It is worthwhile to single out the work of Vickery [90, 91] who provided the basis for the method employed in the HAZUS hurricane model by the US Federal Emergency Management Agency (FEMA) [18]. This study contains analysis on wind speed data, wind loads on buildings and the performance of building components. More specifically, the focus is on the behaviour of the various components of a building envelope under wind loads in combination with engineering judgement. Salient features included in this work are the modelling of damage due to wind-borne debris and the effects of changing internal wind pressure due to the progressive failure of building envelope components.

From these studies, it stems that the essential elements for the development of engineering-based vulnerability models, are the classification of buildings according to their characteristics, the probabilistic estimation of the actual wind loads on buildings, corresponding to the estimated wind speeds to which the building may be exposed (hazard), but also of the components' performance at each wind speed level. These aspects reflect the possibility of including in the model the uncertainties and non-linearities that are typical of the real response of the structures to wind.

Some uncertainty is also associated with the estimation of wind loads associated with the reference wind speed. In fact, codes and standards worldwide consider a condition of isolated buildings on flat terrain for the definition of the latter. However, as seen in previous chapters, the impact of the urban environment has a great impact on the wind characteristics. A study from James Cook University [95] demonstrated with wind tunnel tests how the horizontal forces associated with an urban environment can be significantly less than those prescribed by the standards. On the contrary,

it is possible to observe a much higher uplift force on the roof if the building is higher than the nearby ones.

Non-linearities are often associated with the load variation resulting from a partial failure of the structure during the action of the extreme event; e.g., an opening resulting from failure of a door, window, or part of the roof, can lead to a rise in internal pressures and to the failure of another part of the structure that would have otherwise not occurred.

For this reason, great attention has been given over the years to the study of debris and its impact on structural performance during extreme wind events. Components of nearby buildings such as roofing gravel or eave gutters, become airborne for high wind speeds and hit windows or doors, creating the effect mentioned above. This behavior is reflected by studies such as the one by Sparks and Bhindarwala [79] that shows a steep slope of the empirical vulnerability curve for houses for higher wind speeds.

In conclusion, it can be said that the most reliable and sophisticated engineering-based methods are those that have the most detailed information on the behavior of building components and wind load and that consider the interaction between component failures.

Component-based wind vulnerability

Component-based vulnerability derivation is historically the earliest engineering-based method developed. For the definition of the vulnerability of a structure to wind, this method employs the fragility functions of the structure's constituent components. One pioneering investigation of this approach was carried out by Unanwa et al. in 2000 [87]. In their work, these authors developed so-called vulnerability bands (Figure 1.2 - right), i.e., two vulnerability curves constituting a lower and an upper bound of losses, representing the most favorable and unfavorable condition, respectively. Such bands are developed for low-rise (1-3 floors) and mid-rise (4-10 floors) buildings (residential, commercial/industrial, government/institutional), considering alternative component and connection configurations that exhibit the lowest and highest probability of failure. In order to quantify these vulnerability bounds, the *damage degree* at given hazard wind level IM , $DD(IM)$,

is defined according to the following formulations:

$$DD(IM) = \sum_{i=1}^n P[\text{failure}|IM]_i \cdot CCF_i \cdot \alpha_i \quad (5.7)$$

in which $P[\text{failure}|IM]_i$ is the i-th component fragility, CCF_i the i-th *component cost factor*, n the number of components used in the damage model, and α_i the i-th *component location parameter*. More specifically, the latter parameter takes into account the case that a component may be very extended and therefore located in areas exposed to different wind effects. Using expert judgement, the components considered in the damage model (i.e., those most likely to fail) were identified by the authors to be the roof covering, roof structure, exterior doors and windows, exterior wall, interior, structural system and foundation. The *fault tree* considered by the authors is shown in Figure 5.9. In this figure it is possible to observe how each component (except interior and structural system) is connected by three lines. While the first one is related to the direct damage due to the action of wind or debris (*basic damage*), the second and third are related to the damage that the component causes or suffers from another (*propagational damage*). In this way, the fragility of the component is defined by the study of two different contributions.

The fragility of each element is then studied through a fault tree analysis in which the top event is the failure of the component as shown in Figure 5.10 for the roof covering. However, this analysis has not been performed for all components identified previously since for the foundations and the structural system the failure probability is orders of magnitude smaller. Finally, the wind load was assumed in a deterministic way as is usual to find in these early engineering-based methods.

Simulation-based wind vulnerability

The engineering- simulation-based approach is considered the most sophisticated approach in the state-of-the-art of wind vulnerability development [70]. Developed on a probabilistic framework, the study of components

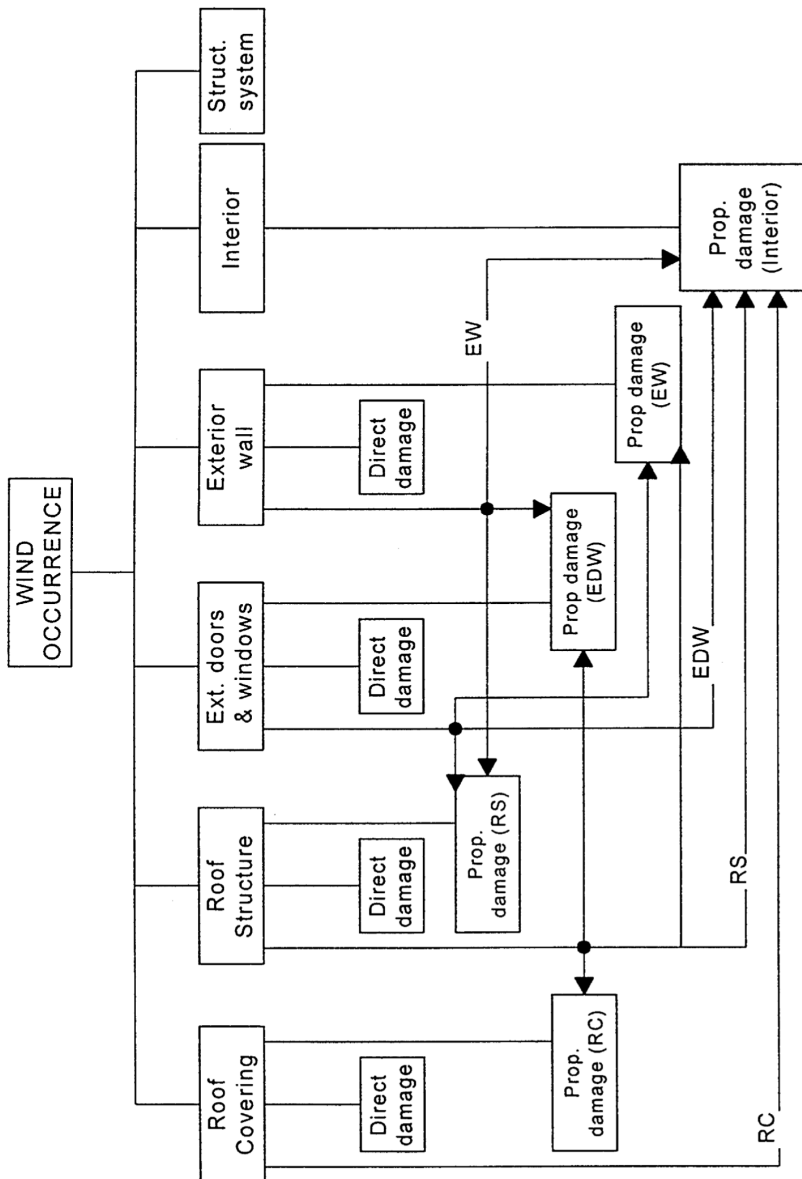


Figure 5.9: Wind damage process (adapted from [87]).

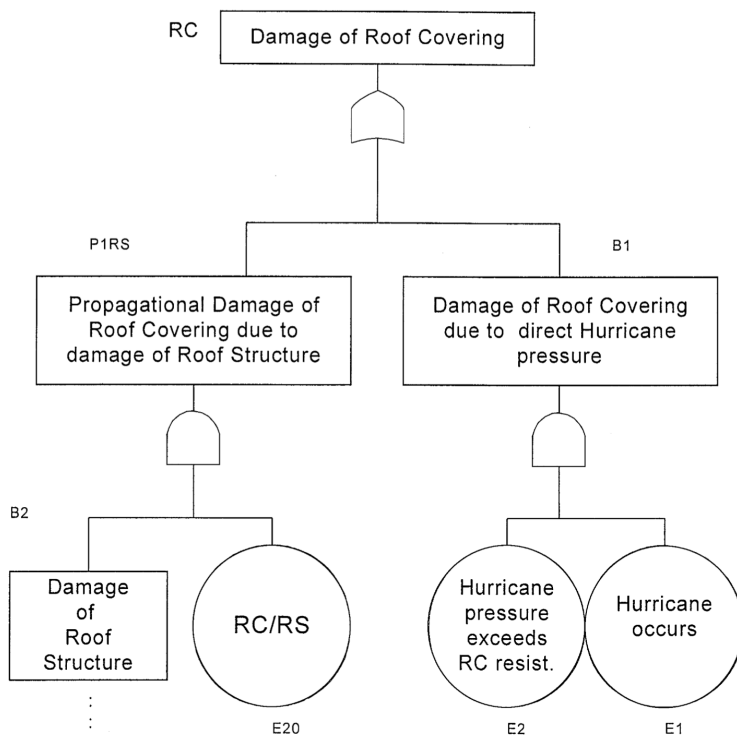


Figure 5.10: Fault tree scheme for roof covering damage (adapted from [87]).

damages and their propagation due to the wind is carried out usually through *Monte Carlo simulations*, over time. In this way it is possible for each simulation to sample a resistance and load value for the whole structure. Then, for every interval of time, each component failure and the effects of the latter on the entire structure is accounted via the development of sophisticated algorithms. The flexibility of the latter allows to include in the model crucial parameters in the definition of the structural response, from the variation of wind characteristics (e.g., direction and intensity) to the impact of windborne debris. By repeating the process for a sufficient number of Monte Carlo realizations, it is possible to develop average results both in terms of fragility and vulnerability (Figure 5.11).

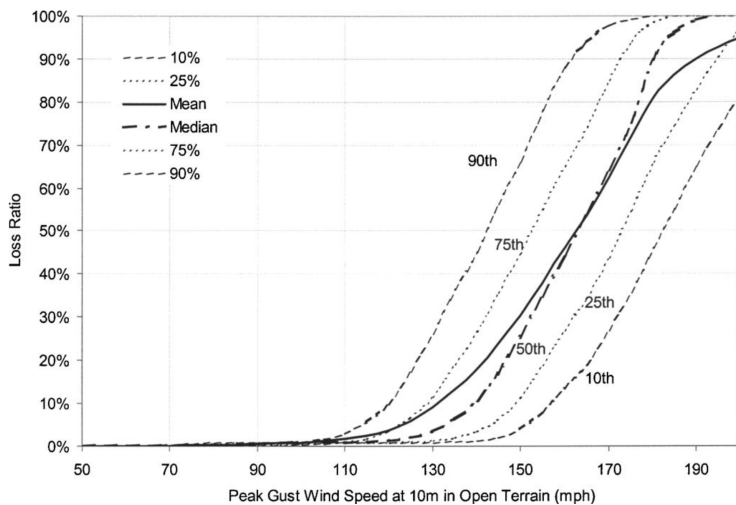


Figure 5.11: Vulnerability curve percentiles (adapted from [91]).

The great flexibility of this approach lies in the definition of a detailed algorithm that takes into account all the non-linearities in the model. One of the most detailed results the one developed by Vickery for HAZUS in Figure 5.12.

This algorithm involves studying the response of the structure to a simulated hurricane, for time intervals of 15 minutes. For each simulation,

a component resistance, the error on the building pressure distributions, the building orientation and the shielding effects of surrounding buildings are sampled. In each time step, wind speed and direction is computed and applied to the structure according to pressure coefficients theory. It is then assessed whether any components failed in this load step (also taking into account windborne debris) and if so, the internal pressure variation is evaluated and the time step is recomputed for the new configuration. This process is then repeated several times until the result is judged satisfactory.

Although HAZUS presents results that are considered reliable for US constructions, in other parts of the world such results are not considered so reliable since construction practices change worldwide. For this reason other models have been developed in more recent years by other authors in other regions. An example is the one developed in Japan by Zhang et al. in 2014 [102]. Although the authors have developed the model for a specific building type (typical Japanese residential building), they have been able to develop a sophisticated model for debris assessment (flying tiles in Figure 5.13).

Advantages and disadvantages of engineering-based wind vulnerability models

The greatest advantage of engineering methods lies in their great flexibility. In fact, these methods move away from the low levels of detail of the previous methods and allow the study of very specific individual characteristics of structural components, from the roof typology to the smallest connecting bolt. Figure 5.12 shows how the variation of one of the smallest elements of the roof connection, the washer, can lead to a very different result in roof vulnerability terms. A real limitation is therefore in the existence and availability of reliable information on the capacity of the elements and strong wind-structure interaction models. However, the great flexibility allows an improvement of models over time, when more detailed studies become available, study of mitigation measures, building code improvements, and identification of the weakest links in the component-chain. In addition,

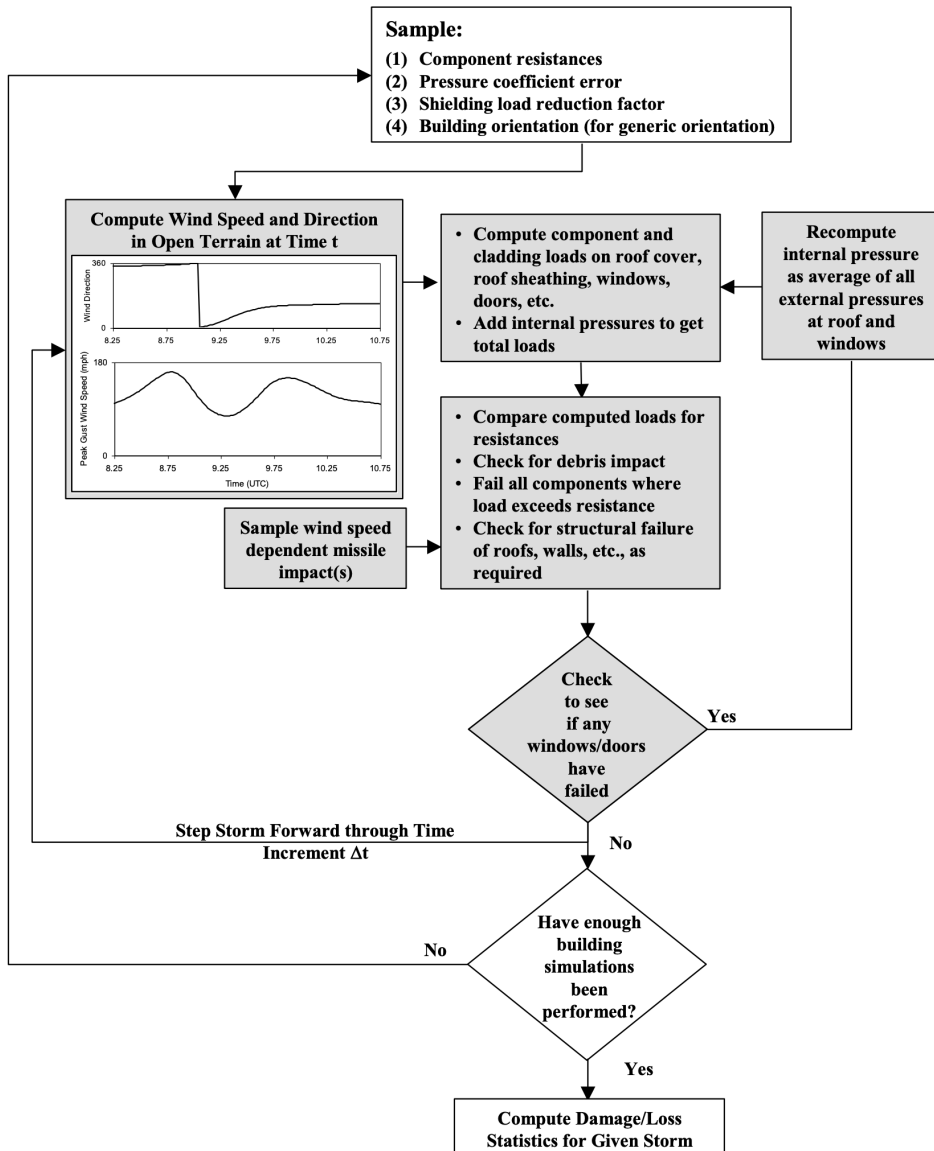


Figure 5.12: HAZUS hurricane damage estimation algorithm (adapted from [91]).

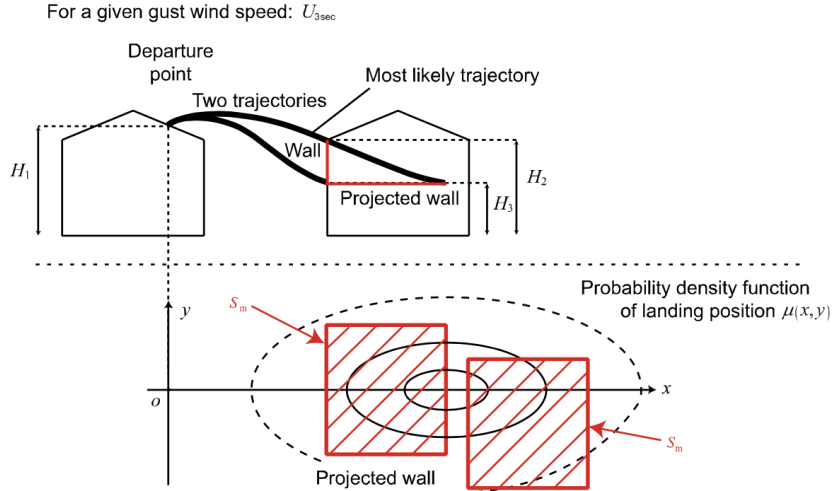


Figure 5.13: Flying debris model (adapted from [102]).

the development of simulation techniques makes it possible to increase the reliability of the models and to study the behaviour of the structure over a wide range of intensity measurements. Compared, for example, to the past-loss data approach, such models do not suffer from gaps in the definition of the intensity measure. However, the disadvantage of these models lies in their great complexity. For this reason, some authors have focused on an in-depth study of just the most vulnerable components, such as the roof structure (e.g., [52]).

5.1.4 Comparison between approaches of vulnerability assessment

As a concluding remark, a summary of the salient differences between the main approaches for wind vulnerability modelling is provided. First of all, it can be observed that models based on past loss-data information coming from post-event insurance claims or surveys. On the other hand, the

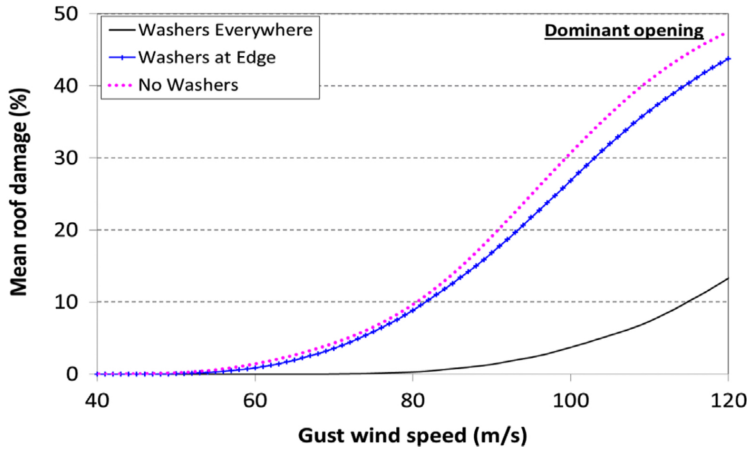


Figure 5.14: Vulnerability curves for a roofs for a given direction of the wind, a dominant opening, and different configurations of cyclone washer for the connection (adapted from [52]).

same data are used in the case of the heuristic approach to calibrate specific vulnerability models and in the case of engineering-based approaches, as a means of verifying model robustness. The core of engineering-based wind vulnerability is the explicit use of structural engineering concepts and mechanical modelling, which allows for distinguishing between individual building types – a distinction that claims usually cannot capture. Another issue examined in this report is the treatment of the various sources of uncertainty. While in empirical models all sources of uncertainty are implicitly accounted for in the vulnerability curve, heuristics and engineering-based models require that these sources of uncertainty be handled explicitly. This means that in these cases, the modeller is allowed to control how uncertainty is handled, but on the other hand, it may not always be possible to cover all sources thereof. However, greater control over handling uncertainty translates into higher complexity and therefore higher modelling costs. On the other hand, empirical models simply employ regression of past

loss data, which require less time and effort, when compared to, for example, simulation-based methods. Finally, the exportability of vulnerability models to other regions is another issue that brings forward a difference between the modelling approaches. While empirical models exhibit limited exportability because they are based on data that refer to specific regions with their own specific construction and territorial characteristics, heuristic and engineering-based models are more flexible in this respect, because the differences in local construction practice and building codes can be explicitly accounted for in the vulnerability modelling. This flexibility also allows for results that are relevant to risk mitigation, such as being able to identify which building components are mostly at risk, in order to plan remedial measures and potentially update the vulnerability model. This is not possible for empirical models, that are based on past loss data and therefore only reflect the building stock characteristics at a specific time, without the possibility to account for the future evolution of construction techniques, potentially triggered by the natural catastrophe. A summary presentation of this comparison between methodologies for estimating wind vulnerability is provided in Table 5.2.

Table 5.2: Comparison of the features of vulnerability methodologies

Approach	Past-loss data	Heuristic	Engineering-component-based	Engineering-simulation-based
Control of uncertainty	Implicit	Implicit/ Explicit	Explicit	Explicit
Development complexity	Low	Medium	Medium/High	High
Development time	Short	Short	Medium/Long	Medium/Long
Exportability	Low	Medium	Medium/High	Medium/High

Chapter 6

Wind fragility

Among the different vulnerability curve development methods discussed in the previous chapters, the present thesis focuses on engineering methods. These methods have seen a gradual migration of the academic community towards them in recent years, resulting in an increase of results both in terms of wind vulnerability and fragility of structures but also of their components. However, more attention has been paid to the development of fragility rather than vulnerability curves (e.g., [58, 18, 41, 60, 102, 101]), since the definition of the latter is often linked to loss terms that limit their exportability between different regions.

The building fragility, in performance-based approaches, is usually defined as the probability of exceeding a k -th damage state, given an intensity measure [22], i.e., $P[DS \geq ds_k | im]$. In common risk frameworks, fragility can be used to define the probability of k -th damage state occurrence (given im) according to:

$$P[DS = ds_k | im] = P[DS \geq ds_k | im] - P[DS \geq ds_{k+1} | im] \quad (6.1)$$

with k lower than the highest damage state. Nevertheless, building fragility functions also suffer from exportability problems [102] as they are usually derived for coarse taxonomies, e.g., industrial or residential buildings. It

is easy to understand how typical residential buildings are very different in US and Japan in many aspects like geometry or characteristics of non-structural elements such as roof shape and roof tiles. Then, in recent years, as also remarked in the previous chapter, the academic focus has been put on the study of some detailed building components most vulnerable to wind. Thus, many existing fragilities have been developed for them. Being consequence functions related to components less common, it is more difficult to assess the overall building losses from component fragilities. Since that, over the years an effort has been directed in the direction of building fragility composition and this thesis also attempts to provide an example. In fact, a method for the definition of building fragility is proposed herein, using a composition of component fragilities. This approach makes some simplifying assumptions that will require validation (to follow), yet it allows for a rapid evaluation of a building's wind fragility when its component fragilities can be available, without resorting to laborious structure-specific analyses.

The next section analyzes this method developed in accordance with the PBWE framework presented. It also shows a simple illustrative application, which provides some degree of validation for the method.

6.1 Building fragility composition

Component-specific wind fragility studies are often motivated by the difficulty inherent in modelling the whole building system and the interaction between damage to its components, the so-called *damage propagation*: for example, failure of a window can lead to a rise in internal pressure and a consequent failure of the whole roof structure. Engineering-based approaches to vulnerability assessment allow to model the damage propagation among building components and simulate the response of the entire building. However, despite the enhanced accuracy, these methods tend to be both structure-specific and time-consuming. Therefore, some studies propose methods to expedite component fragility composition, for example fault tree analyses [87, 29, 40, 24, 69].

A simplified probabilistic fragility composition approach is also proposed here, aimed at cost-effective and rapid building fragility assessment, consistent with the PBWE framework of Section 1.2. For each realization of the intensity measure, this method evaluates the fragility of a building from those of its components, through the definition of a damage matrix. Therefore, the key assumptions at the basis of this approach include the availability of the damage matrix and the related component fragility curves.

For a given im , building fragility for the $k - th$ damage state, ds_k , can be evaluated through the summation of the probability of occurrence of damage states greater and equal than k :

$$P[DS \geq ds_k | im] = \sum_{j=k}^{n_{ds}} P[DS = ds_j | im] \quad (6.2)$$

with n_{ds} being the discrete number of building damage states considered. According to the assumptions of Section 1.2, the probability of occurrence of the $j - th$ building damage state, ds_j , can be defined as:

$$P[DS = ds_j | im] = \sum_{m=1}^{n_{\{edp\}}} P[DS = ds_j | \{EDP\} = \{edp\}_m] \cdot P[\{EDP\} = \{edp\}_m | im] \quad (6.3)$$

where $n_{\{edp\}}$ is the number of possible realizations of the vector of engineering demand parameters, $\{edp\}$, defined by the building component damage states. All the possible realisations of this vector, collected into the sample space $\{EDP\}$, are determined through the definition of the damage matrix, used to univocally return the building damage states from the ones of its components. As an example, the damage matrix in Figure 6.1 defines the building in a certain damage state (minor damage) if *any* of the shaded component damage states in the corresponding row occurs (failure of one fenestration or between 2% and 15% of the roof cover or both). Also, in the same figure, it is possible to observe how the first damage state for the roof cover component occurs for a failure between 2% (excluded) and 15%

(included) of the whole component, the second for a failure between 15% (excluded) and 50% (included), and the third for a failure greater than 50% (excluded). It is essential to point out how the previous damage states have been numbered in ascending order based on severity of the damage and are not related to the definition of the building or other component damage states. This principle, applied for each component, defines the useful *numerical damage matrix* as the type in Table 6.1 for the damage matrix in Figure 6.1. In this matrix each row refers to a different damage state of the building while each column refers to a different component of the building.

Damage State	Qualitative Damage Description	Roof Cover Failure	Window Door Failures	Roof Deck	Missile Impacts on Walls	Roof Structure Failure	Wall Structure Failure
0	No Damage or Very Minor Damage Little or no visible damage from the outside. No broken windows, or failed roof deck. Minimal loss of roof over, with no or very limited water penetration.	$\leq 2\%$	No	No	No	No	No
1	Minor Damage Maximum of one broken window, door or garage door. Moderate roof cover loss that can be covered to prevent additional water entering the building. Marks or dents on walls requiring painting or patching for repair.	$>2\% \text{ and } \leq 15\%$	One window, door, or garage door failure	No	<5 impacts	No	No
2	Moderate Damage Major roof cover damage, moderate window breakage. Minor roof sheathing failure. Some resulting damage to interior of building from water	$>15\% \text{ and } \leq 50\%$	$> \text{one and } \leq \text{the larger of } 20\% \text{ & } 3$	1 to 3 panels	Typically 5 to 10 impacts	No	No
3	Severe Damage Major window damage or roof sheathing loss. Major roof cover loss. Extensive damage to interior from water.	$>50\%$	$> \text{the larger of } 20\% \text{ & } 3 \text{ and } \leq 50\%$	$>3 \text{ and } \leq 25\%$	Typically 10 to 20 impacts	No	No
4	Destruction Complete roof failure and/or, failure of wall frame. Loss of more than 50% of roof sheathing.	Typically $>50\%$	$>50\%$	$>25\%$	Typically >20 impacts	Yes	Yes

Figure 6.1: Damage matrix for residential building (adapted from [18]).

Actually, this expedient allows to handle with numerical combinations of component damage states, deemed as engineering demand parameters, corresponding to each building damage state. In fact, it is possible to associate to each possible realisation of $\{\text{edp}\}$, i.e. to each set of component damage states, the corresponding damage state of the entire building. This can be done by identifying for each nonzero element of $\{\text{edp}\}$ (for each

Table 6.1: Numerical damage matrix from residential building (Figure 6.1), excluding missile impacts on the walls.

Building	Roof cover	Window/ door	Roof deck	Roof structure	Wall structure
0	0	0	0	0	0
1	1	1	0	0	0
2	2	2	1	0	0
3	3	3	2	0	0
4	3	4	3	1	1

component damage state) its corresponding row in the numerical damage matrix and then associating the damage state corresponding to the lowest row thus identified damage state to the building as a whole.

Therefore, it is possible to collect all possible combinations of $\{edp\}$ associated with a specific DS , according to the following procedure. Given the selected $j - th$ building damage state, the corresponding row on numerical damage matrix shows a value for each $i - th$ component, $edp_{j,i}$. This value allows to define a vector of damage states, $\{0; \dots; edp_{j,i}\}$, for each building component. From the selection of a single element at a time for each of these vectors comes all the possible combination of the component damage states corresponding to a building damage states lower or equal to j . Collecting all these combinations in a subassembly, it is possible to find the ones corresponding univocally to the $j - th$ (grater than the first, defined by all 0), $\{EDP\}_{ds_j}$, from its difference with subassembly corresponding to ds_{j-1} . Therefore, for each possible realization $\{edp\}_m$, it results:

$$P[DS = ds_j | \{EDP\} = \{edp\}_m] = \begin{cases} 1 & \{edp\}_m \in \{EDP\}_{ds_j} \\ 0 & \{edp\}_m \notin \{EDP\}_{ds_j} \end{cases} \quad (6.4)$$

with $\{EDP\} = \bigcup_{j=1}^{n_{ds}} \{EDP\}_{ds_j}$.

Once defined the first term of the product into the summation of Equation 6.7 has been defined, it remains to define the second one. Assuming the

occurrence of building components' damage states *stochastically independent* from each other, the probability of occurrence of a specific combination of building component damage states results:

$$P[\{EDP\} = \{edp\}_m | im] = \prod_{i=1}^{n_c} P[EDP_i = edp_{i,m} | im] \quad (6.5)$$

with n_c the number of the considered building components (lower or equal to n_{ds}). Although the previous hypothesis is very strong given the well-known interaction between component failures, the independence between component damage states events have been yet investigated to some extent in the literature [24, 69]. Recognising a certain degree of applicability of this hypothesis in the literature, it has been deemed adequate for the purposes of this thesis.

Each terms in the product of Equation 6.5 can be calculated through the fragility functions of the i -th building component, in analogy with the Equation 6.1:

$$\begin{aligned} P[EDP_i = edp_{i,m} | im] &= \\ P[EDP_i \geq edp_{i,m} | im] - P[EDP_i \geq edp_{i,m} + 1 | im] \end{aligned} \quad (6.6)$$

with $edp_{i,m}$ lower than the highest component damage state.

Finally, for a given im , according to the previous equations, the fragility of the building can be derived by the definition of the numerical damage matrix, knowing the fragility functions of its components, as:

$$\begin{aligned}
P[DS \geq ds_k | im] &= \sum_{j=k}^{n_{ds}} P[DS = ds_j | im] = \\
&\sum_{j=k}^{n_{ds}} \sum_{m=1}^{n_{\{edp\}}} P[DS = ds_j | \{EDP\} = \{edp\}_m] \cdot P[\{EDP\} = \{edp\}_m | im] = \\
&\sum_{j=k}^{n_{ds}} \sum_{m=1}^{n_{\{edp\}}} P[DS = ds_j | \{EDP\} = \{edp\}_m] \cdot \prod_{i=1}^{n_c} P[EDP_i = edp_{i,m} | im] = \\
&\sum_{j=k}^{n_{ds}} \sum_{m=1}^{n_{\{edp\}}} P[DS = ds_j | \{EDP\} = \{edp\}_m] \cdot \prod_{i=1}^{n_c} (P[EDP_i \geq edp_{i,m} | im] - \\
&\quad P[EDP_i \geq edp_{i,m} + 1 | im]) \quad (6.7)
\end{aligned}$$

with

$$P[DS = ds_j | \{EDP\} = \{edp\}_m] = \begin{cases} 1 & \{edp\}_m \in \{EDP\}_{ds_j} \\ 0 & \{edp\}_m \notin \{EDP\}_{ds_j} \end{cases}$$

6.1.1 Illustrative application

With the aim to clarify the proposed fragility composition approach of the previous section, a simple example is provided. The damage matrix (Figure 1.8) and the associated fragility curves (Figure 6.2) have been selected from the HAZUS technical manual [18], for an industrial building (typology G.1). The corresponding numerical damage matrix is presented in Table 6.2 (considering only the components for which the fragility curves have been developed).

To the first building damage state (first row in Table 6.2), ds_0 , correspond a numerical value for each i -th component, $edp_{0,i}$, equal to 0. For this reason the only building component damage states combination corresponding to ds_0 is $\{0; 0; 0; 0; 0\} = \{EDP\}_0$.

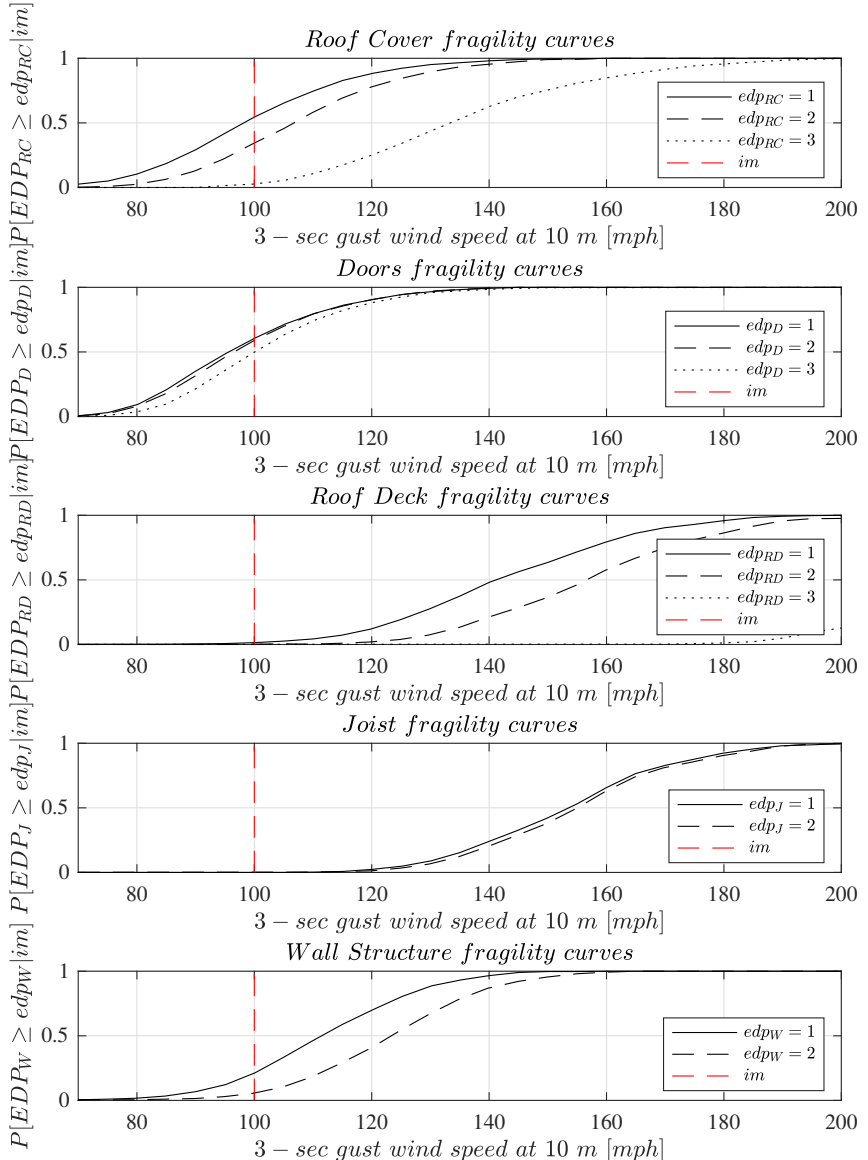


Figure 6.2: Industrial building (G.1) component fragility curves (adapted from [18]).

Table 6.2: Numerical damage matrix for the first three industrial building damage states, according to [18]

Building <i>DS</i>	Roof cover { EDP_{RC} }	Roof deck { EDP_{RD} }	Joist { EDP_J }	Doors { EDP_D }	Wall { EDP_W }
0	0	0	0	0	0
1	1	0	0	1	0
2	2	1	0	2	0
3	3	2	1	3	1

For the second damage state, since $edp_{0,RC} = edp_{0,D} = 1$ and $edp_{0,RD} = edp_{0,J} = edp_{0,W} = 0$, all the possible combination of the component damage states corresponding to a building damage states lower or equal to ds_1 are: {0; 0; 0; 0; 0}, {1; 0; 0; 0; 0}, {0; 0; 0; 1; 0}, and {1; 0; 0; 1; 0}. The difference between them and $\{EDP\}_0$ provides the subassembly $\{EDP\}_1$: {1; 0; 0; 0; 0}, {0; 0; 0; 1; 0}, and {1; 0; 0; 1; 0}. (In order to simplify the discussion, the more numerous combinations for the following building damage states are not listed.)

According to the composition approach of Section 6.1, knowing the fragility curve for each of the building components, the probability of occurrence of ds_0 , for a given im , results:

$$\begin{aligned}
 P[DS = 0|im] &= \\
 P[\{EDP\} = \{0; 0; 0; 0; 0\}|im] &= P[EDP_{RC} = 0|im] \cdot P[EDP_{RD} = 0|im] \cdot \\
 P[EDP_J = 0|im] \cdot P[EDP_D = 0|im] \cdot P[EDP_W = 0|im] &= \\
 (1 - P[EDP_{RC} \geq 1|im]) \cdot (1 - P[EDP_{RD} \geq 1|im]) \cdot (1 - P[EDP_J \geq 1|im]) \cdot \\
 (1 - P[EDP_D \geq 1|im]) \cdot (1 - P[EDP_W \geq 1|im]) & \quad (6.8)
 \end{aligned}$$

In the same way, it is possible to define the occurrence probability of ds_1 :

$$\begin{aligned}
 P[DS = 1|im] &= P[\{EDP\} = \{1; 0; 0; 0; 0\}|im] + \\
 P[\{EDP\} &= \{0; 0; 0; 1; 0\}|im] + P[\{EDP\} = \{1; 0; 0; 1; 0\}|im] = \\
 P[EDP_{RC} = 1|im] \cdot P[EDP_{RD} = 0|im] \cdot P[EDP_J = 0|im] \cdot \\
 P[EDP_D = 0|im] \cdot P[EDP_W = 0|im] + P[EDP_{RC} = 0|im] \cdot \\
 P[EDP_{RD} = 0|im] \cdot P[EDP_J = 0|im] \cdot P[EDP_D = 1|im] \cdot \\
 P[EDP_W = 0|im] + P[EDP_{RC} = 1|im] \cdot P[EDP_{RD} = 0|im] \cdot \\
 P[EDP_J = 0|im] \cdot P[EDP_D = 1|im] \cdot P[EDP_W = 0|im] \quad (6.9)
 \end{aligned}$$

Developing the same calculations for all damage states of the building, it is possible to define its fragility curves, shown in Figure 6.3. This figure also shows the comparison with fragility curves provided by HAZUS via its engineering- simulation-based approach. It is possible to observe as the presented composition-based approach returns results with a certain degree of agreement with those provided by HAZUS simulation, with a maximum difference of about 0.1, greater as the building damage state increases and for wind speed ranging between 90 and 120 mph.

6.2 Building component fragility composition

Through refined engineering-based methods for wind vulnerability assessment, over the years, some authors have increased the level of detail of their studies to the level of *building sub-components* but also *building elements* (e.g., a single bolt or tile). Then, some of them presented fragility results for *sub-components* and *element*.

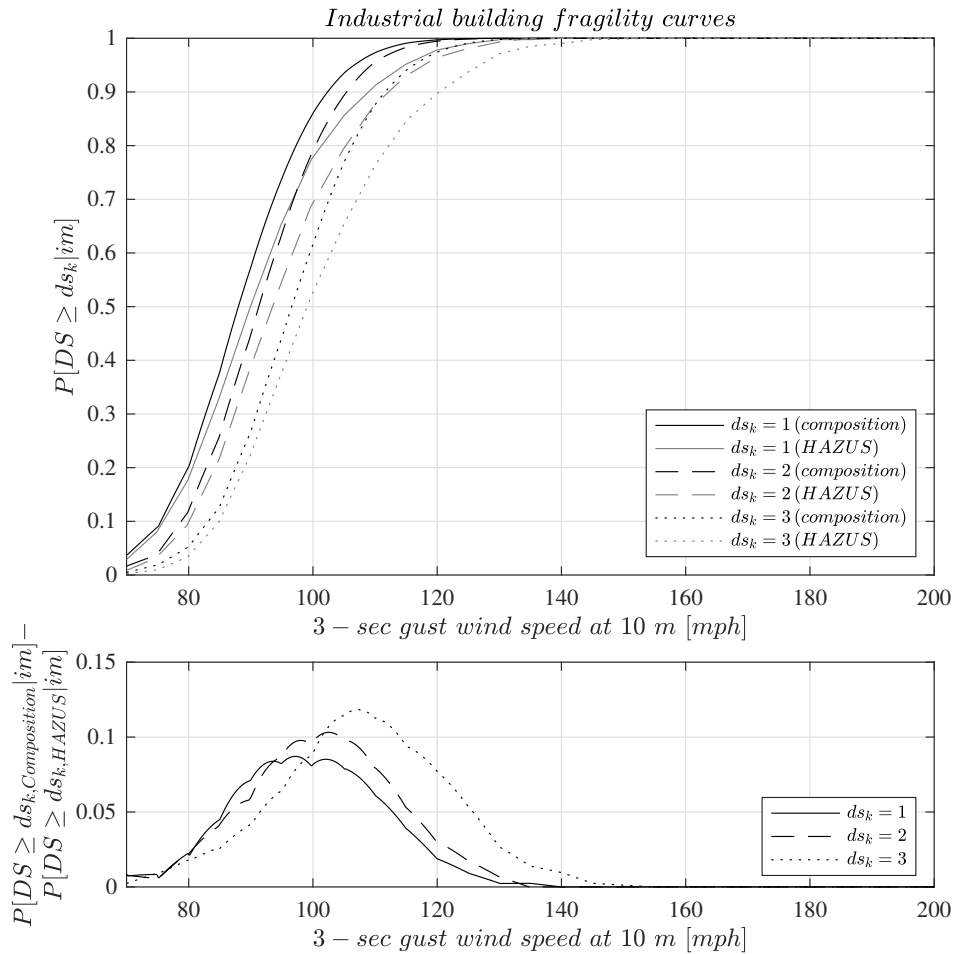


Figure 6.3: Industrial building fragility curves comparison.

Therefore, the author of this thesis has investigated these fragilities, trying to derive results that can be used in the composition approach described in Section 6.1, which has been developed on a lower level of detail. This process is motivated by the common definition of the damage matrix for a limited number of generic macro-components, typical of the building type, but also by the aim of increasing the population of useful results for the development of the composition approach.

A first analysed aspect involves the composition of building sub-components to assess the one of the main component, e.g., composition of roof deck and tile system fragility to derive a more generalized roof covering main component fragility. This problem has been addressed in the same way of the previous composition procedure, specifying in this case that *DS* refers to the damage state of the main component while *EDP* represents the damage states of the sub-components. For this reason its discussion will not be further detailed.

The author's attention has also focused on two other main issues: the fragility functions association with existing damage states definitions and the study of single element fragility for the definition of a main component fragility. A study which enabled both of these aspects to be investigated is the one of Zhang et al. that, in 2014, developed a model for vulnerability definition of a typical residential building in Japan [102]. More specifically, they focus on three components of the structure, roof tiles, windows, and roof sheathing, and provide results in terms of fragility and vulnerability of the structure, its components, but also elements.

Then, although the authors do not formalise the damage states in their study, it has been possible to associate some of their results with the damage states provided by HAZUS for residential buildings. It is the case of window fragility in Figure 6.4 where the abscissa corresponds to the probability that at least one window fails.

Given the five HAZUS residential building damage state definitions for windows - no damage, one window failure, between 2 and 3 failures (or 20% of total number), between 4 and 50%, and greater than 50% - the window fragility curves developed by Zhang et al. are compatible with the ones corresponding to the first *HAZUS damage state (HDS)*. However, this

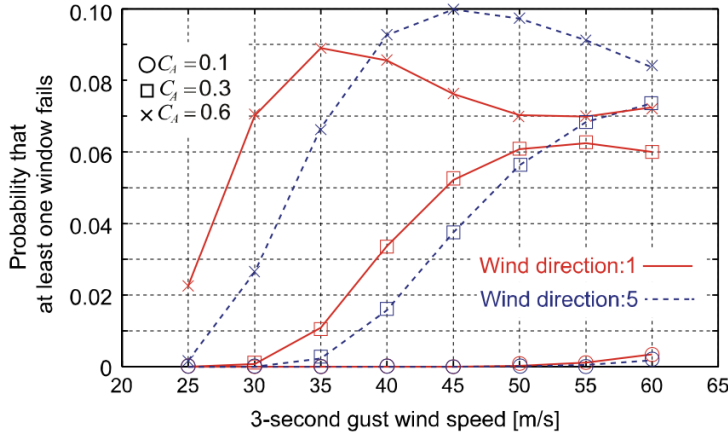


Figure 6.4: Windows fragility curves for different values of wind direction and spatial density of buildings (adapted from [102]).

aspect is mainly a product of an expert judgement.

Therefore, the more rigorous aspect of the element fragility composition results a more delicate and complex task. The next dedicated section explores this issue.

6.2.1 Roof covering fragility composition

This section aims to present the developed composition procedure for the definition of ad-hoc HAZUS-compatible building component (roof covering) fragility curves from the ones of its single element (typical Japanese tile) provided by Zhang et al. [102]. Also the feasibility of this method is discussed through a results comparison.

The fragility of a single tile, i.e., the probability of failure given a wind speed, $P[\text{Tile failure}|\text{IM}]_{C_p}$, is shown in Figure 6.5 for different values of *external pressure coefficient*, C_p , from -0.30 to -0.25. C_p is a widely used multiplicative coefficient in fluid dynamics, defining the relative pressure in a flow field.

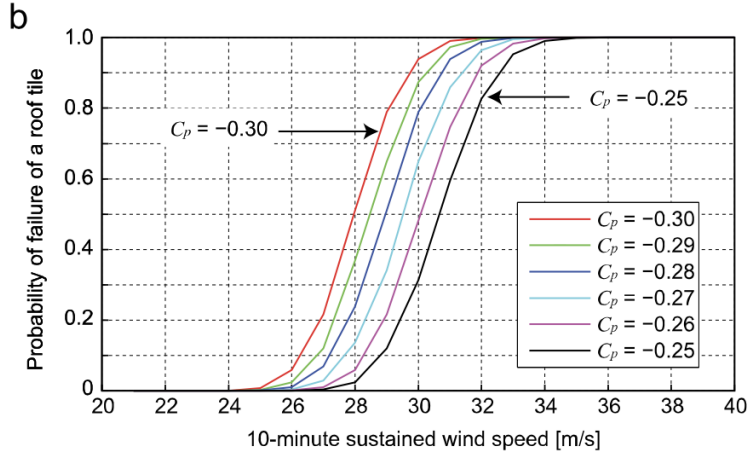


Figure 6.5: Single tile fragility curves for different values of external pressure coefficient, C_p (adapted from [102]).

Assuming that the failure of each roof tile is *independent* from the failure of the others and $P[\text{Tile failure}|IM]_{C_p}$ *identically distributed* on whole roof covering system (i.e., the same for each roof tile), has been defined a binomial distribution in order to assess the conditional probability (to IM) of k roof tile failures:

$$P[\text{No. failure} = k|IM]_{C_p} = \binom{n}{k} \cdot P[\text{Tile failure}|IM]_{C_p}^k \cdot (1 - P[\text{Tile failure}|IM]_{C_p})^{n-k} \quad (6.10)$$

where $n = 1152$ is the total number of roof tiles.

In order to provide a validation of the previous assumptions, a comparison was made with Zhang et al. results in terms of the expected value of roof tiles failures percentages (Figure 6.6), knowing the expected value of

the binomial distribution:

$$E[\% \text{ failure} | IM]_{C_p} = \frac{E[\text{No. failure} | IM]_{C_p}}{n} \cdot 100 = P[\text{Tile failure} | IM]_{C_p} \cdot 100 \quad (6.11)$$

However, Figure 6.6 shows result for different conditions in terms of *spatial densities* of buildings, C_A , and wind direction, *normal-to-ridge* (5) or *parallel-to-ridge* (1). Additionally, not all tiles are subject to the same external pressure coefficient as shown by their cumulative number in Figure 6.7 (parallel-to-ridge wind direction). This figure shows a great variability of C_p for $C_A = 0.1$. This variability decreases for growing C_A and, for $C_A = 0.6$, it results very small. For this reason, assuming on the whole roof covering an uniform C_p distribution equal to -0.25 , the only consistent comparison of results provided by Equation 6.11 is with the expected percentage of failed roof tiles for $C_A = 0.6$ and the wind direction parallel-to-ridge. The good agreement between the results is shown in Figure 6.8.

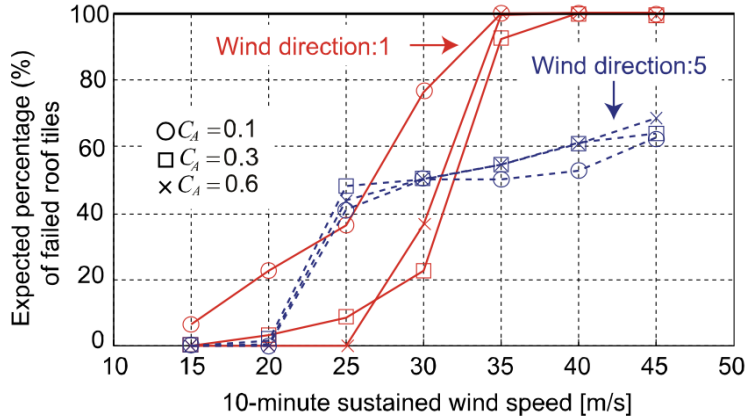


Figure 6.6: Expected percentage of failed roof tiles for different values of wind direction and spatial density of buildings (adapted from [102]).

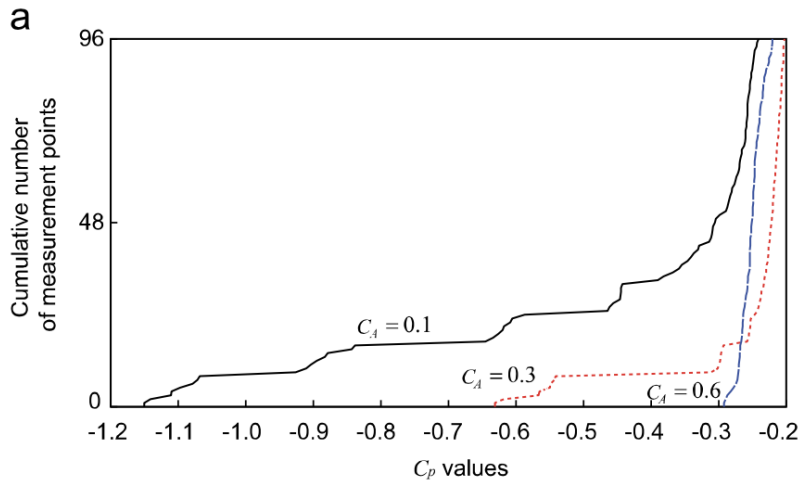


Figure 6.7: Cumulative number of measurement points as function of external pressure coefficient for parallel-to-ridge wind direction (adapted from [102]).

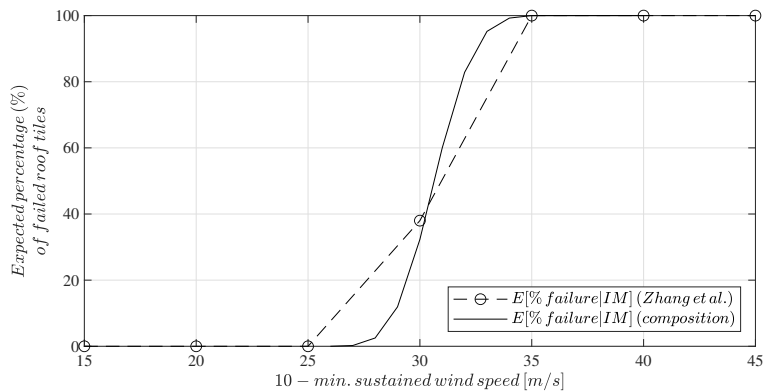


Figure 6.8: Result comparison ($C_A = 0.6$, $C_p = -0.25$ and parallel-to-ridge wind direction).

As stated before, the assumption of a uniform C_p distribution equal to -0.25 for a different C_A (e.g., 0.3) is more weak, as shown in Figure 6.9.

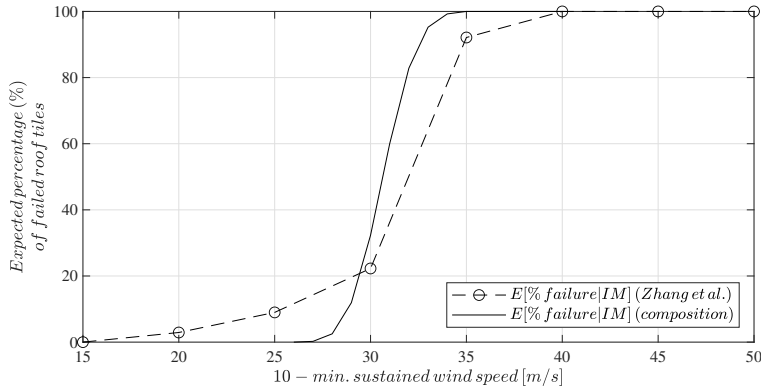


Figure 6.9: Result comparison ($C_A = 0.3$, $C_p = -0.25$ and parallel-to-ridge wind direction).

Given the observed agreement between the previous results, for $C_p = -0.25$, $C_A = 0.1$, and parallel-to-ridge wind direction, the author developed ad-hoc HAZUS-compatible roof covering (RC) fragility curves (Figure 6.10), according to the binomial distribution in Equation 6.10 and the damage matrix limits provided by HAZUS for residential buildings (Figure 6.1):

$$P[EDP_{RC} \geq 1|IM] = P[\text{No. failure} > 23|IM] = \sum_{k=24}^{1152} \binom{1152}{k} \cdot P[\text{Tile failure}|IM]_{C_p}^k \cdot (1 - P[\text{Tile failure}|IM]_{C_p})^{1152-k} \quad (6.12)$$

$$\begin{aligned}
P[EDP_{RC} \geq 2|IM] &= P[\text{No. failure} > 172|IM] = \\
&= \sum_{k=173}^{1152} \binom{1152}{k} \cdot P[\text{Tile failure}|IM]_{C_p}^k \cdot (1 - P[\text{Tile failure}|IM]_{C_p})^{1152-k}
\end{aligned} \tag{6.13}$$

$$\begin{aligned}
P[EDP_{RC} \geq 3|IM] &= P[\text{No. failure} > 576|IM] = \\
&= \sum_{k=577}^{1152} \binom{1152}{k} \cdot P[\text{Tile failure}|IM]_{C_p}^k \cdot (1 - P[\text{Tile failure}|IM]_{C_p})^{1152-k}
\end{aligned} \tag{6.14}$$

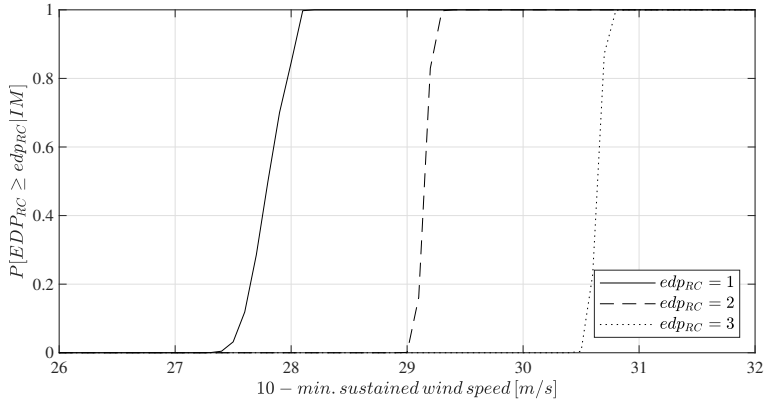


Figure 6.10: HAZUS-compatible roof covering fragility curves from composition approach ($C_p = -0.25$, $C_A = 0.1$, and parallel-to-ridge wind direction).

6.3 Damage matrix

The fragility composition approach discussed in the previous sections assumes the availability of a damage matrix to link a combination of main component damage states to the building ones.

Nowadays, the most comprehensive collection of different building damage matrices in extreme wind condition is provided by the FEMA's HAZUS-MH Program [90, 91, 18]. This condition is confirmed by several authors using nowadays such matrices (e.g., [2, 4]) and thus supporting a trend to keep them as globally accepted benchmarks.

However, in some cases, some literature studies have developed fragilities using slightly different definitions of damage states (e.g., a different percentage of total failure of a component) or addressing parts of buildings for which a damage matrix has not been specifically developed, as in the case of single element fragility. Although the latter case was addressed to some extent in Section 6.2, developing ad-hoc component fragility curves from the ones of their elements, the former has been addressed by the author proposing a slightly modification of some *HAZUS damage state (HDS)* definitions introducing the *Hazus-Based Damage States (HBDS)*. The next section discusses an example case of such a modification.

6.3.1 Hazus-based damage matrix

Lee and Rosowsky (*L&R*), in 2005, studied the uplift of roof sheathing (*RSh*) for five wood-frame buildings [55] by numerical simulations. The authors analyzed different configurations of these typical US single-family structures and carried on a study on log-normal complementary fragility curves (Equation 6.15) for four different roof sheathing damage states $EDP_{RSh,L\&R}$ (Figure 6.11): no damage ($edp_{RSh,L\&R} = 1$) i.e. no failure of sheathing panel, no more than one sheathing panel failure ($edp_{RSh,L\&R} = 2$), between one and 10% of total number of sheathing panels failure ($edp_{RSh,L\&R} = 3$) and between 10% and 25% ($edp_{RSh,L\&R} = 4$).

$$P[EDP_{RSh,L\&R} \leq i | IM] = 1 - \Phi \left[\frac{\ln(IM) - \eta_i}{\beta_i} \right] \quad (6.15)$$

with i the considered $i - th$ damage state.

According to the previous equation, for each damage state $edp_{RSh,L\&R}$

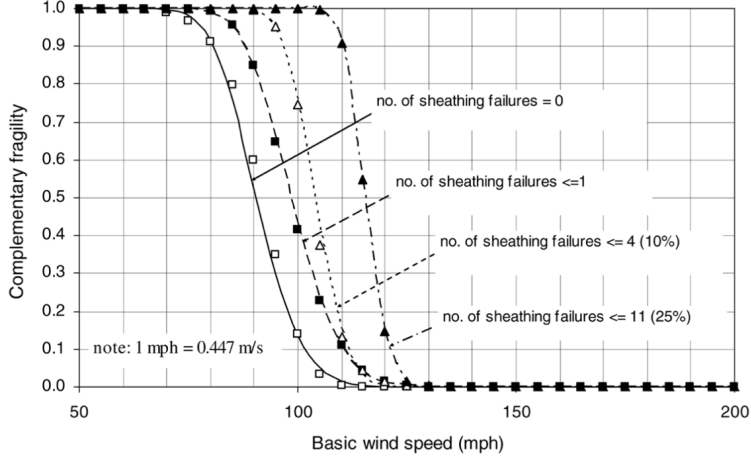


Figure 6.11: Complementary fragility curves for structure type 2, exposure C and 8d nail (adapted from [55]).

it results:

$$\begin{aligned}
 P[No. failure = 0|IM] &= \\
 1 - \Phi\left[\frac{\ln(IM) - \eta_1}{\beta_1}\right] &= 1 - P[No. failure \geq 1|IM] \implies \\
 \Phi\left[\frac{\ln(IM) - \eta_1}{\beta_1}\right] &= P[No. failure \geq 1|IM] \quad (6.16)
 \end{aligned}$$

$$\begin{aligned}
 P[No. failure \leq 1|IM] &= \\
 1 - \Phi\left[\frac{\ln(IM) - \eta_2}{\beta_2}\right] &= 1 - P[No. failure > 1|IM] \implies \\
 \Phi\left[\frac{\ln(IM) - \eta_2}{\beta_2}\right] &= P[No. failure > 1|IM] \quad (6.17)
 \end{aligned}$$

$$\begin{aligned}
P[\% \text{ of failure} \leq 10\% | IM] &= \\
1 - \Phi \left[\frac{\ln(IM) - \eta_3}{\beta_3} \right] &= 1 - P[\% \text{ of failure} > 10\% | IM] \implies \\
\Phi \left[\frac{\ln(IM) - \eta_3}{\beta_3} \right] &= P[\% \text{ of failure} > 10\% | IM] \quad (6.18)
\end{aligned}$$

$$\begin{aligned}
P[\% \text{ of failure} \leq 25\% | IM] &= \\
1 - \Phi \left[\frac{\ln(IM) - \eta_4}{\beta_4} \right] &= 1 - P[\% \text{ of failure} > 25\% | IM] \implies \\
\Phi \left[\frac{\ln(IM) - \eta_4}{\beta_4} \right] &= P[\% \text{ of failure} > 25\% | IM] \quad (6.19)
\end{aligned}$$

with *No. failure* the number of sheathing panel failures and *% of failure* the percentage of failure of the whole roof sheathing component.

In a similar way, for the residential construction class, HAZUS (*H*) [18] defines fragility curves (Figure 6.12) for four damage states of roof sheathing (i.e., roof deck), $edp_{RSh,H}$: no damage ($edp_{RSh,H} = 0$), between 1 and 3 sheathing panel failures ($edp_{RSh,H} = 1$), between 4 and 25% (of total number) of roof sheathing panels failed ($edp_{RSh,H} = 2$) and greater than 25% ($edp_{RSh,H} = 3$).

Applying these definitions to the building analysed by Lee and Rosowsky, it descends:

$$P[EDP_{RSh,H} \geq 1 | IM] \equiv P[No. \text{ failure} \geq 1 | IM] \quad (6.20)$$

$$P[EDP_{RSh,H} \geq 2 | IM] \equiv P[No. \text{ failure} > 3 | IM] \quad (6.21)$$

$$P[EDP_{RSh,H} \geq 3 | IM] \equiv P[\% \text{ of failure} > 25\% | IM] \quad (6.22)$$

Watching at the previous equations, in some cases, a direct correspondence between the damage states defined by Lee and Rosowsky and HAZUS rises: Equation 6.16 and 6.19, and Equation 6.20 and 6.22, respectively. On

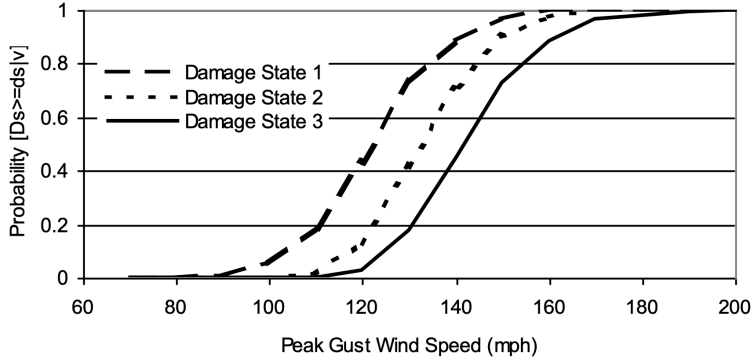


Figure 6.12: Roof sheathing fragility curves for residential building (one Story, 6d roof sheathing nails, strapped roof trusses, gable roof, no garage, unreinforced masonry walls, $z_0 = 0.03$ m - adapted from [18]).

the other hand, it is not possible to associate to the damage state definition in the log-normal cumulative fragility curve of Equation 6.17, a corresponding HDS. However, it is possible for Equation 6.18 and the second HDS, under the assumption of 10% of roof sheathing equal to 3. This is the case of type 1, 4, and 5 structures for Lee e Rosowsky (see Section A.2.2 for details) while in the case of type 2 and 3 structures it results:

$$\Phi \left[\frac{\ln(IM) - \eta_3}{\beta_3} \right] = P[\text{No. fail} > 4 | IM] \quad (6.23)$$

With the aim to make the composition approach more general, given the equivalence of the buildings treated by HAZUS and Lee and Rosowsky and the previous accordance between Equation 6.18 and the second HDS, the author suggests to use in the composition approach of Section 6.1, for residential building, a lower limit of the second roof sheathing damage state equal to 10% of the whole component. This defines a first slight modification to the damage states defined by HAZUS, de facto defining the previously introduced more general HAZUS-Based Damage States (HBDS).

6.3.2 Roof sheathing fragility composition

This section proposes a procedure to define roof sheathing Hazus-compatible fragility curves from single element fragility and shows their reliability by the comparison with Lee and Rosowsky results. The authors provide roof sheathing single panel fragility, $P[\text{Roof sh. failure}_{type} | IM]$ (Figure 6.13), for different *types* of panel (1 to 4 depending on location and dimension) and their relative number on the total, n_{type} (Figure 6.14).

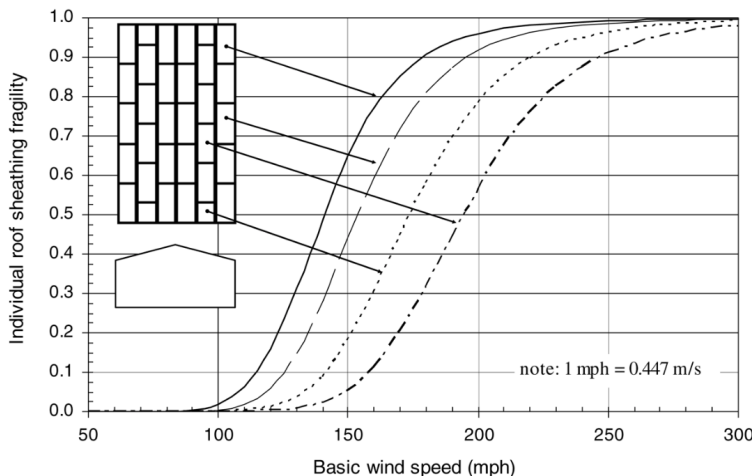


Figure 6.13: Roof sheathing panels failure probability (all directions wind; structure type 1; exposure B; 8d nails - adapted from [55])

Counting the panel failures, according to Lee and Rosowsky conservative assumption of their independence [55], fragility curve for HAZUS-

Figure 6.14: Gust pressure scheme for structure Type 1 (exposure B; 8d nails - adapted from [55]).

compatible damage state 1 (Equation 6.20) results:

$$\begin{aligned}
P[No. \text{ failure} \geq 1 | IM] &= 1 - P[No. \text{ failure} = 0 | IM] = \\
1 - (1 - P[Roof sh. \text{ failure}_1 | IM])^{n_1} \cdot (1 - P[Roof sh. \text{ failure}_2 | IM])^{n_2} \cdot \\
(1 - P[Roof sh. \text{ failure}_3 | IM])^{n_3} \cdot (1 - P[Roof sh. \text{ failure}_4 | IM])^{n_4} = \\
1 - \prod_{i=1}^4 (1 - P[Roof sh. \text{ failure}_i | IM])^{n_i} \quad (6.24)
\end{aligned}$$

Similarly, HAZUS-compatible damage state 2 (Equation 6.21):

$$\begin{aligned}
P[No. failure \geq 2 | IM] &= 1 - (P[No. failure = 0 | IM] \\
&+ P[No. failure = 1 | IM]) = 1 - \left[\prod_{i=1}^4 (1 - P[Roof sh. failure_i | IM])^{n_i} + \right. \\
&(1 - P[Roof sh. failure_1 | IM])^{n_1-1} \cdot P[Roof sh. failure_1 | IM] \cdot \\
&(1 - P[Roof sh. failure_2 | IM])^{n_2} \cdot (1 - P[Roof sh. failure_3 | IM])^{n_3} \cdot \\
&(1 - P[Roof sh. failure_4 | IM])^{n_4} + (1 - P[Roof sh. failure_1 | IM])^{n_1} \cdot \\
&(1 - P[Roof sh. failure_2 | IM])^{n_2-1} \cdot P[Roof sh. failure_2 | IM] \cdot \\
&(1 - P[Roof sh. failure_3 | IM])^{n_3} \cdot (1 - P[Roof sh. failure_4 | IM])^{n_4} + \\
&(1 - P[Roof sh. failure_1 | IM])^{n_1} \cdot (1 - P[Roof sh. failure_2 | IM])^{n_2} \cdot \\
&(1 - P[Roof sh. failure_3 | IM])^{n_3-1} \cdot P[Roof sh. failure_3 | IM] \cdot \\
&(1 - P[Roof sh. failure_4 | IM])^{n_4} + (1 - P[Roof sh. failure_1 | IM])^{n_1} \cdot \\
&(1 - P[Roof sh. failure_2 | IM])^{n_2} \cdot (1 - P[Roof sh. failure_3 | IM])^{n_3} \cdot \\
&\left. (1 - P[Roof sh. failure_4 | IM])^{n_4-1} \cdot P[Roof sh. failure_4 | IM] \right] \quad (6.25)
\end{aligned}$$

The same concept can be applied for the following damage states.

According to these fragility formulations, their comparison with Lee and Rosowsky numerical simulation results is shown in Figure 6.15. It is possible to observe a good match for the first damage state while the curve related to the second damage state shows a greater fragility compared to Lee and Rosowsky results.

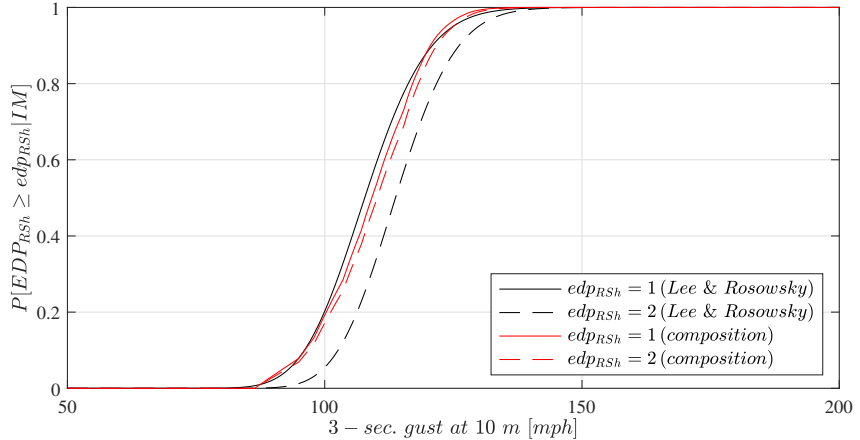


Figure 6.15: Results comparison (all directions wind; structure type 1; exposure B; 8d nails).

A justification for this discrepancy could be found in the authors definition of fragility curves according to two different scenarios for the building, depending on whether or not a first failure occurred: *partially enclose* and *enclosed*, respectively. Partially enclose condition changes the internal pressure of the building, changing the load on panels and then their fragility. Concerning the Figure 6.14 curves only the enclosed case, this justifies the accordance of results for $edp_{RSh} = 1$ and the less comparability for $edp_{RSh} = 2$ that requires the fragilities for a partially enclose condition.

In conclusion, it is possible to conclude that the presented method of composition shows a good agreement with the more complex and time-consuming numerical simulations but requires great caution in choosing the appropriate fragility for each damage state.

LOSS

In order to complete the risk analysis, it is necessary to define the distribution $G_{L|DS}[l|ds]$ of Equation 1.6 representing the measure of losses as function of the damage state of the building. The loss assessment has received much more attention from the insurance industry than the engineering community [59] that deals mainly with *direct losses*. These represent repair or replacement costs of damage, or damage to interiors, from the perspective of a physical damage to a building. One of the major contributions to direct losses in extreme wind phenomena is due to water penetration following the opening of breaches in the building envelope [58, 55]. However, a series of *indirect damages*, i.e., immaterial damages, need consideration and often represent a large contribution to the total loss. An example is provided by business interruption or the need of alternative accommodations for families whose home has been damaged.

Due to the complexity and multidisciplinary nature of the latter aspects, only direct losses are discussed in this thesis.

7.1 Building direct losses

Frequently, the losses of a building are defined through the definition of a *damage (or cost) ratio*, DR , i.e., the ratio of the direct loss suffered by the building to its (insured) value, as a function of the building damage state. Given the probabilistic nature of this parameter, it should be described through a probability distribution. However, only synthetic parameters such as the expected value are often provided, calibrated by the insurance industry on a large number of claims, e.g., Table 7.1, for five commercial building damage states (according to HAZUS definitions [18]).

Table 7.1: Example of expected damage ratios value for five commercial building damage states.

DS	Damage Ratio
0	0.00
1	0.15
2	0.25
3	0.30
4	0.45

Given the unavailability of the distribution of losses as a function of the damage state, in this case it is possible to adapt the formulation of Equation 1.6 in terms of expected values. Under the assumption of uncorrelated number of events and expected loss given the event, *the expected annual loss* results:

$$E[L] = \int_{IM} \sum_{j=1}^{n_{ds}} \sum_{m=1}^{n_{\{edp\}}} E[L|ds_j] \cdot P[DS = ds_j | \{EDP\} = \{edp\}_m] \cdot P[\{EDP\} = \{edp\}_m | im] \cdot |d\lambda_{im}| \quad (7.1)$$

Part IV

Software & Conclusion

Chapter **8**

ERMESS - ExtReMe wind risk assESSment software

The ExtReMe wind risk assESSment (prototype) Software, ERMES, is the result of a three-year research agreement (2019-2022) between the University of Naples Federico II and the insurance company AXA-XL which is specialised in the management of complex risks. This agreement falls under the thematic area of building vulnerability to wind-induced actions, as part of a framework for risk assessment against natural hazards. The principal objective is to provide a probabilistic description of potential economic losses resulting from wind-related natural hazards, with a focus on industrial facilities. This objective is pursued through the collection of as many such functions as can be found published in the scientific literature or in manuals of risk assessment practice, categorise and store them in a database along with relevant metadata and render all of this information readily available to AXA-XL through the development of an interactive standalone software; i.e., a wind version of FRAME developed for earthquakes by Petruzzelli and Iervolino in 2014 [68].

The software is developed on the MATLAB® platform [61] through the *App Designer*, an interactive development environment for designing

an app layout and programming its behaviour.

The framework of the software reflects the one of the PBWE approach presented in this thesis and its interface (Figure 8.1) clearly points out the main risk components: hazard, vulnerability, and exposure.

After the description of the software flow chart in the next section, the main modules of the software and their sub-modules will be presented in the following sections.

8.1 Flow chart

This section presents the software's logical flow in performing the risk analysis, i.e., its *flow chart*. However, as it is designed, its algorithm does not follow a one-way path and the user can, in some cases, change parameters on the run.

Figure 8.2 represents the first part of the flow chart concerning the hazard module developed according to the Part II of this thesis. The user is intuitively asked to input some site parameters of the structure. First of all, the geographical coordinates, the typology of the hazardous event under analysis (tropical cyclone or tornado), and the roughness of the terrain. The relevance of these parameters is detailed in Section 3.1. More specifically, in ERMESS these parameters are necessary to carry out specific operations such as the conversion of the intensity measures. The user is given the choice of performing or not a scenario analysis, i.e., given the occurrence of a certain intensity of the event. In this case, the user can define the intensity measure using the ERMESS's build-in hazard maps described Section 4.1, defining a certain return period for the tropical cyclone or the intensity of the phenomenon in the case of a tornado. This allows to define a hazard value. Alternatively, in case the user requires to define his own intensity measure, he is asked to define a return period for it. In the case of risk analysis (i.e., non-scenario), in the same way, the user can choose to let ERMESS define the hazard curve or define his own input. However, in the latter case, since it is necessary to define a hazard curve instead of a value, a *comma-separated values* (.csv) file is required for this operation.

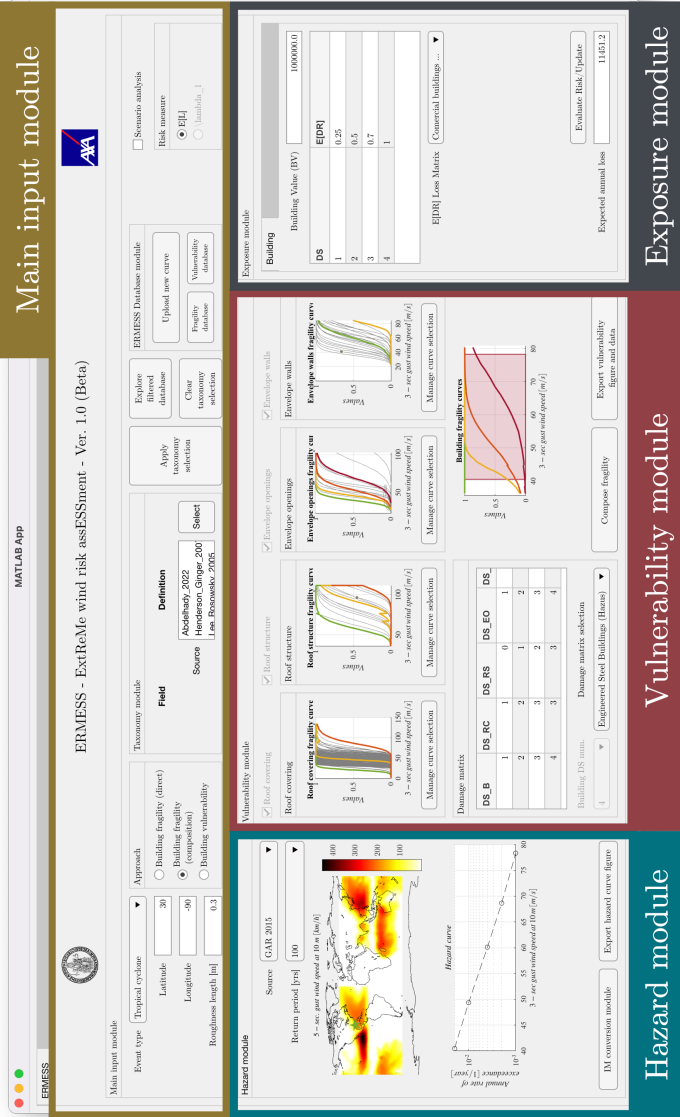


Figure 8.1: ERMESS main interface and modules.

Once the hazard is defined, the software homogenises the intensity measurements to the reference value of 3 second wind speed at 10 m, if necessary. A conversion sub-module of the intensity measures is therefore integrated into the hazard module according to the procedures described in Section 3.4.

Figure 8.3 collects the second part of the flow chart related to the vulnerability and exposure modules according to Part III of this thesis. Once the hazard is defined, the user is offered the possibility to follow three approaches for vulnerability assessment: a direct definition of the building vulnerability, the direct definition of its fragility, or the composition of the latter through the fragilities of its main components. In the first two cases, the user is offered the possibility of direct selection from the ERMESST database of the vulnerability or fragility curves (Appendix A) of the building or of direct input of their own curves (.csv). In the case of the composition approach, the user is asked to define/select a damage matrix and the subsequent definition of the relative fragility curves of the main components, according to Section 6. Also in this case, the user is given the possibility to choose these curves from the database or to define them manually through .csv files.

Finally, the exposure module, given the building fragility curves, defines the losses of the structure through appropriate consequence functions. Once the hazard and vulnerability of the structure have been defined, through their integration, it is possible to reach the definition of the selected risk measure between λ_l or $E[L]$, according to Equation 1.6 or 7.1, respectively.

8.2 Hazard module

The *hazard module* is located on the left side of the ERMESST main interface (Figure 8.1). This module (Figure 8.4,a) shows an input section in the upper half and an output section in the lower part. The first input that the user provides for the risk analysis is the type of event considered. In fact, as described by Section II, the characteristics of extreme wind phenomena

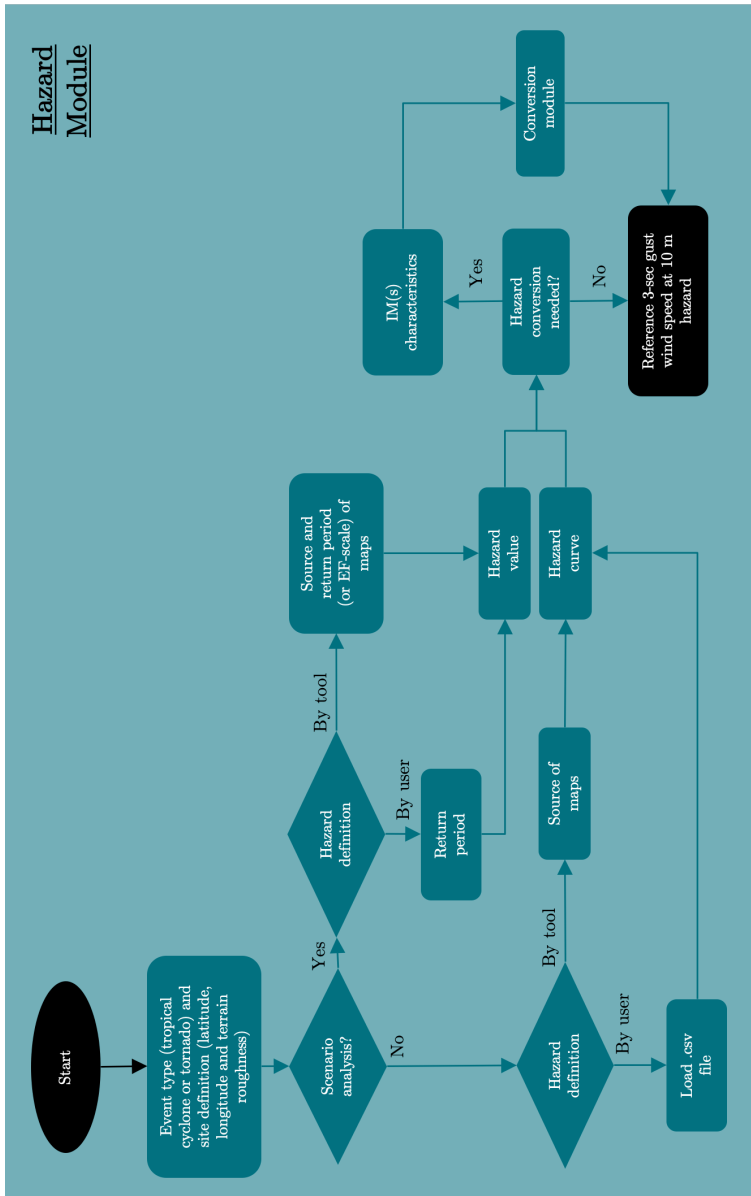


Figure 8.2: Hazard module flow chart.

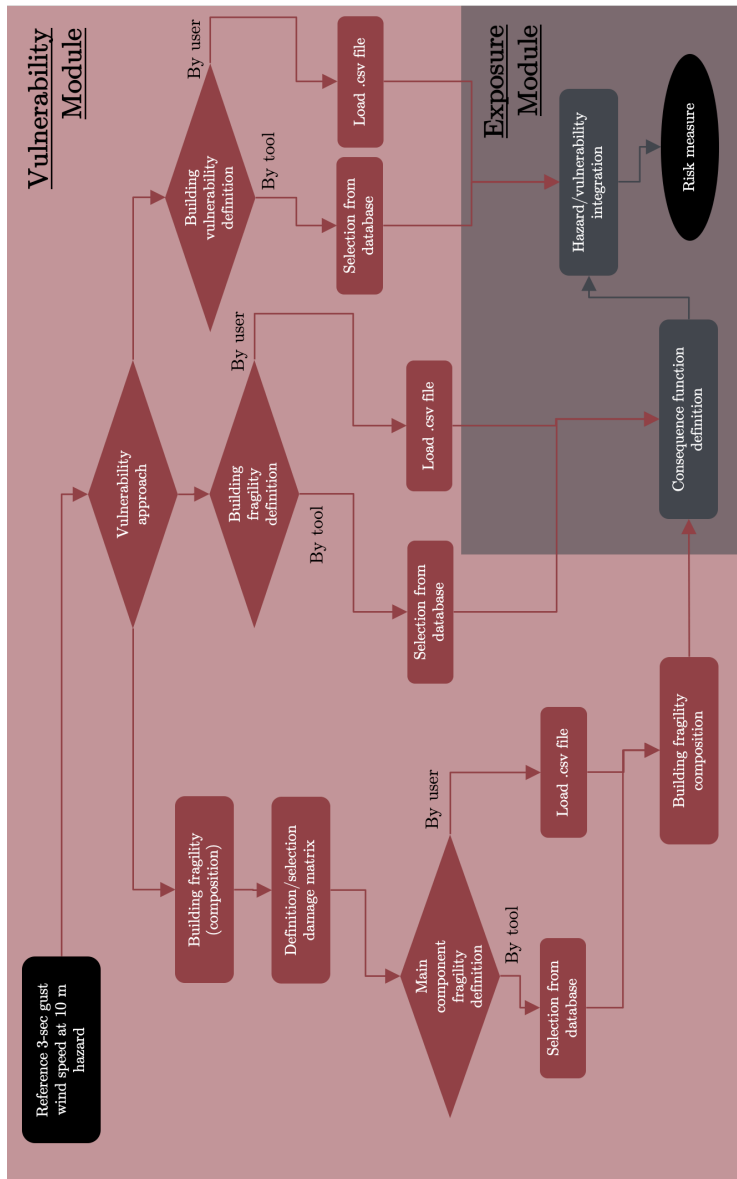


Figure 8.3: Vulnerability and exposure modules flow chart.

usually differ and should be treated differently. In ERMESS only two types of hazardous events are handled given the lack of freely available maps for other wind phenomena: tropical cyclones and tornadoes (Figure 8.4,b). However, ERMESS is able to integrate additional maps once they become available.

The remaining inputs concern the geographic coordinates of the site and the roughness of the terrain. The geographic coordinates identify the site as a green star on the hazard map (related to the return period selected) in the centre of the panel.

In case the analysis is developed for tropical cyclones, in addition to being able to enter his own hazard values (Figure 8.4,c), to the user is offered the possibility to use the GAR built-in hazard maps (Section 4.1.1). Since the maps implemented in ERMESS for tropical cyclone conditions concern 5 return periods (from 50 to 1000 years - Figure 8.4,d), it is possible to build the hazard curve for the site on the bottom of the hazard module.

In the same way, if the user chooses to develop a risk analysis for tornadoes, in addition to his own input, he is offered the possibility to use the built-in hazard curve developed by the fitting of the hazard values provided for US by Standohar-Alfano and van de Lindt (Section 4.1.2) for the six intensities EF0-EF5 (Figure 8.4,e).

As anticipated in the previous section, the user is also able of performing scenario analysis. By checking the appropriate box, to the user is highlighted the IM value for the selected map (Figure 8.4,f) or is allowed to enter his own value. In the latter case (as well as in the case of own input of the hazard curve) the value need to be expressed in the intensity measure terms considered as a reference for ERMESS, i.e., 3-sec gust wind speed at 10 m.

Since the GAR built-in maps express the IM in terms of 5-sec gust wind speed at 10 m, a conversion has become necessary and an ad-hoc sub module has been developed in ERMESS (Figure 8.4,g). This *IM conversion sub module* is accessible at the bottom of the hazard module and shows inputs and outputs of the conversion, in addition to the approach followed between the ones described in Section 3.4.1 and 3.4.2. Since this conversion makes use of the input parameters of geographic location and terrain roughness,

this clarifies their necessary a-priori definition in the module.

In conclusion, the output of this module is the hazard curve or the hazard value used by ERMES in the following risk or scenario analysis, respectively.

8.3 Vulnerability module

The *vulnerability module* is located in the central part of the ERMES main interface (Figure 8.1). The upper left corner of the central input section is dedicated to the choice of the approach to follow in the assessment of vulnerability, which can be of three different types. The first way involves the direct definition of the fragility of the building, the second the composition of this fragility through the ones of its main components, and the third concerns the definition of the vulnerability of the building. In Figure 8.5,a is shown the second most complex case. In the remaining cases the module is reduced to a single figure panel.

In the main input module central part is the *taxonomy sub module* of ERMES that allows the selection of the database curves of interest, according to the taxonomy developed by the author and discussed in Section A.1. According to the chosen vulnerability approach and the building characteristics for which the risk analysis is developed, the selection of the database occurs. This selection can then be applied, managed, and visualised through dedicated buttons on the right.

The vulnerability module, according to the fragility composition approach discussed in Section 6.1, shows the damage matrix and the four fragility curve selection panels for the building (B) main components: roof covering (RC), roof structure (RC), envelope openings (EO) and envelope walls (EW).

Once the damage matrix is selected among those ERMES built-in or defined ad-hoc, on the basis of the number of the main components damage states (less than or equal to 4), the definition and management of their fragility curves is allowed,. In fact, through the dedicated button it is possible to open the *component fragility sub module* (Figure 8.5,b).

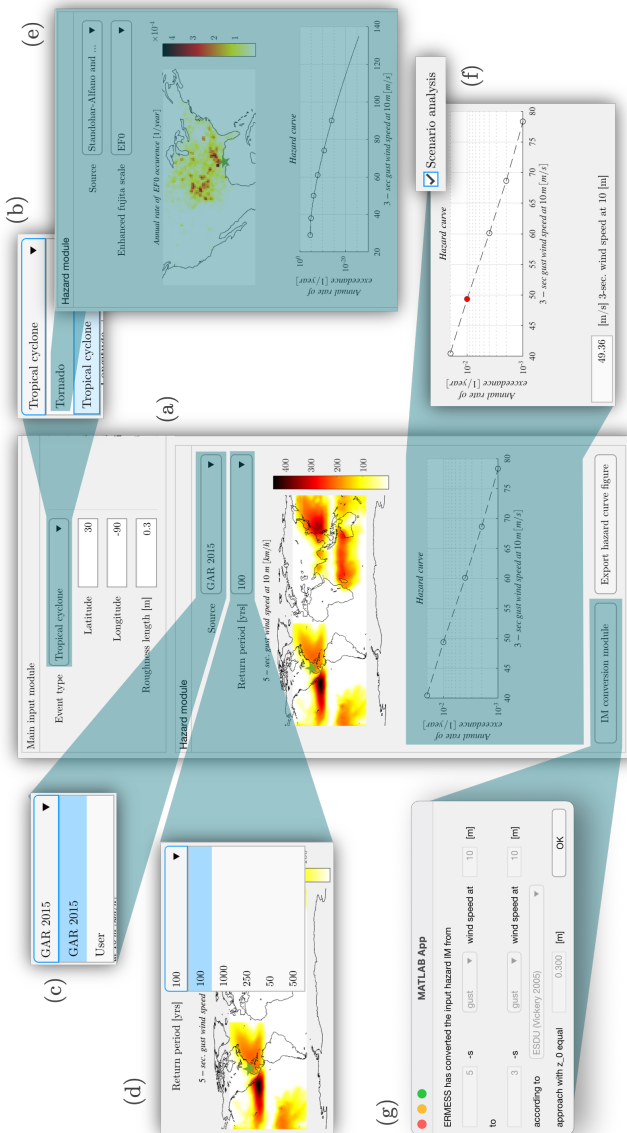


Figure 8.4: Hazard module interface.

This sub module presents on the left a panel for the definition of the fragility curve related to each damage state defined by the damage matrix. On the right, an overview panel offers a synthesis of the selected curves; the green curve refers to the first damage state, the yellow curve to the second, the orange curve to the third, and the red curve to the fourth. The user is offered the possibility to choose these curves among the database or to load own curves (.csv). In the first case, a sub taxonomy panel helps the user in the curve selection from the database, showing only the taxonomy items related to the selected main component. A drop menu allows the selection of a synthetic curve (e.g., mean or median) or a specific one (Tag).

Once fragility curves for each main component are defined, they are displayed on the main panel of ERMES and it is therefore possible, through the dedicated button, to *Compose fragility* of the building (see Section 6.1 for details). This fragility panel also shows the IM range (in red) for which the hazard curve has been defined. (In the case of scenario analysis, this area is limited to a solid line.)

8.4 Loss module

Once the building fragility curves are known, the risk measures can be defined in the exposure panel, given appropriate consequence functions. The ERMES *exposure module* is located to the right of its main interface. In the input area (Figure 8.6,a - top), it provides the definition of the type of analysis (scenario or not) and of the risk measure. The latter can be chosen between the expected annual loss $E[L]$ according to Equation 7.1 or the exceedance rate of losses λ_l of Equation 1.6.

(To date, given the lack of reliable $G_{L|DS}(l|ds)$ distributions related to building damage states to wind, in ERMES is implemented only the expected annual losses $E[L]$ computation. The calculation of λ_l is part of the next future development of ERMES.)

Expressing consequence functions in terms of damage ratios (DR), a drop menu enables the definition of their most appropriate values (between the ERMES built-in ones) for each damage state (Figure 8.6,b). According

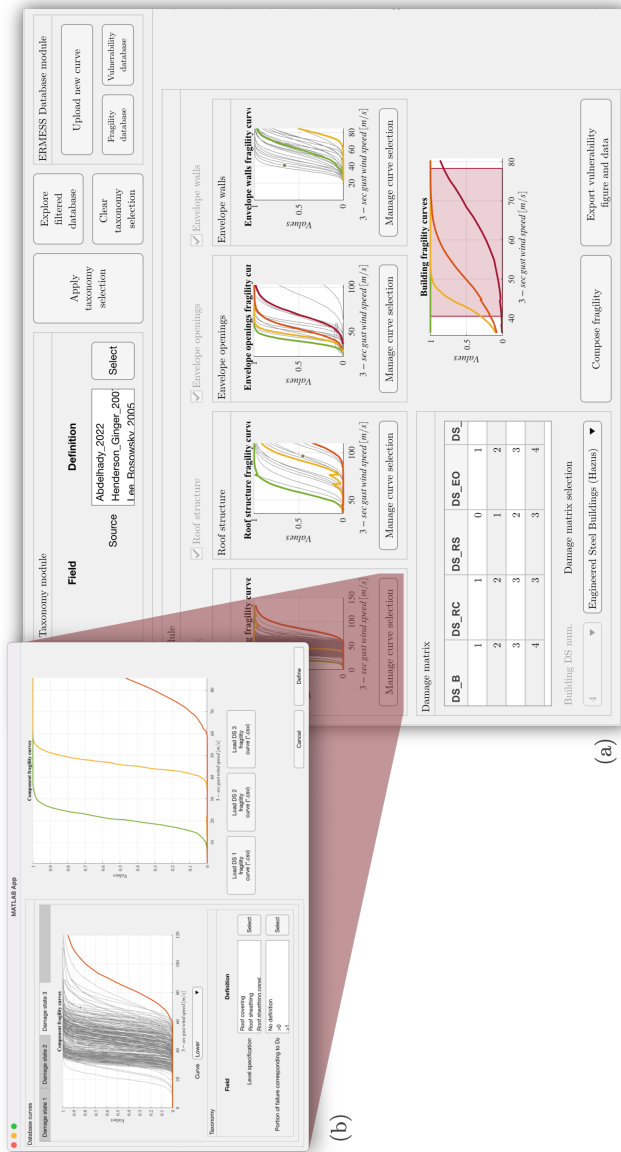


Figure 8.5: Vulnerability module interface.

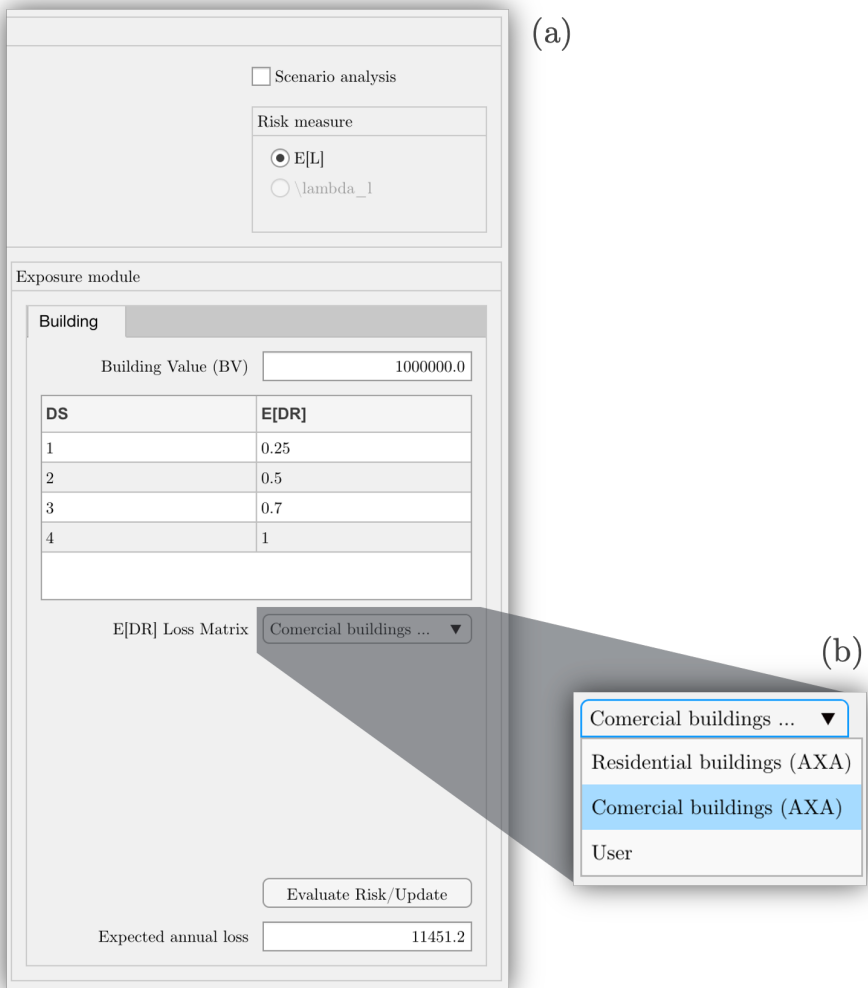


Figure 8.6: Exposure module interface.

to Equation 7.1, expected annual damage ratio value is calculated through the following formulation:

$$E[DR] = \int_{IM} \sum_{j=1}^{n_{ds}} \sum_{m=1}^{n_{\{edp\}}} E[DR|ds_j] \cdot P[DS = ds_j | \{EDP\} = \{edp\}_m].$$

$$P[\{EDP\} = \{edp\}_m | im] \cdot |d\lambda_{im}| \quad (8.1)$$

In order to express the building loss in appropriate monetary terms, ERMESS implements the opportunity to define its generic value, *Building Value (BV)*, before the evaluation of the expected annual loss as:

$$E[L] = BV \cdot E[DR] \quad (8.2)$$

Chapter **9**

Final remarks

This concluding segment outlines the results of this doctoral study and discusses potential future developments. The present thesis, after an extensive and in-depth study of the available literature, proposes a PBWE-oriented methodology for risk assessment of structures to extreme winds. This approach, although containing some simplifying assumptions, allows to account for parameters that are recognised in the literature as fundamental, such as the interaction between the most vulnerable building components to extreme winds. Furthermore, the framework on which the method is based, is flexible enough to allow for additional relevant features to be accounted for in the risk analysis.

More specifically, this simplified probabilistic approach proposes the composition of building fragility from component fragilities available from the literature. This may also entail combining single-element fragility models into new component fragilities. Some illustrative examples of this methodologies have also been developed and presented in this thesis. One such example has shown the feasibility building fragility composition, using the fragilities of five main components, provided that an appropriate damage matrix can be defined. Another example illustrates the development of building component fragility using fragility models of a single elements,

such as a roof tile.

These preliminary validation attempts of this methodology have shown promising agreement with the results obtained via more accurate, yet complex and time-consuming, methods. However, the applicability of this methodology hinges on the availability and quality of the input component fragility. For this reason, effort has been dedicated to collect as many of them as possible from the literature but also from sources outside the academic community. As a result, a wide database has been compiled, containing a large number of fragility and vulnerability functions.

Putting together this database required an extensive preliminary study into existing approaches for the definition of vulnerability functions with the purpose of categorising them. Special attention was given to the intensity measure of interest in wind engineering, that is wind speed. In fact, the details of its multiple possible definitions and the methods of conversion from one to another are crucial for compiling a homogeneous database.

For this reason, details pertaining to wind speed definition and other relevant parameters also had an impact on the definition of an ad-hoc taxonomy that was developed to categorise the large number of collected fragility and vulnerability functions. This taxonomy, in addition to allowing a great level of detail to the database, collects all those parameters deemed as essential in the response of structures to extreme winds and necessary for the development of the fragility composition methods.

As a culmination of this research, the author implemented these procedures into a software tool for the risk assessment of structures in extreme wind conditions: ExtReMe wind risk assESment Software, ERMES. This tool, commissioned by the insurance company AXA-XL, allows the rapid probabilistic assessment of this type of risk.

This tool contains the aforementioned database as an in-built feature and implements the method for fragility composition from those of the building components. The potential of this tool lies in its applicability to any site or building, while maintaining simplicity in the risk analysis. The main advantage of ERMES is its ability to compute, in a simplified and expedient manner, wind fragility curves for buildings for which no specific study exists, without the use of sophisticated and time-consuming methods.

This work constitutes a starting point for the development of a more comprehensive framework for risk assessment of structures exposed to extreme winds. Actually, the framework is based on assumptions that need to be further validated on a case-by-case basis, e.g., the conditional stochastic independence between different components of the structure reaching specific damage states. Moreover, further upgrades can include the implementation of procedures accounting for other wind-related phenomena that can influence the risk assessment, such as the issue of airborne debris. Furthermore, recent years have seen a growing interest in wind phenomena other than tropical cyclones and tornadoes, such as downbursts and local winds, which points the way for another possible extension of this risk computation framework into a wider set of wind-related natural hazards.

Appendices

Appendix A

Database

The purpose of this appendix is to describe the fragility and vulnerability curve database compiled by the author and the related taxonomy. The importance of an adequately large database and its applications have been discussed extensively in the previous chapters.

The database has been developed on a MATLAB® [61] *structure*, a data type whose *fields* are defined as *taxonomy items*. These items represent the entries of the taxonomy developed by the author, based on the study of relevant extreme wind risk analysis literature, and will be discussed in the next section. The remaining part of this appendix reviews the studies whose results are collected into the first version of the database and defines their taxonomy entries, divided into fragility or vulnerability functions for buildings, components, or elements.

The database implemented in ERMESS does not include all entries presented in this appendix, primarily because the conversion of intensity or loss measures to the reference values has not been possible in all cases. In addition, the ERMESS database integrates fragility curves from a recent study by Ascolese "Analisi di rischio da vento estremo per portafogli di edifici, basata su fragilità di componenti" [8]. In this master's degree thesis, the author provides the parameters of log-normal distribution fits of about

4500 digitized building and component fragility curves from the FEMA HAZUS–MH 2.1 Technical Manual [18].

A.1 Taxonomy

In this section the previously introduced taxonomy entries are described for each curve (or function) collected for the database. These items are grouped in the following macro-areas:

- Source
- Site
- Building
- Damage state
- Roof
- Roof covering
- Envelope wall
- Envelope openings
- Curve measures
- Other

The *source* macro-area collects the taxonomy items judged as necessary to identify the study from which the fragility or vulnerability curves have been extracted and some key features. Then, the first taxonomic item, **source**, concerns a tag composed according to an Author(s)_Year scheme (e.g., Henderson_Ginger_2007 or Li_Ellingwood_2006). The following items define the **year** of the study publication and the **region** of interest. Both these characteristics have been considered relevant to the classification of curves since analysis techniques differ between nations and evolve over time.

Therefore, in the author's opinion, it is important to set the curves in a spatial and temporal location. Furthermore, given the different features of the extreme wind phenomena, it was considered necessary to link each curve to the type of event for which it has been developed (e.g., a tropical cyclone or tornado) through the definition of the taxonomic entry **event type**. Finally, the last item in this macro-area area concerns the **approach** followed for the development of the curve according to the classification presented in Section 5.1: past-loss data, heuristic and engineering based.

The second taxonomy macro-area, *site*, concerns the parameters that most influence the local wind field and the loads on structures. The **wind pressure model** entry defines the employed model for conversion of wind speed into pressure on structures (e.g., the ASCE Standard 7-02 [7] or the Tokyo Polytechnic University aerodynamic database [85]). Also the contribution of wind **direction** and **terrain roughness** parameters are known to affect the definition of the local wind field and loads on the structure, as described in Chapter 3. Since the terrain roughness is not usually defined as a number and it is categorised differently between national standards and codes worldwide, the following items concern the definition of a **terrain category** and its **reference code**. However, since some codes do not actually define a terrain feature but rather a level of site exposure, **surrounding conditions**, **exposure**, and its **reference code** are additional items needed for the definition of the wind field (but also for the issue of wind-borne debris).

After the site characteristics have been defined, it is possible to move on to those of the *building*. **Date of building construction** and **reference building code** represent items that have the aim to link the building to a specific date and design technique, respectively (e.g., PCI design manual of 1971 or Queensland Home building code of 1981). The following items define some rough characteristics of the building: **technology** (e.g., high-, mid- or low-rise wood-frame or masonry), **type of use** (e.g., residential or commercial), **geometry**, and **number of stories**. Then, two taxonomy items are dedicated to the **enclosure classification** and its **criteria**. Modern standards classify the actions on the structure following the definition of this parameter since openings are widely accepted as a key parameter in

the definition of building internal pressure. Finally, the **curve (or data) level** entry defines the vulnerability or fragility curve first detail level between whole building, building component, or building component element, while **level specification** defines a second (e.g., roof tile, roof sheathing, or envelope opening).

In order to employ the database for risk assessment via the fragility composition approach described in Chapter 6 of this thesis, the following entries define, where possible, the **amount of damage corresponding to the Hazus-based damage state (HBDS)**, the **corresponding HBDS** and, in the case of components and elements, the **HBDS corresponding to the building or the component**, respectively. In this way it is possible to categorise the fragility curves according to the HAZUS-based damage state approach.

After the *damage state* macro area, the next ones concern the taxonomic entries required to describe the characteristics of the main components of a structure's envelope.

The most vulnerable component in the wind risk analysis of structures is the *roof* and for this reason great attention is dedicated to its taxonomy. The **typology of roof** provides a first level information (e.g., hip or gable roof) together with its **technology** (e.g., wood-frame). Then additional items allow to go more deeper into the detail level through the definition of the **slope**, the presence or not of **overhangs**, the **height together with its definition** and the **roof-to-wall connections**. This information can be importany for the definition of the response of the structure to wind loads and their modifications result in a great difference in the roof but also whole building capacity, as shown by a wide number of studies focused only on this component.

Roof covering macro area defines the characteristics of this main component through the definition of its **typology** (e.g., panels or tiles), **technology** (e.g., metal or wood panels), element **dimension** and **connection** (e.g., 8d or skew nails). The study of this component is essential for the roof damage definition but also for the debris analysis since the roof covering is one of its main sources.

The taxonomy entries related to the *envelope walls* are the **typology**

(e.g., unreinforced masonry) and **technology**. The details are not very extensive since it is the main component that is usually less vulnerable to extreme winds.

The same cannot be said for *envelope openings* whose failure is the main source of increasing internal pressure and then of the progressive failure of the structure. Given the possibility of failure of this component due to wind pressure but also to debris impact, an important parameter for its characterisation is the **percentage of openings** in proportion to the building envelope (the probability of debris impact increases with the size of the openings on the envelope), in addition to **typology** (e.g., glass doors or windows) and **technology** (size and thickness).

The *curve measures* macro-area refers to the intensity measure and the related vulnerability measure of each collected curve. This thesis highlighted the importance of the different features in the definition and conversion of IM. therefore the taxonomic entries provide the definition of **reference height** (e.g., 10 m), **reference time** (e.g., 3-sec or 10-min), **typology** (mean or gust) and **unit of measurement** (e.g., m/s or mph). Regarding the vulnerability measure, the items **values model** (e.g., discrete or parametric) and **values unit of measurement** (e.g., MDR or probability of exceedance a damage state) are defined.

The last taxonomic items concern the *other* characteristics considered fundamental in the risk assessment of structures. Firstly, taking into account the **debris** phenomenon in the development of fragility and vulnerability curves is essential in some situations such as residential environments. A number of different models have been developed to study this phenomenon and are collected in the taxonomic entry **debris model** (e.g., Abdelhady or Lin & Vanmarcke models). However, also the **shielding** effect of the structure, i.e., the protection provided by nearby buildings, the **damage due to water penetration** from the breaches that occur in the envelope, and the **secondary damage to people** are characteristics that some authors deem to be necessary in the definition of extreme wind vulnerability. Therfore, for each of these aspects two taxonomic entries are considered, the first describing whether or not this phenomenon has been taken into account while the second describes the employed **model**.

Finally, the last two taxonomic items refer to the management of the **uncertainties** and a numerical **tag** is assigned to each curve for its unambiguous identification into the database. For practical purposes, the database has been separated into one collecting fragility curves (*fragility database*) and one collecting vulnerability curves (*vulnerability database*).

It is worth mentioning that, since the definition of taxonomic entries has been the result of a process of synthesis of different studies, among the collected data some taxonomy items are not specified. This is due to the intrinsic difference between vulnerability and fragility curves but also to the choice of some authors not to take into account certain characteristics or, in the case of the older literature, due to lack of knowledge.

Additionally, in the previous discussion it emerged that the developed taxonomic entries cover the general characteristics of the building also when the curve refers to a single component or element and vice versa. This is due to the interaction between the components failure, i.e., the progressive damage, that is a key factor in the reliable assessment of their wind vulnerability. For example, in the analysis of the fragility of the roof or the whole building, it is important to take into account the characteristics of the openings of the envelope since their failure implies an increase in the internal pressure of the whole structure. For this reason, at each level of detail, the taxonomy entries include information on the other levels.

A.2 Fragility curves

A.2.1 Building fragility curves

Henderson and Ginger (2007), “Vulnerability model of an Australian high-set house subjected to cyclonic wind loading.” [41]

The Henderson and Ginger study analyses, in a probabilistic way, the vulnerability of typical northern Australian '60-'70 houses (Figure A.1): high-set, timber framed houses with rectangular plan, fibre cement sheet exterior wall cladding and metal roof cladding on a low to flat pitch gable end roof. The authors take into account the progressive failure.

- Source: reference tag for this study is **Henderson_Ginger_2007**.
- Year: **2007**.
- Region: **Australia**.
- Event type: **cyclone**.
- Curve typology: **fragility curves**.
- Approach: **engineering-based** approach.
- Wind pressure model: Wind loads and pressures are derived according to Australian Standard **AS/NZS 1170.2 of 2002** [81] for ultimate limit state design.
- Direction of wind: -
- Terrain roughness: -
- Terrain category: curve are presented according to **category 2** for intensity measure (flat terrain). However, analyses are carried out considering buildings located in suburban terrain of category 2.5.
- Terrain category reference code: **AS/NZS 1170.2 of 2002**.



Figure A.1: High-set house examples in Townsville (top) and Darwin (down) adapted from [56].

- Surrounding condition: -
- Exposure category: -
- Exposure category reference code: -
- Date of building construction or retrofit: **1960-1970**.
- Reference building code: the considered building reference code is the **Queensland Home Building Code of 1981** [31].
- Structure technology: **high-set wood-framed** house elevated on piers about 2 m high, with internal lining of either hardboard or plasterboard. Some frame layout details are shown in Figure A.2.

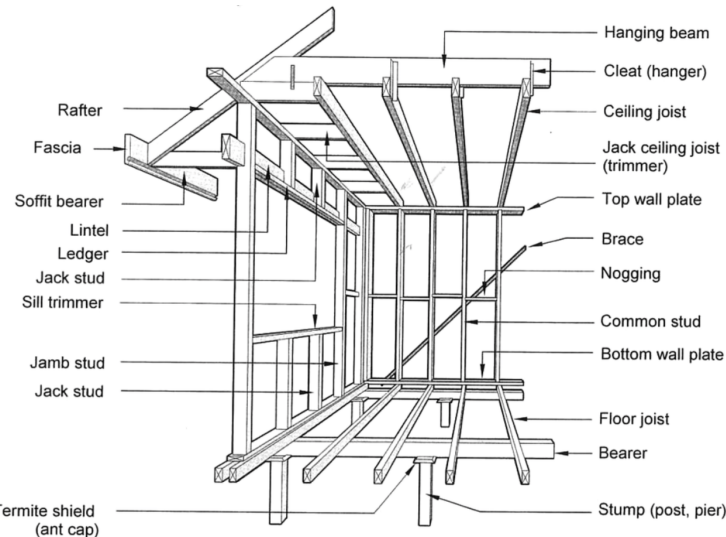


Figure A.2: High-set house frame layout details (adapted from [41]).

- Type of use: **residential**.
- Geometry in plan: 12-14 x 8 [m] **rectangular** plan .

- Number of storey: **1-2 storeys.**
- Enclosure classification: a dominant opening on the envelope is considered on 0% to 90% of building population for gust wind speed ranging between 40 [m/s] to 80 [m/s].
- Criteria for enclosure classification: damage **surveys**.
- Curve or data level: results are presented for both **whole building** and **building components**.
- Level specification: different connections failures are aggregated into failure modes of 4 sub-structure classes to consider their interaction (Figure A.3). Sub-structure classes are: **roof envelope (roof covering), roof structure, envelope wall structure, envelope wall cladding** and subfloor bracing support of piers (**foundation**). Fragility curves of sub-structure (Figure A.4) consider the independence between their failure mode while overall results (Figure A.5) (percentage of failed buildings) consider the failure tree scheme presented in Figure A.6. Curves in Figure A.5 have been loaded into the database as whole building fragility curves.

Sub-structure class	Failure mode
A Roof envelope	Cladding pulling over fastener or Cladding fastener pulling out of batten or Batten joint failing at Rafter
B Roof structure	Rafter joint failing at ridge or Rafter joint failing at top plate which also includes graded purlin construction.
C Wall structure	Wall racking failure from bracing component failure or wall collapse following loss of support from failure of roof structure
D Subfloor bracing support of piers	Subfloor bracing failure which does not consider footing failure or overturning.

Figure A.3: Failure modes (adapted from [41]).

- Amount of damage corresponding to Damage State DS: -
- Corresponding Hazus-type Damage State (HDS): -

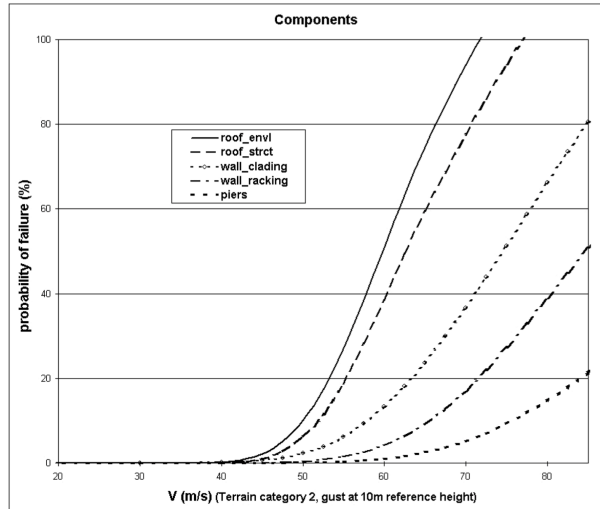


Figure A.4: Estimated probability of failure of components in the modeled houses (adapted from [41]).

- Corresponding HDS upper level: -
- Roof typology: gable roof.
- Roof technology: wood-frame with 100×50 [mm] rafters, 900 [mm] spaced, skew nailed to the wall top plate. 75×50 [mm] collar ties on every second rafter pair, and 100×50 [mm] ceiling joists adjacent to the rafters (Figure A.7). Cyclone rods are present in perimeter walls.
- Roof slope: relatively low or flat roof.
- Roof overhang: yes.
- Roof height definition: -
- Roof height: -
- Roof-to-wall connection: skew nails.

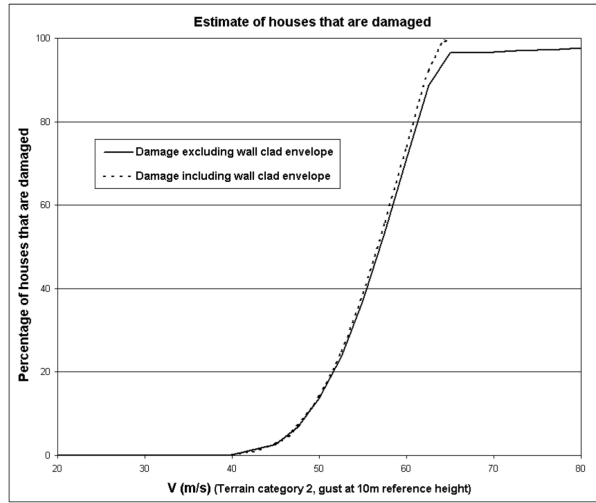


Figure A.5: Estimated percentage houses damaged with increasing wind speed (adapted from [41]).

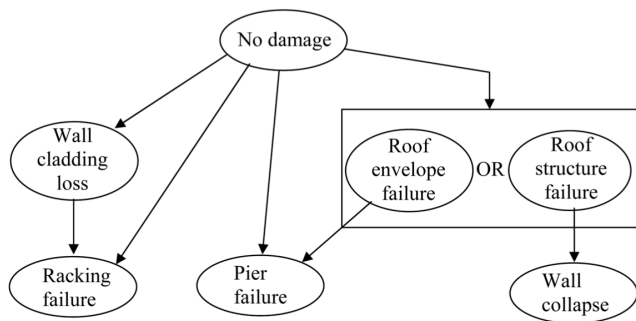


Figure A.6: Tree diagram of failure modes and propagation paths (adapted from [41]).

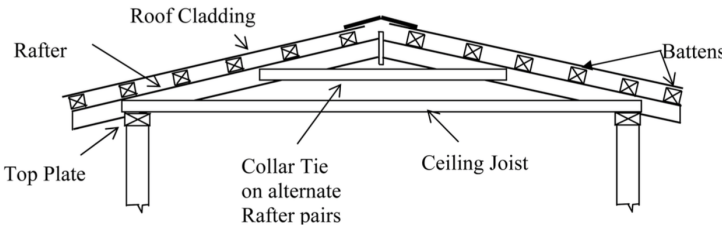


Figure A.7: High-set house roof details (adapted from [41]).

- Covering typology: **roof sheeting panels**.
- Covering technology: **metal panel** screw fixed, at spacings of up to 300 [mm], to timber battens spaced at nominally 900 [mm] apart.
- Covering size: -
- Covering connection: **skew nails**.
- Envelope walls typology: **wall framing** consists of 100 × 50 [mm] studs between top and bottom plates, 450 [mm] spaced with nogging at nominal mid height between the studs.
- Envelope walls technology: external walls cladding with **fibre cement or timber panels**.
- Envelope percentage of openings: -
- Openings typology: -
- Openings technology: -
- IM reference height: **10 [m]**.
- IM reference time: **3-sec.**
- IM typology: **gust**.

- IM unit of measurements: [m/s].
- Values model: **discrete values**.
- Values unit of measurements: **probability of failure** (component) or **probability of damage** (whole building).
- Debris: **take into account**.
- Debris model: -
- Shielding: -
- Shielding model: -
- Water penetration damage: -
- Water penetration damage model: -
- Secondary damage to people: -
- Secondary damage to people model: -
- Uncertainty: **take into account** for the wind action and the components strength.
- Tag: **250-256** of fragility database.

Masoomi and Lindt (2016), “Tornado fragility and risk assessment of an archetype masonry school building.” [60]

The authors of this study assess the fragility and risk of an archetype unreinforced masonry school building (Figure A.8) subject to tornado action in the United States. After pointing out today’s shortcomings in terms of design recommendations and attention to this type of event due to its low probability of occurrence, the authors develop a simulation-based complex engineering-based model. This study has two major purposes: (i) use the results to develop specific design rules and (ii) provide fragility curves for masonry school buildings. These results are presented using two different approaches for wind load definition and five different types of unreinforced masonry structure.

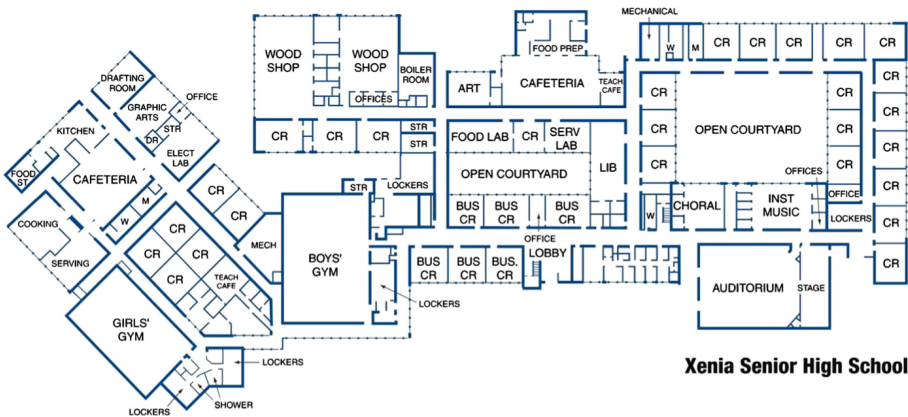


Figure A.8: The high school archetype floor plan (adapted from [60]).

- Source: reference tag for this study is **Masoomi_2016**.
- Year: **2016**.
- Region: **United States**.
- Event type: **tornado**.

- Curve typology: **fragility curves**.
- Approach: simulation- **engineering-based** (according to simulation scheme of Figure A.9).
- Wind pressure model: two different approaches were considered for the calculation of wind loads on the building. *Approach A* uses a **modified ASCE standard 7-10** model while *approach B* uses a **modified ASCE standard 7-16** model. The modifications of these models are based on the use of some *tornado pressure coefficients* to modify ASCE pressure coefficients.
- Direction of wind: **all possible** directions are considered since wind speed can occur from any direction in tornadoes.
- Terrain roughness: -
- Terrain category: -
- Terrain category reference code: -
- Surrounding condition: -
- Exposure category: **C**.
- Exposure category reference code: **ASCE standard 7-10** .
- Date of building construction or retrofit: **1970**.
- Reference building code: **PCI design manual (1971)**.
- Structure technology: the building is representative of an archetype **unreinforced masonry** school.
- Type of use: **school**.
- Geometry in plan: the geometry of the structure is **complex** (Figure A.8).

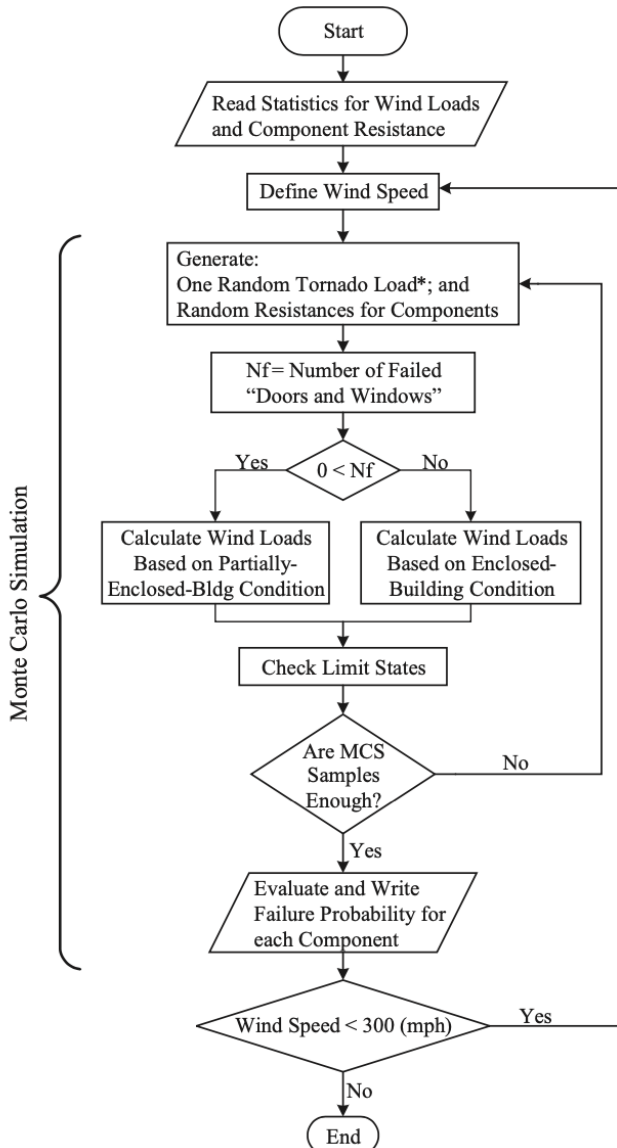


Figure A.9: Simulation scheme (adapted from [60]).

- Number of storey: 1.
- Enclosure classification: **partially enclosed** and **enclosed** building conditions are considered for the assessment of the loads acting on the structure. For A approach, the partially enclosed condition is only used for envelope wall lateral loads. Otherwise, the structure is considered fully sealed.
- Criteria for enclosure classification: according to **ASCE** criteria.
- Curve or data level: results are presented for both **whole building** and **building components**.
- Level specification: fragility curves are developed for both types of approach (A and B) for: the **building**, doors and windows (**envelope openings**), **roof covering**, **roof structure** and five types of **envelope walls**.
- Amount of damage corresponding to Damage State DS: according to HAZUS damage matrix definition (Figure A.10).
- Corresponding Hazus-type Damage State (HDS): according to HAZUS damage matrix definition (Figure A.10).
- Corresponding HDS upper level: according to HAZUS damage matrix definition (Figure A.10).

Damage state	Roof cover failure	Window/door failures	Parapet failure	Non-load-bearing wall failure	Roof structural failure	Load-bearing wall failure
0	<2%	No	No	No	No	No
1	>2% and ≤15%	1 or 2	No	No	No	No
2	>15% and ≤50%	>2 and ≤25%	No	No	No	No
3	>50%	>25%	Yes	Yes	No	No
4	Typically >50%	Typically >25%	Typically Yes	Typically Yes	Yes	Yes

^a Each damage state is defined as occurrence of any of the shaded damage indicators in a given row.

Figure A.10: Damage matrix (adapted from [60]).

- Roof typology: **precast concrete roof** system is considered.
- Roof technology: **hollow-core** and **Single tee** beam types are considered for different parts of the building.

- Roof slope: **flat roof**.
- Roof overhang: -
- Roof height definition: -
- Roof height: -
- Roof-to-wall connection: **bolt #5; 8" or 12' CMU; fully or partially grouted.**
- Covering typology: **build-up** roof cover.
- Covering technology: -
- Covering size: -
- Covering connection: -
- Envelope walls typology: five characteristics of **unreinforced masonry** (URM 1 to 5) is considered.
- Envelope walls technology: the characteristics of the assumed **0.3 m** wall strips are summarised in Figure A.11 in terms of masonry and mortar types.

Type	Masonry and mortar types	Sample Size	Mean	COV	Modulus of rupture in MSJC code	Allowable stress in MSJC code	Ratio of mean to allowable stress
M1	Fully Grouted, M/S, PCL	6	2.0 MPa (289.6 psi)	0.11	1.12 MPa (163 psi)	0.59 MPa (86 psi)	3.37
M2	Partially Grouted, M/S, PCL	- ^a	1.47 MPa (213.0 psi)	0.31	0.61 MPa (88 psi)	0.32 MPa (46 psi)	4.63
M3	Ungrouted, M/S, PCL	80	1.29 MPa (186.5 psi)	0.48	0.43 MPa (63 psi)	0.23 MPa (33 psi)	5.65
M4	Ungrouted, N, PCL	61	0.69 MPa (100.5 psi)	0.45	0.33 MPa (48 psi)	0.17 MPa (25 psi)	4.02
M5	Ungrouted, N, MC	17	0.36 MPa (52.7 psi)	0.45	0.16 MPa (23 psi)	0.08 MPa (12 psi)	4.39

^a The values for partially grouted masonry are determined on the basis of linear interpolation between fully grouted hollow units and ungrouted hollow units.

Figure A.11: Statistics of masonry typologies (adapted from [60]).

- Envelope percentage of openings: -
- Openings typology: -
- Openings technology: -

- IM reference height: roof height.
- IM reference time: **3-sec.**
- IM typology: **gust**.
- IM unit of measurements: [mph].
- Values model: **parametric values**.
- Values unit of measurements: **probability of failure** (Figure A.12) or **probability of damage state exceedance** (Figure A.13).

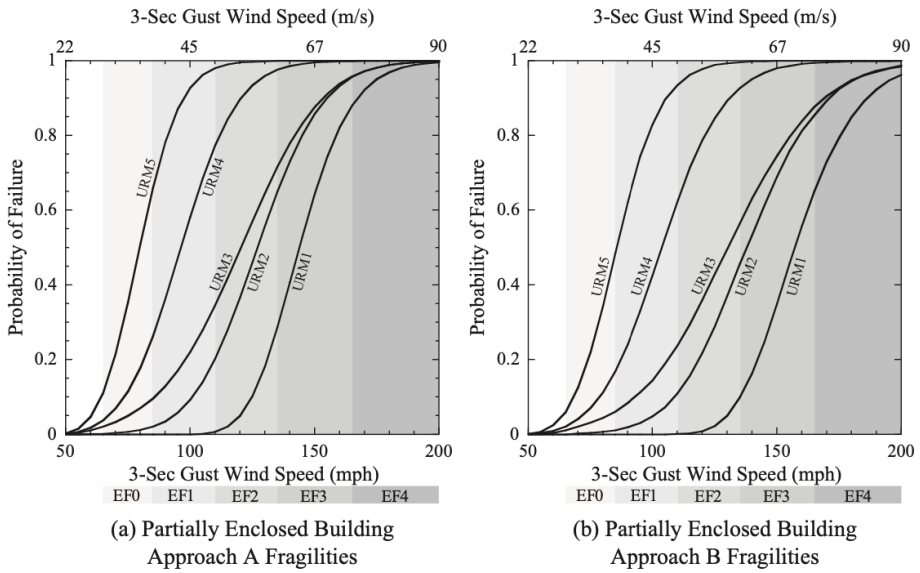


Figure A.12: Fragility curves for different typology of envelope wall (adapted from [60]).

- Debris: -
- Debris model: -

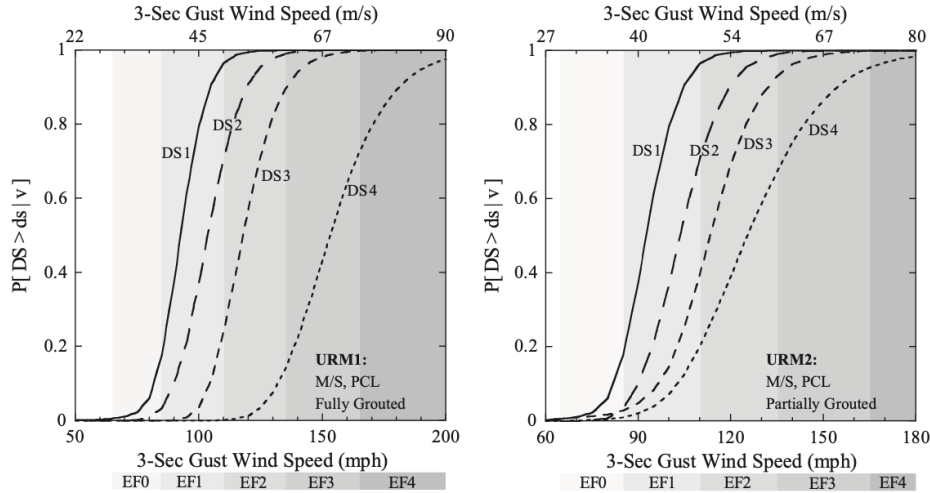


Figure A.13: Building fragility curves (adapted from [60]).

- Shielding: -
- Shielding model: -
- Water penetration damage: -
- Water penetration damage model: -
- Secondary damage to people: -
- Secondary damage to people model: -
- Uncertainty: -
- Tag: **490-584** of fragility database.

Abdelhady, Spence, and McCormick (2022), “Risk and fragility assessment of residential wooden buildings subject to hurricane winds.” [2]

The main focus of the authors of this study is on the hurricane-imposed risk assessment and fragility analysis of residential wooden buildings. Based on Monte Carlo simulation, building fragilities for 3-sec gust wind speed are estimated considering two main damage mechanisms: the excessive dynamic wind pressure and impact of windborne debris. Different construction cases are studied (from the most weak, 1, to the most resistant, 10) for three different *floor-area ratios* (FAR): 0.1, 0.3, and 0.6. Log-normal fragility curves are provided for a residential gable-roof wooden building (Figure A.14), according to the 5 damage states defined according to HAZUS.

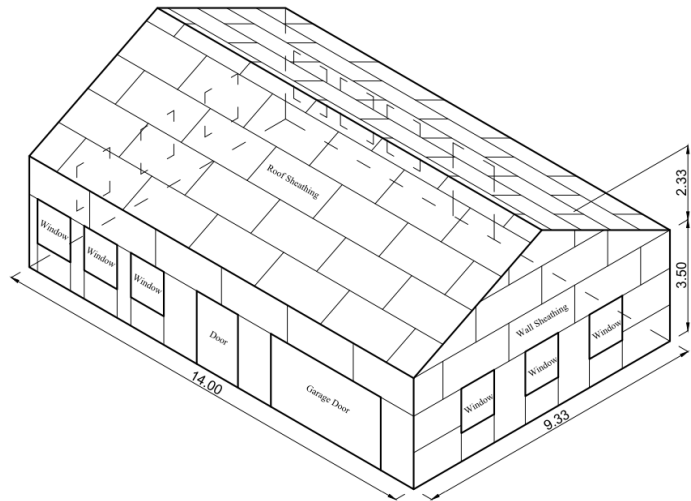


Figure A.14: Gable-roof building archetype (adapted from [2])

- Source: reference tag for this study is **Abdelhady_2022**.
- Year: **2022**.

- Region: **United States**.
- Event type: **hurricane**.
- Curve typology: building **fragility curves**.
- Approach: **engineering-based**.
- Wind pressure model: net pressures on building is obtained by external and internal pressure coefficients provided by **Tokyo Polytechnic University aerodynamic database** ([//www.wind.arch.t-kougei.ac.jp/info_center/windpressure/grouplowrise/mainpage.html](http://www.wind.arch.t-kougei.ac.jp/info_center/windpressure/grouplowrise/mainpage.html)) [85] and **Holmes** [43], respectively.
- Direction of wind: -
- Terrain roughness: -
- Terrain category: -
- Terrain category reference code: -
- Surrounding condition: flor-to-area ratio (FAR) equal to **0.1, 0.3 and 0.6**.
- Exposure category: -
- Exposure category reference code: -
- Date of building construction or retrofit: -
- Reference building code: -
- Structure technology: .
- Type of use: **residential**.
- Geometry in plan: **rectangular** 14 x 9.33 [m] plan.
- Number of storey: **1**.

- Enclosure classification: -
- Criteria for enclosure classification: -
- Curve or data level: **whole building**.
- Level specification: **building**.
- Amount of damage corresponding to Damage State DS: 5 qualitative measures of the building damage are provided, according to HAZUS classification for residential buildings: **no damage, minor damage, moderate damage, severe damage and destruction** (Figure A.15).

Damage state	Qualitative measure	Roof/Wall cover failure	Window/Door failure	Roof/Wall sheathing failure	Roof-Wall connection failure
0	No damage	$\leq 2\%$	No	No	No
1	Minor damage	$> 2\% \text{ and } \leq 15\%$	1	No	No
2	Moderate damage	$> 15\% \text{ and } \leq 50\%$	2 or 3	1-3	No
3	Severe damage	$> 50\%$	$> 3 \text{ and } \leq 8$	$> 3 \text{ and } \leq 25\%$	No
4	Destruction	Typically $> 50\%$	> 8	$> 25\%$	Yes

Figure A.15: Damage states for residential wooden buildings according to HAZUS (adapted from [2])

- Corresponding Hazus-type Damage State (HDS): previous qualitative measure correspond to HAZUS building damage states **0, 1, 2, 3 and 4**, respectively.
- Corresponding HDS upper level: -
- Roof typology: **gable roof**.
- Roof technology: -
- Roof slope: **26.5°**.
- Roof overhang: **no**.
- Roof height definition: **eave height**.
- Roof height: **3.5 [m]**.

- Roof-to-wall connection: -
- Covering typology: **roof sheathing and roof covering**.
- Covering technology: -
- Covering size: -
- Covering connection: -
- Envelope walls typology: **wall sheathing and wall covering**.
- Envelope walls technology: -
- Envelope percentage of openings: -
- Openings typology: **windows, doors and garage door**.
- Openings technology: -
- IM reference height: -
- IM reference time: **3-sec..**
- IM typology: **gust wind speed**.
- IM unit of measurements: **[m/s]**.
- Values model: **parametric values** .
- Values unit of measurements: **probability of damage state exceedance** (Figure A.16).
- Debris: both **taken into account and not**.
- Debris model: extension of neighbouring buildings defined by the radius r value according to [1] (Figure A.17) and windborne debris trajectories traced using the probabilistic 6-DOF debris trajectory model by Grayson [32].

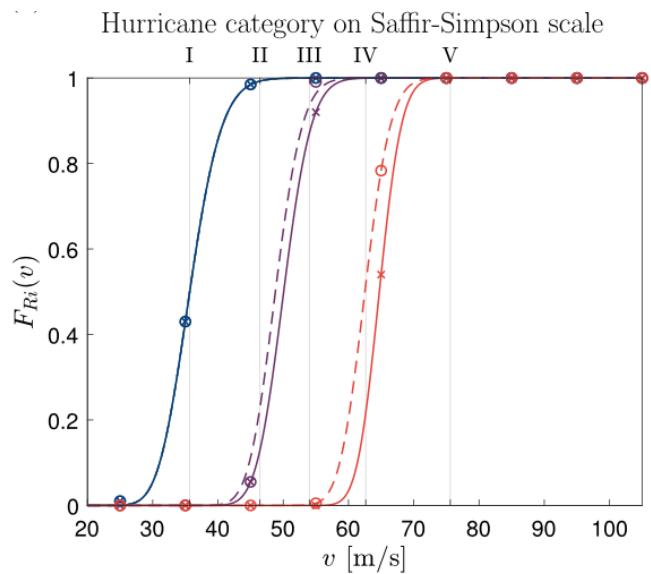


Figure A.16: Simulation results (scatters) and fitted case 3 building fragility curves (lines) for FAR equal to 0.3. Dotted line represent no debris condition, while the solid lines represent the debris condition (adapted from [2])

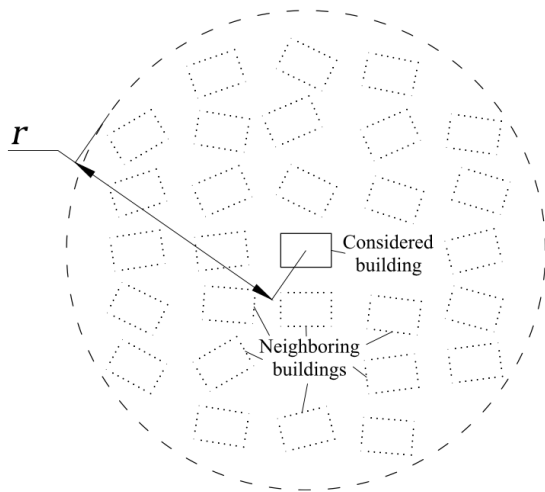


Figure A.17: Surrounding condition scheme according to considered radius r (adapted from [2])

- Shielding: -
- Shielding model: -
- Water penetration damage: -
- Water penetration damage model: -
- Secondary damage to people: -
- Secondary damage to people model: -
- Uncertainty: **taked into account** using Monte Carlo simulation.
- Tag: **257-489** of fragility database.

A.2.2 Components fragility curves

Lee (2004), “Site-specific hazards and load models for probability-based design.” [54] and Lee and Rosowsky (2005), “Fragility assessment for roof sheathing failure in high wind regions.” [55]

The study of Lee and Rowosky [55] concerns a fragility model for roof sheathing uplift assessment, given available fastener test data. More specifically, the authors develop (complementary) fragility curves as a function of wind speed (3-sec gust at 10 m in open terrain), with the aim of their use in performance-based design. Fragility curves are developed for roof sheathing uplift of light frame wood construction in United States, considered as one of the main source of building envelope breach and therefore a great source of water ingress and losses, during hurricanes. More details are provided in Lee’s 2004 Ph.D. thesis [54].

- Source: reference tag for this study is **Lee_Rosowsky_2005**.
- Year: **2005**.
- Region: **United States**.
- Event type: **hurricane** (Tropical cyclone).
- Curve typology: **fragility curves**.
- Approach: **engineering based**.
- Wind pressure model: according to **ASCE Standard 7-02** standards [7].
- Direction of wind: three cases are considered; **all possible** direction of the wind (using a directionality factor according to [7]), **normal-to-ridge** direction and **parallel-to-ridge** direction (Figure A.18).
- Terrain roughness: -
- Terrain category: -

nominal GCp (ASCE 7-02)			Type 1 (roof slope = 18.4°)		
Zone 3	Zone 2	Zone 1	GCp values at each panel		
-2.6	-1.7	-0.9	all directions	normal-to-ridge	parallel-to-ridge
Nominal ^a	Mean ^b	COV	Number of panels		
			All directions	Normal-to-ridge direction	Parallel-to-ridge direction
a b c d	-1.861 -1.532 -1.500 -0.900	0.12 0.12 0.12 0.12	8 12 4 8	0 10 0 16	4 2 2 10
			32	26	18

Figure A.18: Summary data for structure Type 1 (adapted from [55])

- Terrain category reference code: -
- Surrounding condition: -
- Exposure category: **B, C and D** exposure conditions are investigated.
- Exposure category reference code: ASCE Standard 7-02 [7].
- Date of building construction or retrofit: -
- Reference building code: -
- Structure technology: 5 quite different type **light-frame wood** construction are studied. (Figure A.18-A.22).
- Type of use: **residential**.
- Geometry in plan: **rectangular**.

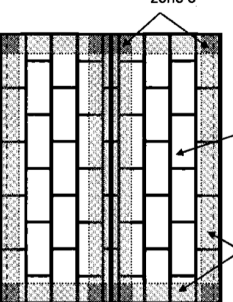
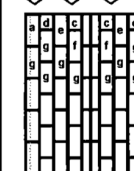
nominal GCp (ASCE 7-02)						
Zone 3	Zone 2	Zone 1				
-3.7	-2.2	-0.9				
zone 3						
						
zone 1						
zone 2						
Type 2 (roof slope = 26.6°)						
GCp values at each panel						
all directions	normal -to-ridge	parallel-to-ridge				
						
number of panels						
nominal*	mean**	COV	all directions	normal -to-ridge direction	parallel-to-ridge direction	
a	-2.540	-2.413	0.12	4	0	2
b	-1.989	-1.890	0.12	6	5	0
c	-2.811	-2.670	0.12	4	0	2
d	-1.875	-1.781	0.12	4	0	2
e	-1.388	-1.318	0.12	4	0	2
f	-1.739	-1.652	0.12	8	6	2
g	-0.900	-0.855	0.12	14	11	10
			44	22	20	

Figure A.19: Summary data for structure Type 2 (adapted from [54])

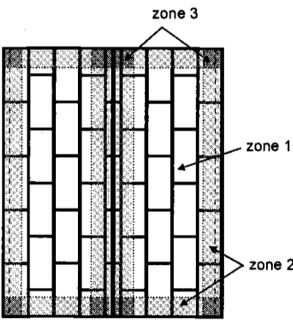
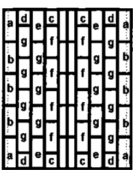
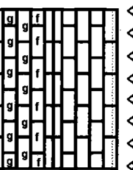
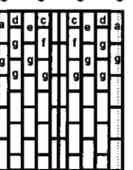
nominal GCp (ASCE 7-02)						
Zone 3	Zone 2	Zone 1				
-2.0	-2.0	-1.0				
						
Type 3 (roof slope = 33.7°)						
GCp values at each panel						
all directions	normal -to-ridge	parallel-to-ridge				
						
number of panels						
nominal*	mean**	COV	all directions	normal -to-ridge direction	parallel-to-ridge direction	
a	-1.938	-1.841	0.12	4	0	2
b	-1.901	-1.806	0.12	6	5	0
c	-1.849	-1.757	0.12	4	0	2
d	-1.750	-1.663	0.12	4	0	2
e	-1.375	-1.306	0.12	4	0	2
f	-1.396	-1.327	0.12	8	6	2
g	-1.000	-0.950	0.12	14	11	10
			44	22	20	

Figure A.20: Summary data for structure Type 3 (adapted from [54])

nominal GCp (ASCE 7-02)			Type 4 (roof slope = 18.4°)		
Zone 3 ***	Zone 2	Zone 1	GCp values at each panel		
-1.7	-1.7	-0.9	all directions	normal -to-ridge	parallel-to-ridge
nominal*	mean**	COV	number of panels		
			all directions	normal -to-ridge direction	parallel-to-ridge direction
a -1.171	-1.113	0.12	8	4	4
b -1.532	-1.455	0.12	8	3	1
c -1.281	-1.217	0.12	8	6	4
d -1.519	-1.443	0.12	4	2	2
e -1.405	-1.335	0.12	2	1	0
f -0.900	-0.855	0.12	4	4	6

Figure A.21: Summary data for structure Type 4 (adapted from [54])

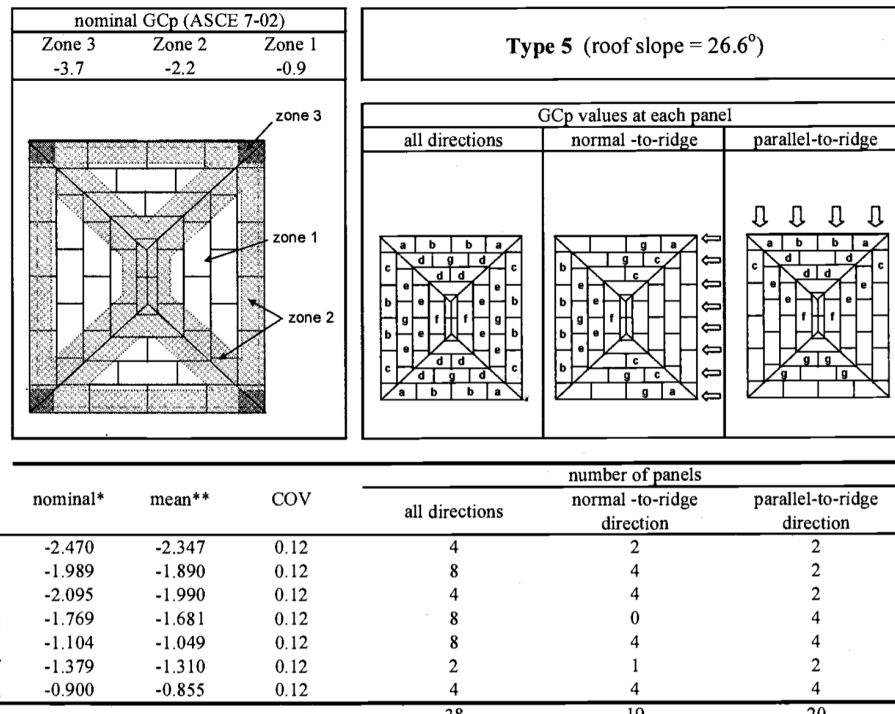


Figure A.22: Summary data for structure Type 5 (adapted from [54])

- Number of storey: only Type 3 structure has **2** stories while all the other types have **1** storey.
- Enclosure classification: the authors distinguish between two condition of the building: **enclosed** building and **partially enclosed**.
- Criteria for enclosure classification: the status of partially enclosed building follow the failure of the first roof sheathing panel. For this reason damage states greater than 1 (**at least one panel failure**) correspond to a partially enclosed condition while first damage state (**no panel failure**) corresponds to an enclosed condition.
- Curve or data level: the study concern **building component** and **building component element** fragility.
- Level specification: the considered component is the whole **roof sheathing system** (Figure A.23) and the element is the single **roof sheathing** (Figure A.24).

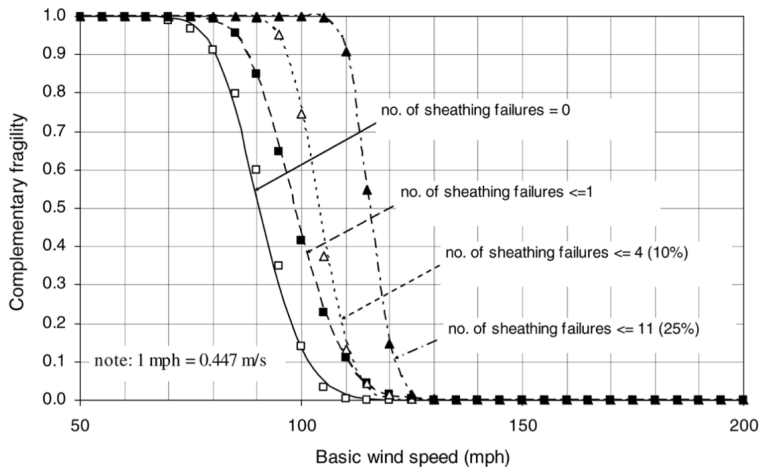


Figure A.23: Lognormal fitted roof system complementary fragilities (structure Type 1; exposure B; 8d nail - adapted from [55]).

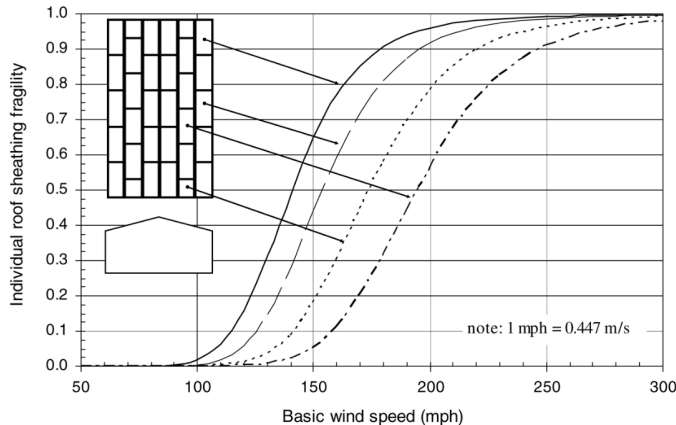


Fig. 2. Fragilities for individual roof sheathing failure (Structure Type 1/Exposure B/8d nail — 6 in./12 in. spacing).

Figure A.24: Fragility curves for individual roof sheathing failure (enclosed building; structure Type 1; exposure B; 8d nail - adapted from [55]).

- Amount of damage corresponding to Damage State DS: the authors define fragility curves for **single element failure** and for four roof sheathing system damage levels: **no sheathing failures (1)**, **no more than one sheathing panel failure (2)**, **fewer than 10% of sheathing panels failed (3)** and **fewer than 25% of sheathing panels failed (4)**.
- Corresponding Hazus-type Damage State (HDS): see Section 6.3.1.
- Corresponding HDS upper level: see Section 6.3.1.
- Roof typology: type 1, 2 and 3 are characterised by **gable** roofs while 4 and 5 by **hip** roofs (Figure A.18-A.22).
- Roof technology: **light-wood** system. The roof framing (50 mm x 100 mm spruce-pine-fir (SPF) rafters) spacing is the same for all the building typology: 610 mm.

- Roof slope: Roof slope are considered in three different values: **4:12 (18.4°), 6:12 (26.6°) and 8:12 (33.7°).**
- Roof overhang: Type 2, 3 and 5 structure have **overhang** while Type 1 and 4 do not.
- Roof height definition: **eave height.**
- Roof height: **2.44 m** for structural types 1, 2, 4 and 5. Instead, Type 3 has a **4.88 m** eave height.
- Roof-to-wall connection: -
- Covering typology: **roof sheathing panels.**
- Covering technology: **12 mm CDX plywood panels.**
- Covering size: **1.22 m x 2.44 m and 1.22 m x 1.22 m .**
- Covering connection: smooth-shank hand-driven common nails long 63.5 mm with 3.33 mm diameter (**8d**) or long 50.8 mm with 2.87 mm diameter (**6d**).The nailing schedule is 150 mm along the edge of the panel and 300 mm at interior locations. See Figure A.25 for resistance statistics.

Nail type/spacing	Panel size	Mean	COV	CDF
8d nail ^a 6 in./12 in. (15.2 cm/30.5 cm)	4 ft × 8 ft (1.22 m × 2.44m)	57.7 psf (2.76 kN/m ²)	0.20	Normal
	4 ft × 4 ft (1.22 m × 1.22 m)	73.3 psf (3.51 kN/m ²)	0.20	Normal
6d nail ^b 6 in./12 in. (15.2 cm/30.5 cm)	4 ft × 8 ft (1.22 m × 2.44 m)	25.0 psf (1.20 kN/m ²)	0.15	Normal
	4 ft × 4 ft (1.22 m × 1.22 m)	32.0 psf (1.53 kN/m ²)	0.15	Normal

^a 0.131 in. (3.33 mm) diameter, 2.5 in. (63.5 mm) long.

^b 0.113 in. (2.87 mm) diameter, 2.0 in. (50.8 mm) long.

Figure A.25: Summary of resistance statistics for different nail types and configurations (adapted from [55])

- Envelope walls typology: -
- Envelope walls technology: -

- Envelope percentage of openings: -
- Openings typology: -
- Openings technology: -
- IM reference height: **10 m.**
- IM reference time: **3-sec.**
- IM typology: **gust**.
- IM unit of measurements: **mph**.
- Values model: **parametric** (Log-normal).
- Values unit of measurements: the unit of measurements is a **limit state probability of exceedence** for component fragility (Figure A.23) or **probability of failure of single roof sheathing element** (Figure A.24).
- Debris: -
- Debris model: -
- Shielding: -
- Shielding model: -
- Water penetration damage: -
- Water penetration damage model: -
- Secondary damage to people: -
- Secondary damage to people model: -
- Uncertainty: -
- Tag: **15-234** of fragility database.

Henderson and Ginger (2007), “Vulnerability model of an Australian high-set house subjected to cyclonic wind loading.” [41]

See Section A.2.1 for details.

Zhang, Nishijima, and Maruyama (2014), “Reliability-based modeling of typhoon induced wind vulnerability for residential buildings in Japan.” [102]

The present study provides a vulnerability modelling approach for typical residential buildings in Japan (Figure A.26 and A.27) and assesses the performance of the some non-structural components: roof tiles, windows and roof sheathing.

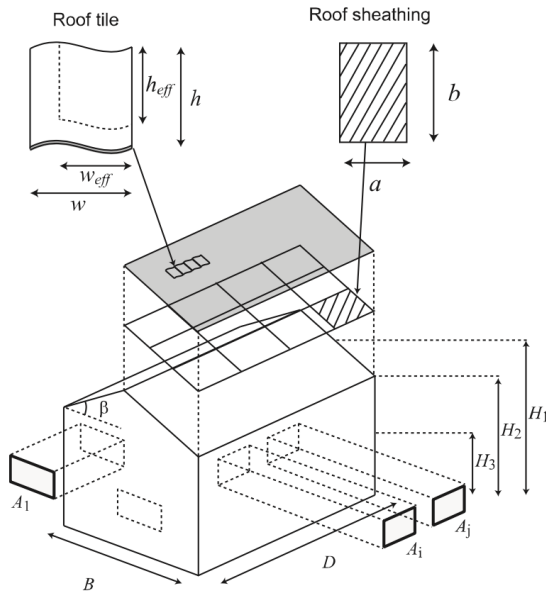


Figure A.26: Geometries of model building and building elements (adapted from [102]).

<i>Building</i>	
H_1 [m]	7.0
H_2 [m]	6.2
H_3 [m]	3.5
B [m]	6.2
D [m]	9.3
β [deg]	26.7
<i>Roof tile</i>	
h [m]	0.315
w [m]	0.295
h_{eff} [m]	0.275
w_{eff} [m]	0.225
ρ_{rt} [kg/m ³]	3000.0
<i>Roof sheathing</i>	
a [m]	1.22
b [m]	2.44

Figure A.27: Parameters of model building, roof tile and roof sheathing (adapted from [102]).

- Source: reference tag for this study is **Zhang_2014**.
- Year: **2014**.
- Region: **Japan**.
- Event type: **Typhoon**.
- Curve typology: the authors present results in terms of building components **fragility**, component elements fragility and building **vulnerability** curves.
- Approach: the study falls under the **simulation-based engineering approach**.
- Wind pressure model: the authors use a **own specific model** to define gust wind load.

- Direction of wind: 13 different direction are introduced by the authors but results are presented only for 2 direction: 1 and 5 in Figure A.28 that correspond to **parallel-to-ridge** and **normal-to-ridge** direction respectively.

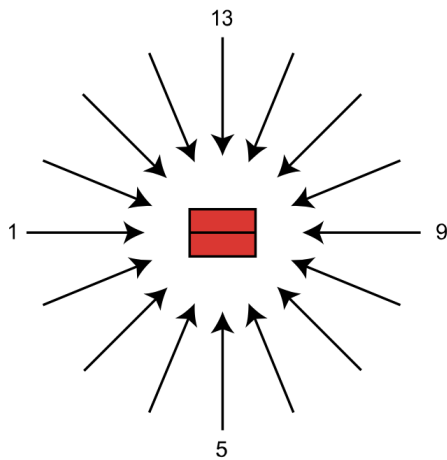


Figure A.28: Direction of the wind relative to building orientation (adapted from [102]).

- Terrain roughness:
- Terrain category: **III**.
- Terrain category reference code: **AIJ** recommendations for loads on buildings [6].
- Surrounding condition: three different surrounding condition are considered according to the **spatial building density**: **0.1, 0.3 and 0.6** (Figure A.29)). The authors assume the building surrounded by buildings that are identical to the model building.
- Exposure category: -

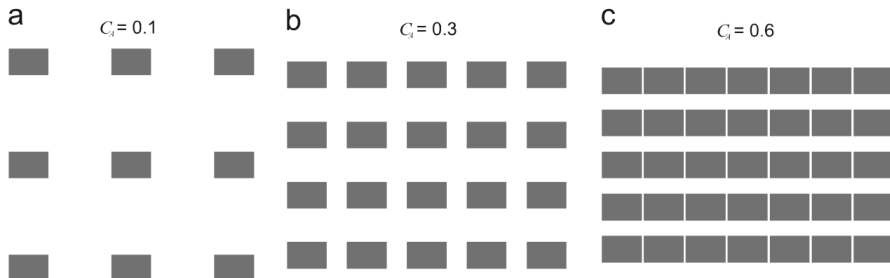


Figure A.29: Different spatial building densities (adapted from [102]).

- Exposure category reference code: -
- Date of building construction or retrofit: -
- Reference building code: -
- Structure technology: **wood-frame building.**
- Type of use: **residential.**
- Geometry in plan: **rectangular.**
- Number of storey: **2.**
- Enclosure classification: -
- Criteria for enclosure classification: -
- Curve or data level: the study outputs are at the scale of: **whole building** in terms of vulnerability; **building component** in terms of both fragility and vulnerability; **building component elements** in terms of fragility.
- Level specification: the study study the behaviour of: **building, roof covering, roof tile, envelope windows.**
- Amount of damage corresponding to Damage State DS: see Section 6.2.

- Corresponding Hazus-type Damage State (HDS): see Section 6.2.
- Corresponding HDS upper level: see Section 6.2.
- Roof typology: **gable roof**.
- Roof technology: -
- Roof slope: **26.7°**.
- Roof overhang: **No**.
- Roof height definition: **eave height**.
- Roof height: **7 [m]**.
- Roof-to-wall connection: -
- Covering typology: the study deals with a **typical Japanase roof cover** and **Roof sheathing panels**.
- Covering technology: the roof covering is composed by **1152 typical Japanase tiles (3000 kg/m³ density** placed on **24 plywood roof sheathing panels** (for more details see Figure A.27).
- Covering size: all the tiles have the same dimensions: **0.315 m x 0.295 m** (0.275 m x 0.225 m considering the overlapping). The roof sheathing panels have dimensions of **1.22 m x 2.44 m**.
- Covering connection: for the tile, the authors consider two different cases characterized respectively by a factor ζ of 1 or 2. This factor multiply the gravity force component orthogonal to the tile plane, considered as the only resistance contribute to orthogonal uplift force. The connection is therefore **proportional to the weight**.
- Envelope walls typology: -
- Envelope walls technology: -

- Envelope percentage of openings: the study consider the windows at the first floor as the **15 % of the area of the whole first floor wall** (the windows on the ground floor are not modeled).
- Openings typology: **glass windows**.
- Openings technology: **windows** are aggregated in one on each side of the building.
- IM reference height: **7 [m]**.
- IM reference time: some results are presented in terms of **10-min.** sustained wind speed while other in **3-sec.** gust wind speed.
- IM typology: 10-min. sustained refers to a **mean** value while 3-sec. represents a **gust**.
- IM unit of measurements: **[m/s]**.
- Values model: output are given in both **discrete** (fragility and component vulnerability) and **parametric** (building vulnerability) way.
- Values unit of measurements: the output unit of measurements are **probability of failure of a roof tile** (Figure A.30), **probability that at least one windows fails** (Figure A.31), **expected percentage of failed roof tiles** (Figure A.32) and **expected consequence** (Figure A.33).
- Debris: the flying tiles are considered the only damage source in the evaluation of window failure due to debris.
- Debris model: the flying trajectory of a roof tile is modeled taking basis in the **2010 Lin and Vanmarcke** model (Figure A.34).
- Shielding: -
- Shielding model: -
- Water penetration damage: -

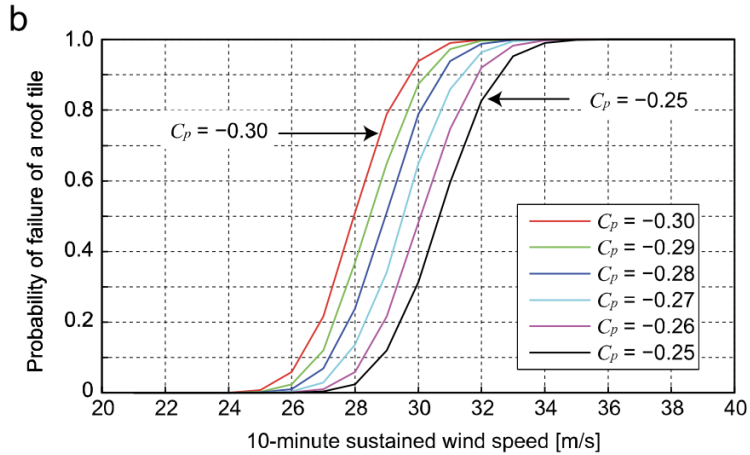


Figure A.30: Single roof tile fragility curves for different external pressure coefficient C_p (adapted from [102]).

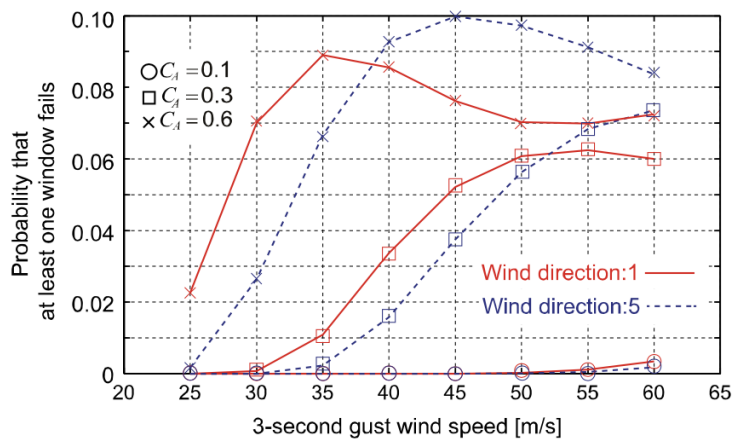


Figure A.31: Windows fragility curves for two different wind direction (adapted from [102]).

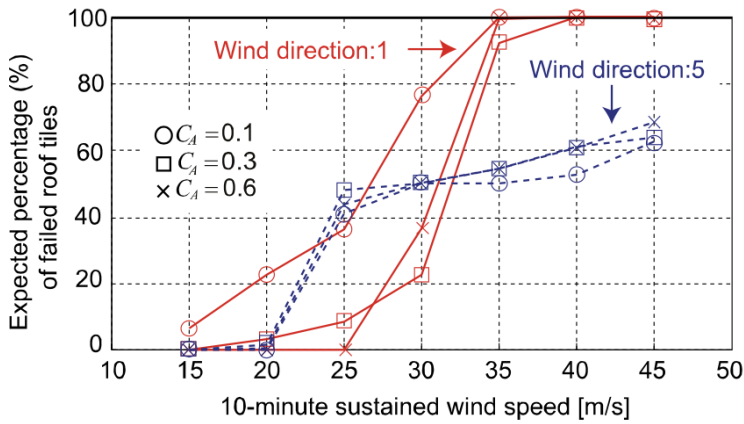


Figure A.32: Expected percentage of failed roof tiles for two different wind direction (adapted from [102]).

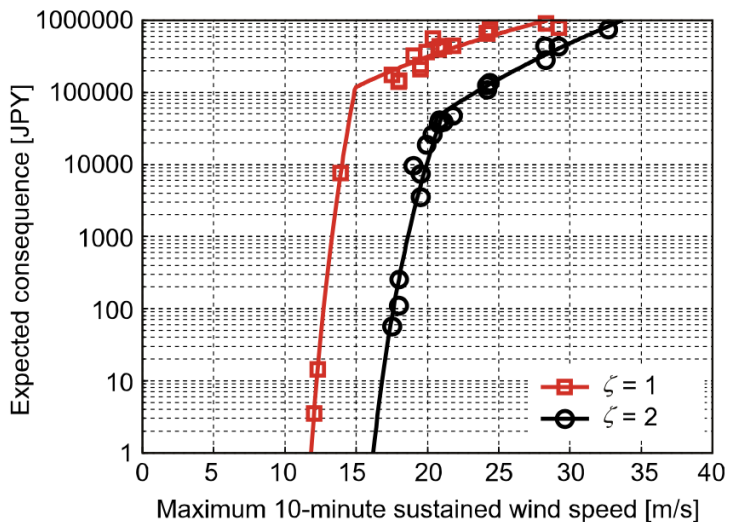


Figure A.33: Building vulnerability curves (adapted from [102]).

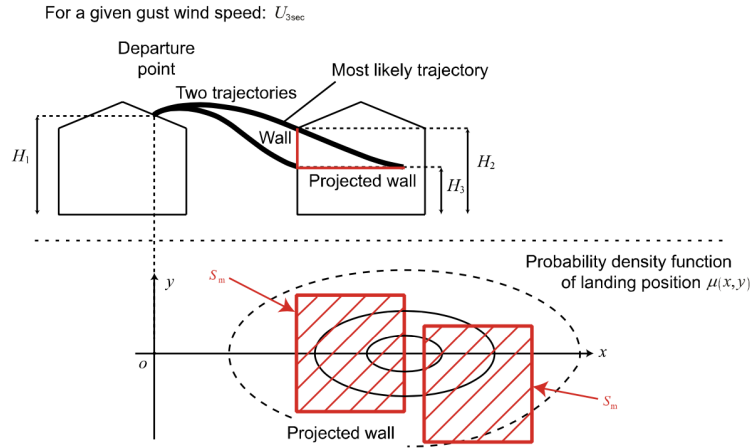


Figure A.34: Flying debris trajectories and criterion for debris hit on the wall.
(adapted from [102]).

- Water penetration damage model: -
- Secondary damage to people: -
- Secondary damage to people model: -
- Uncertainty: the uncertainties are taken into account.
- Tag: **235-246** of fragility database and **25-32** of vulnerability database.

A.2.3 Element fragility curves

Zhang, Nishijima, and Maruyama (2014), “Reliability-based modeling of typhoon induced wind vulnerability for residential buildings in Japan.” [102]

See section A.2.2 for details.

Lee (2004), “Site-specific hazards and load models for probability-based design.” [54] and Lee and Rosowsky (2005), “Fragility assessment for roof sheathing failure in high wind regions.” [55]

See section A.2.2 for details.

Li and Ellingwood (2006), “Hurricane damage to residential construction in the US: Importance of uncertainty modeling in risk assessment.” [57]

The authors present a probabilistic approach to assess the reliability of low-rise wood residential construction in hurricane-prone regions of the United States through the fragility curves of building elements (e.g. roof panels and windows). By the convolution of structural fragility models and wind ad-hoc computed hazard curves, they define the probability of failure under a series of possible hurricane winds. They also address the sources of uncertainty.

- Source: reference tag for this study is **Li_Ellingwood_2006**.
- Year: the year of the study is **2006**.
- Region: the study analyze the southeast hurricane-prone region of **United States**.
- Event type: the study event is **hurricane** (tropical cyclones).
- Curve typology: the study develops a probabilistic risk assessment method to assess performance and reliability of specific low-rise light-frame wood residential buildings by its components **fragility curves**.

- Approach: the fragility curves of most vulnerable components (Figure A.35 to A.38) were obtained with an **engineering-based** approach, directly by a first-order reliability analysis of the governing limit state equation. The statistics of wind load and component capacity are shown in Figure A.39 and A.40 respectively.

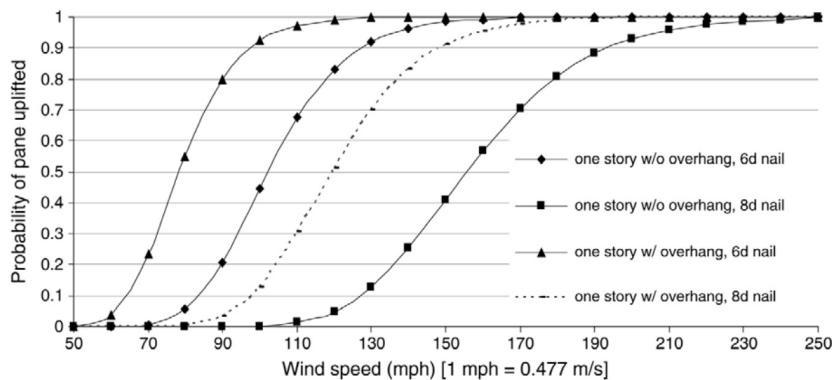


Figure A.35: Root panel fragility of two typical house (Exposure B) (adapted from [57])

- Wind pressure model: according to ASCE Standard 7-02 procedure [7].
- Direction of wind: given the use by the authors of a directional factor, they implicitly consider **all possible** directions for the wind.
- Surrounding condition: -
- Terrain roughness: -
- Terrain category: -
- Terrain category reference code: -
- Surrounding condition: -

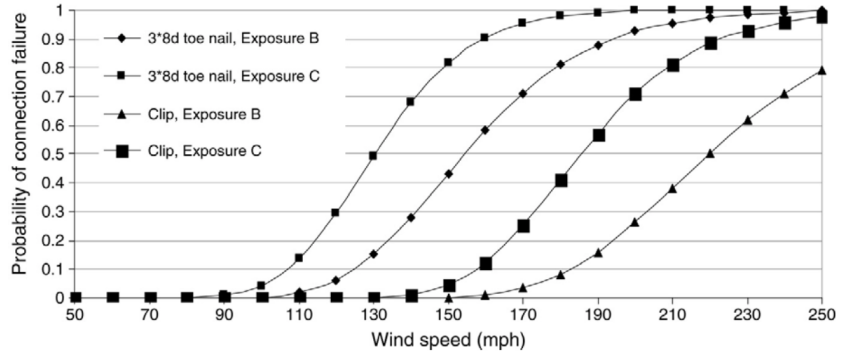


Figure A.36: Roof-to-wall connection fragility of one-story house without roof overhang (adapted from [57])

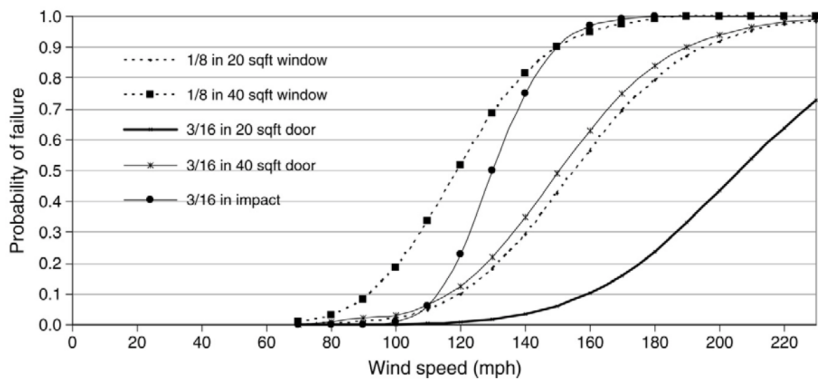


Figure A.37: Glass fragility due to pressure and impact (adapted from [57])

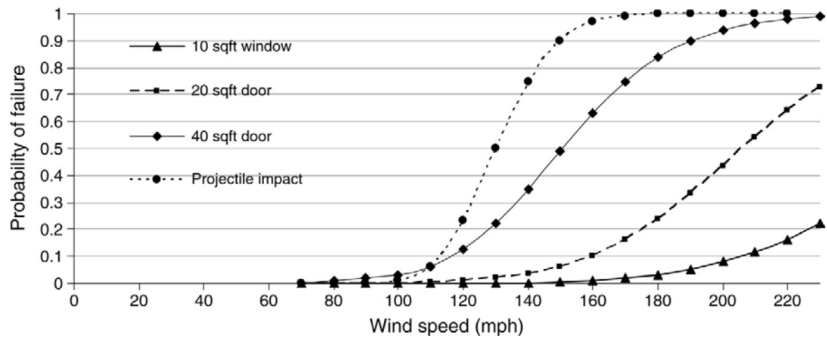


Figure A.38: 3/16 in. (5 mm) glass fragility due to pressure and impact (adapted from [57])

	Mean	COV	CDF
K_z (Exposure B)	0.57	0.12	Normal
K_z (Exposure C)	0.8	0.12	Normal
GC_p (C & C) Zone 3	1.81	0.22	Normal
GC_p (MWFRS)	0.86	0.15	Normal
GC_p (C & C) Zone 4	0.9	0.1	Normal
$GCpi$ (Enclosed)	0.15	0.05	Normal
$GCpi$ (Partial enclosed)	0.45	0.09	Normal
K_d	0.89	0.14	Normal

C & C: Component and cladding.

MWFRS: Main Wind-Force Resisting Systems.

Figure A.39: Wind load statistics (adapted from [57])

Component		Failure mode	Mean	COV	CDF
Roof panel	6d (0.113 in.) nails @ 6/12 in.		25 psf	0.15	Normal
	8d (0.131 in.) nails @ 6/12 in.		60 psf	0.2	Normal
Roof-to-wall connection	3–8d (0.131 in.) toe nails	Uplift	411 lbs	0.34	Normal
	H2.5 Clip		1312 lbs	0.1	Normal
Annealed glass (window and glass door)	1/8 in.; 20 sq ft	Pressure	54.47 psf	0.25	Weibull
	3/16 in.; 40 sq ft		32.04 psf	0.25	
	3/16 in.; 20 sq ft		96.12 psf	0.25	
	3/16 in.; 40 sq ft		51.26 psf	0.25	
3/16 in. thickness		Missile impact ^a	22.8 mph	0.07	Lognormal

1 in. = 25.4 mm; 1 ft² = 0.093 m²; 1 lb = 4.45 N; 1 psf = 47.9 Pa.

^a Assume 15 m of acceleration of 0.005 kg missile, impact velocity is 35% of carrying wind speed. Glass resistance is adjusted to 3 s duration loading.

Figure A.40: Capacity statistics (adapted from [57])

- Exposure category: the fragility curves are developed for **Exposure B and C**.
- Exposure category reference code: **ASCE Standard 7-02** [7].
- Date of building construction or retrofit: -
- Reference building code: -
- Structure technology: the fragility curves are developed for typical **low-rise light-frame wood** building components. Two typical one-story single-family houses, A and B, are considered depending on the presence or not of overhang, respectively.
- Type of use: the type of use is **residential**.
- Geometry in plan: both type of construction are **rectangular** in plan.
- Number of storey: both type of construction have **1** storey.
- Enclosure classification: -
- Criteria for enclosure classification: -

- Curve/data level: the focus of the study is on building component **elements**.
- Level specification: the considered building component elements are: **roof panel, roof truss-to-wall connection and openings** (windows and doors).
- Amount of damage corresponding to Damage State DS: the authors define fragility curves for **single element failure** in several configurations.
- Corresponding Hazus-type Damage State (HDS): -
- Corresponding HDS upper level: -
- Roof typology: the roof typology is **gable roof**, for both type A and B constructions.
- Roof technology: the **light-wood** systems, for both type A and B constructions, are characterized by roof trusses spaced 0.6 m on center.
- Roof slope: **26.57°** (6:12).
- Roof overhang: The type A roof has an **overhang** extending 0.6 m from the wall, while the type B roof does not have overhang.
- Roof height definition: **mean roof height**.
- Roof height: **3.75 m**.
- Roof-to-wall connection: the study develops roof truss-to-wall connection fragility only for roof without overhang, in Exposures B and C. More specifically, the authors consider the following cases: **H2.5 hurricane clips** and **8d toe-nails** (3.3 mm diameter).
- Covering typology: the roof cover studied is composed by **roof panels**.
- Covering technology: **wood panels**.

- Covering size: 1.2 m by 2.4 m.
- Covering connection: the nail patterns are of two types according to nail diameter: **6d** (diameter of 2.9 mm) and **8d** (diameter of 3.3 mm). The nails spacing is of 150 mm at the perimeter panel and 300 mm in the interior panel.
- Envelope walls typology: -
- Envelope walls technology: -
- Envelope percentage of openings: -
- Openings typology: two different thicknesses of **annealed glass** for windows or sliding glass doors are considered.
- Openings technology: the study analyze two different thicknesses of annealed glass, **3 mm** and **5 mm**, and two different areas **small** ($1.9 m^2$) and **large** ($3.7 m^2$), for windows or sliding glass doors.
- IM reference height: **10 m.**
- IM reference time: **3-sec.**
- IM typology: **gust.**
- IM unit of measurements: **mph**
- Values model: The fragility curves of Figure A.35 to A.38 were obtained as **discrete values**, directly from a first-order reliability analysis without distribution assumptions beyond the load and resistance statistics.
- Values unit of measurements: as usually for fragility curves, the unit of measurements is a **probability of failure** of the component.
- Debris: a failure mode of openings by wind-borne debris is take into account.

- Debris model: Figure A.40 describes glass breakage in windows and doors due to wind-borne debris.
- Shielding: -
- Shielding model: -
- Water penetration damage: -
- Water penetration damage model: -
- Secondary damage to people: -
- Secondary damage to people model: -
- Uncertainty: both categories of uncertainties (aleatory and epistemic) and their impact are addressed in this paper.
- Tag: **1-14** of fragility database.

A.3 Vulnerability curves

A.3.1 Building vulnerability curves

Leicester and Reardon (1976), “Statistical Analysis of the Structural Damage by Cyclone Tracy.” [56]

The Cyclone Tracy on Darwin of 1974, has been considered one of the greatest structural disaster occurred in Australia. With the aim of vulnerability curve definition (about 1500 elevated houses, 750 low-set houses, 300 non-residential buildings and 200 light steel industrial building), the authors undertook a quantitative survey one week after the occurrence of this extreme event. Analysing the site wind speed distribution and the evolution of the building design in that region, the mean value of the damage repair index is given for the considered classes of building (Figure A.41). Abnormal cost of construction following a disaster are not taken into account.

- Source: reference tag for this study is **Leicester_Reardon_1976**.
- Year: the year of the study is the 1976 while the year of the event is the **1974**.
- Region: the city under study is Darwin, in the **northern part of Australia**.
- Event type: the event is the **hurricane** (Tropical Cyclone) Tracy.
- Curve typology: six **vulnerability discrete value sets** are developed for the same number of building typologies (see "Type of use" field for more specifications).
- Approach: since the nature of the surveys, the approach is considered as **past-loss data**.
- Wind pressure model: the authors develop an **own specific model** to map the wind pressure in the region.
- Direction of wind: -

TABLE III
Damage Caused by Cyclone Tracy.

Building type	Mean damage repair index	Sample size	Estimated mean wind gust velocity (m s^{-1})
<i>Elevated houses</i>	.39	1486	48
<i>Low set houses*</i>			
A.C. sheet	.23	127	48
brick	.21	532	51
concrete block/brick	.53	71	53
concrete panel	.15	29	53
<i>Non-residential one storey buildings</i>			
modern	.14	94	45
old	.20	70	45
<i>Modern 2 or 3 storey buildings</i>	.22	143	47
<i>Steel-industrial buildings</i>			
modern	.14	200	45
old	.63	5	46

Figure A.41: Effect of wind velocity on damage (adapted from [56])

- Terrain roughness: -
- Terrain category: According to the Australian code AS 1170 [80] the site condition is similar to the **Terrain Category 3**.
- Terrain category reference code: **Australian code AS 1170**.
- Surrounding condition: Most of the surveys concern with **uniform built-up area in flat terrain**.
- Exposure category: the buildings are considered as having an exposure category **C**.
- Exposure category reference code: **Australian code AS 1170**.
- Date of building construction or retrofit: maps of construction years are provided. The authors identify constructions **from pre-1956 to 1974**.
- Reference building code: -
- Structure technology: the considered building types are generically classified as **elevated houses, low set brick houses, low set a.c. sheet wall houses, one storey non-residential building, two and three storey buildings and light modern steel industrial building**.
- Type of use: as stated before, the buildings fall into the following categories: **houses, non-residential or industrial building**.
- Geometry in plan: the authors refer to **standard plans**.
- Number of storey: there are **no more specification** than that given in the in previous Type of use label. It should be find in some previous report [93, 37].
- Enclosure classification: -
- Criteria for enclosure classification: -

- Curve/data level: the curve resolution is at the level of the **whole building**
- Level specification: **building**.
- Amount of damage corresponding to Damage State DS: a relation between the damage repair index (see "Values unit of measurements" field) and the damage class, for the various building types, is given in Figure A.42 and A.43.

TABLE I
Definition of Damage Level for Non-industrial Buildings

Damage class	Worst damage feature	Damage repair index*				
		Elevated houses	Low-set houses		One-storey non-residential buildings	Top floor of multi-storey buildings
Brick walls	Asbestos cement walls					
1	Negligible	0.00	0.00	0.00	0.00	0.00
2	Missile damage to cladding or windows	0.05	0.05	0.05	0.05	0.05
3	Loss of half roof sheeting	0.10	0.10	0.10	0.10	0.10
4	Loss of all roof sheeting	0.20	0.20	0.15	0.15	0.20
5	Loss of roof structure	0.25	0.25	0.20	0.20	0.25
6	Loss of half walls	0.50	0.65	0.60	0.60	0.55
7	Loss of all walls	0.75	0.90	0.90	0.90	0.80
8	Loss of half floor	0.85	—	—	—	—
9	Loss of all floor	0.95	—	—	—	—
10	Collapse of floor support piers	1.00	—	—	—	—

$$\text{*Damage repair index} = \frac{\text{cost to repair damage}}{\text{initial cost of building}}$$

Figure A.42: Relation between the damage repair index and the damage class for non-industrial building (adapted from [56])

- Corresponding Hazus-type Damage State (HDS): -

TABLE II
**Definition of Damage Level for Modern
 Steel Industrial Buildings**

Damage class	Worst damage feature	Damage repair index*
1	Negligible	0.00
2	Loss of half wall or half roof sheeting	0.05
3	Loss of all wall or all roof sheeting	0.15
4	Failure of non-load bearing gable end wall	0.20
5	Loss of all wall and all roof sheeting	0.30
6	Failure of load bearing gable end wall	0.40
7	Failure of some secondary structural members	0.60
8	Failure of some primary structural members	0.80
9	Total collapse of primary structure	1.00

$$* \text{Damage repair index} = \frac{\text{cost to repair damage}}{\text{initial cost of building}}$$

Figure A.43: Relation between the damage repair index and the damage class for modern steel industrial building (adapted from [56])

- Corresponding HDS upper level: -
- Roof typology: -
- Roof technology: -
- Roof slope: -
- Roof overhang: -
- Roof height definition: -
- Roof height: -
- Roof-to-wall connection: -
- Covering typology: -
- Covering technology: -
- Covering size: -
- Covering connection: -
- Envelope walls typology: -
- Envelope walls technology: -
- Envelope percentage of openings: -
- Openings typology: -
- Openings technology: -
- IM reference height: -
- IM reference time: **3 seconds**
- IM typology: **gust**
- IM unit of measurements: m/s.

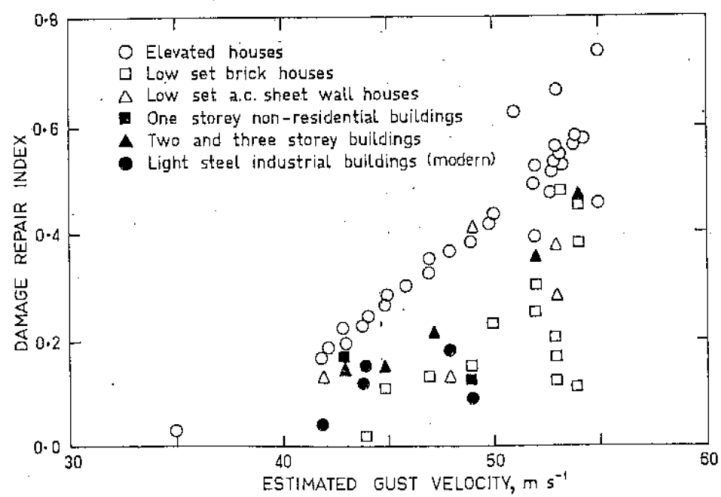


Fig. 6. Effect of wind velocity on damage.

Figure A.44: Mean damage repair index for building classes (adapted from [56])

- Values model: the curves are composed by **discrete values** (Figure A.44).
- Values unit of measurements: the vulnerability measure for the one-storey building is the **damage repair index** defined as the ratio between the cost for damage repair and the initial cost of the building. For multi-storey building a similar index is defined, applied only to the top floor.
- Debris: as usually for past-loss data analyses, the results **take into account** damage from debris implicitly, without specifications.
- Debris model: -
- Shielding: the effect of shielding of adjacent buildings, is superficially **addressed**.
- Shielding model: -
- Water penetration damage: -
- Water penetration damage model: -
- Secondary damage to people: -
- Secondary damage to people model: -
- Uncertainty: -
- Tag: **6-11** of vulnerability database.

Sparks, Schiff, and Reinhold (1994), “Wind damage to envelopes of houses and consequent insurance losses.” [78]

The study of the authors analyses the insurance claim data of Hugo (1989) and Andrew (1992) hurricanes. Focusing also on the building envelope, the authors reveal its great weight in the overall loss assessment and define its contribution through the so-called *loss magnifier* (Figure A.47). This parameter analyses the effect of the rain entering into houses by envelope breach due to the failure of building components. The study also provides some indications about the conversion between gradient wind speed and standard surface measurement (e.g., 2-sec gust at 10 m). Furthermore, it is shown the relationship for expected loss ratios in hurricane-prone and not hurricane-prone regions. Some indications about the limit-state loads for building envelopes are provided.

- Source: reference tag for this study is **Sparks_1994**.
- Year: the year of the study is the 1994 while the year of the events are **1989** for hurricane Hugo and **1992** for hurricane Andrew.
- Region: the Regions under study are Florida for hurricane Andrew and South Carolina for hurricane Hugo, both in the **east coast of United States**.
- Event type: hurricanes are **Tropical Cyclones** that occur in the Atlantic Ocean and northeastern Pacific Ocean.
- Curve typology: the results of the study are concerns 90000 houses **vulnerability discrete value sets** for Florida and South Carolina. For hurricane Andrew (Florida) are also develop **vulnerability discrete value sets** for the following components: Roof envelope, wall envelope and external facilities (swimming pool, screened enclosures, lighting systems, etc.).
- Approach: since the nature of the claims, the approach is considered as **past-loss data**.

- Wind pressure model: -
- Direction of wind: -
- Terrain roughness: -
- Terrain category: -
- Terrain category reference code: -
- Surrounding condition: In Figure A.45 discrete values are referred to both **urban and flat areas**. The data for the latter case are the ones over 12% at speed less than 70 m/s coming from islands or areas exposed to the ocean and the ones over 60% between 70 and 75 m/s from treeless areas. The remaining discrete values and their trend line refers to the urban areas.
- Exposure category: -
- Exposure category reference code: -
- Date of building construction or retrofit: -
- Reference building code: -
- Structure technology: -
- Type of use: the type of use is generically expressed as **housing**.
- Geometry in plan: -
- Number of storey: -
- Enclosure classification: -
- Criteria for enclosure classification: -
- Curve/data level: While the data in Figure A.45 refer to the **whole building** for the two regions, the ones in Figure A.46 refers to the considered **components** of houses in Florida.

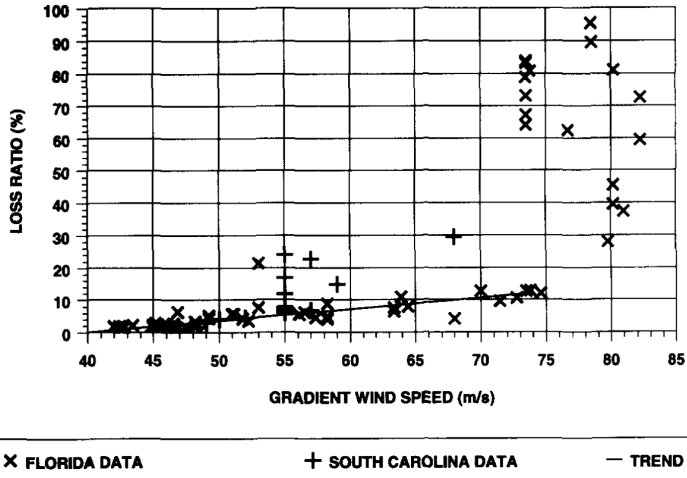


Figure A.45: Relation between average loss ratio and gradient wind speed (adapted from [78])

- Level specification: in addition to the **whole building**, the study develop vulnerability for the following building components: **roof envelope, wall envelope and external facilities**.
- Amount of damage corresponding to Damage State DS: -
- Corresponding Hazus-type Damage State (HDS): -
- Corresponding HDS upper level: -
- Roof typology: -
- Roof technology: -
- Roof slope: -
- Roof overhang: -
- Roof height definition: -

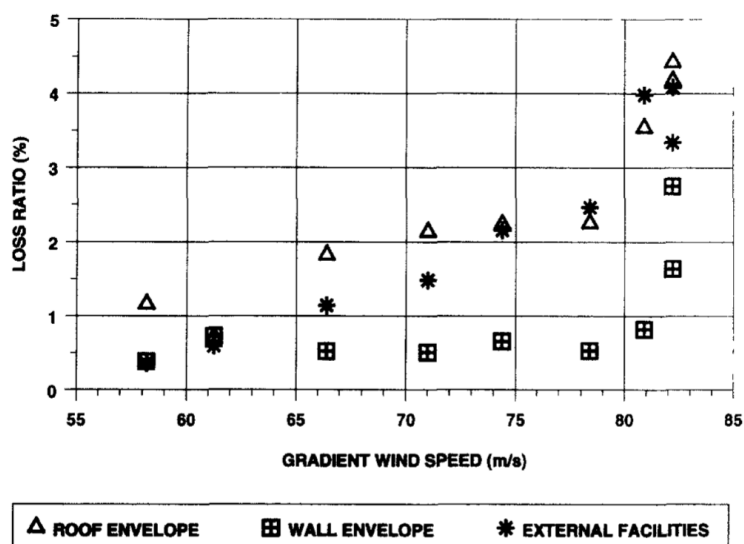


Figure A.46: Relation between component loss ratio and gradient wind speed
(adapted from [78])

- Roof height: -
- Roof-to-wall connection: -
- Covering typology: -
- Covering technology: -
- Covering size: -
- Covering connection: -
- Envelope walls typology: -
- Envelope walls technology: -
- Envelope percentage of openings: -
- Openings typology: -
- Openings technology: -
- IM reference height: -
- IM reference time: -
- IM typology: the IM is expressed as **gradient wind speed**. This measure is given by reconnaissance aircraft flew through the storm at altitudes ranged from 3 to 36 km.
- IM unit of measurements: m/s.
- Values model: the curves are composed mainly by **discrete values** but also exist a trend line for houses in urban areas Figure A.45.
- Values unit of measurements: the vulnerability is expresses in terms of **loss ratio** defined as the total amount paid in claims divided by the total insured value.

- Debris: as usually for past-loss data analyses, the results **take into account** damage from debris implicitly, without specifications (there isn't a debris model).
- Debris model: -
- Shielding: the effect of shielding of adjacent buildings, if any, is **considered** implicitly.
- Shielding model: -
- Water penetration damage: the result of rain entering the building is considered as a consequence of the direct wind damage to the envelope by the definition of the loss magnifier of Figure A.47.

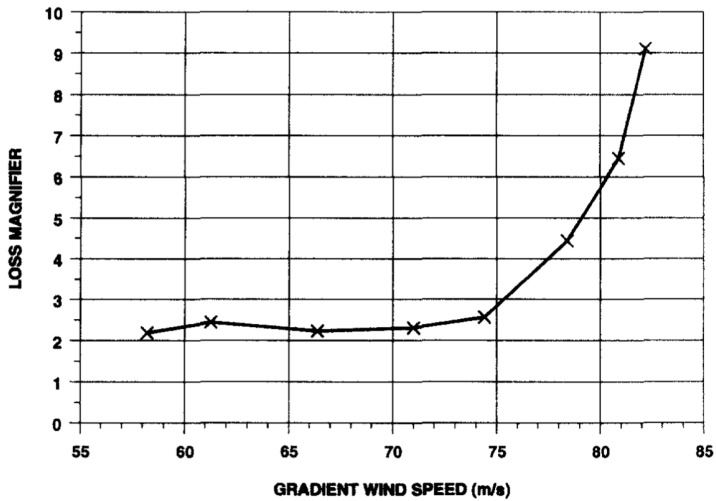


Figure A.47: Relation between average loss magnifier and gradient wind speed (adapted from [78])

- Water penetration damage model: The loss magnifier is defined as the overall building loss, minus the damage to external facilities, divided by the damage to the roof and wall envelopes (Figure A.46).

- Secondary damage to people: -
- Secondary damage to people model: -
- Uncertainty: -
- Tag: **1-5** of vulnerability database.

Khanduri and Morrow (2003), “Vulnerability of buildings to wind-storms and insurance loss estimation.” [50]

In their study, the authors present an innovative disaggregative approach to building vulnerability curve assessment from data of other counties or sites, under specific assumptions. The study provides an example of such an approach for the commercial building class of Puerto Rico, given the insurance past-loss data of two major hurricanes of 1989 and 1998, Hugo and Georges respectively. The authors also analyse the potential future insurance losses for storms of varying intensity and track.

- Source: reference tag for this study is **Khanduri_Morrow_2002**.
- Year: although the study was carried out in 2002, results refers to **1989** Hugo and **1998** Georges hurricanes.
- Region: **Puerto Rico**.
- Event type: **hurricanes** Hugo and Georges.
- Curve typology: **vulnerability**.
- Approach: **past-loss data**.
- Wind pressure model: -
- Direction of wind: -
- Terrain roughness: -
- Terrain category: -
- Terrain category reference code: -
- Surrounding condition: -
- Exposure category: -
- Exposure category reference code: -

- Date of building construction or retrofit: -
- Reference building code: -
- Structure technology: the authors disaggregate the **generic curve** of the buildings class into **wood-frame**, **masonry low-rise** and **reinforced concrete low-rise**.
- Type of use: **commercial**.
- Geometry in plan: -
- Number of storey: low-rise definition denotes **1-3 storeys**.
- Enclosure classification: -
- Criteria for enclosure classification: -
- Curve or data level: **whole building**.
- Level specification: **building**.
- Amount of damage corresponding to Damage State DS: -
- Corresponding Hazus-type Damage State (HDS): -
- Corresponding HDS upper level: -
- Roof typology: -
- Roof technology: -
- Roof slope: -
- Roof overhang: -
- Roof height definition: -
- Roof height: -
- Roof-to-wall connection: -

- Covering typology: -
- Covering technology: -
- Covering size: -
- Covering connection: -
- Envelope walls typology: -
- Envelope walls technology: -
- Envelope percentage of openings: -
- Openings typology: -
- Openings technology: -
- IM reference height: **10 [m]**.
- IM reference time: **3-sec.**
- IM typology: **gust wind speed**.
- IM unit of measurements: **[mph]**.
- Values model: **discrete values**.
- Values unit of measurements: **mean damage ratio** defined as the ratio between the loss and the value of the building (Figure A.48).
- Debris: -
- Debris model: -
- Shielding: -
- Shielding model: -
- Water penetration damage: -

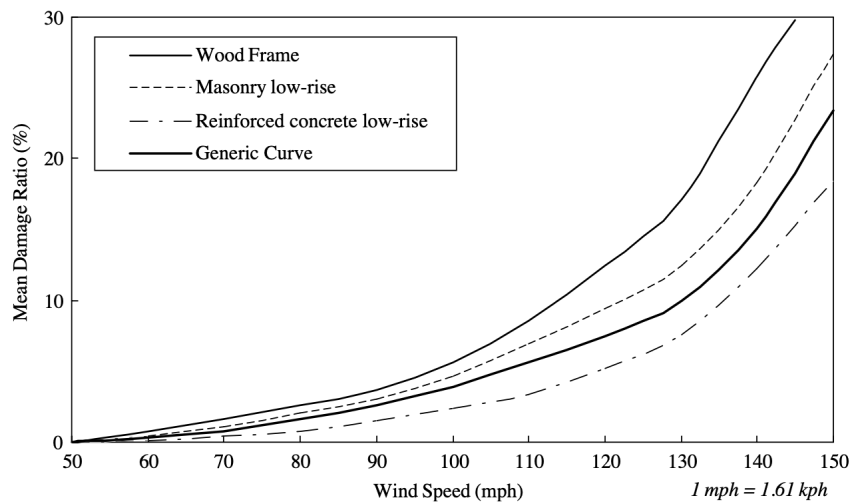


Figure A.48: Hurricane vulnerability curves for commercial building classes in Puerto Rico (adapted from [50])

- Water penetration damage model: -
- Secondary damage to people: -
- Secondary damage to people model: -
- Uncertainty: -
- Tag: **37-40** of vulnerability database.

Pita (2015), Review of CAPRA Vulnerability Module (Hurricane suite). [71]

- Source: reference tag for this study is **CAPRA_2015**
- Year: the year of the report is the **2015**.
- Region: **Caribbean and Central America**.
- Event type: **hurricane**.
- Curve typology: **vulnerability parametric function** (Figure A.49).

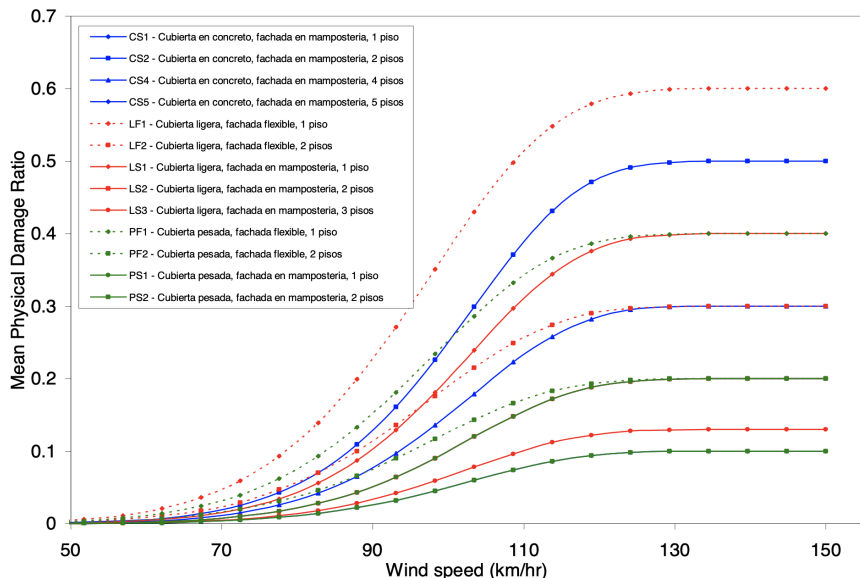


Figure A.49: Available functions in ERN-Vulnerability CAPRA Software (hurricane suite)

- Approach: **heuristic**
- Wind pressure model: -

- Direction of wind: -
- Terrain roughness: -
- Terrain category: -
- Terrain category reference code: -
- Surrounding condition: -
- Exposure category: -
- Exposure category reference code: -
- Date of building construction or retrofit: -
- Reference building code: -
- Structure technology: there are not specification on the structure technology in addition to the roof and facade typology.
- Type of use: -
- Geometry in plan: -
- Number of storey: **from 1 to 5**.
- Enclosure classification: -
- Criteria for enclosure classification: -
- Curve or data level: **whole building**.
- Level specification: **building**.
- Amount of damage corresponding to Damage State DS: -
- Corresponding Hazus-type Damage State (HDS): -
- Corresponding HDS upper level: -

- Roof typology: the author distinguishes the following roof typology: **concrete, light or heavy**.
- Roof technology: -
- Roof slope: -
- Roof overhang: -
- Roof height definition: -
- Roof height: -
- Roof-to-wall connection: -
- Covering typology: -
- Covering technology: -
- Covering size: -
- Covering connection: -
- Envelope walls typology: the author distinguishes the following envelope walls typology: **masonry or flexible**.
- Envelope walls technology: -
- Envelope percentage of openings: -
- Openings typology: -
- Openings technology: -
- IM reference height: -
- IM reference time: **5-sec.**
- IM typology: **gust**.
- IM unit of measurements: **km/h**.

- Values model: **parametric**.
- Values unit of measurements: **mean damage ratio** (MDR) defined as the repair building cost over the total building cost.
- Debris: -
- Debris model: -
- Shielding: -
- Shielding model: -
- Water penetration damage: -
- Water penetration damage model: -
- Secondary damage to people: -
- Secondary damage to people model: -
- Uncertainty: -
- Tag: **12-24** of vulnerability database.

Yum, Kim, and Wei (2020), “Development of vulnerability curves of buildings to windstorms using insurance data: An empirical study in South Korea.” [100]

The authors present a regional-scale study concerning losses in South Korea due to the high winds of Typhoon Maemi (2003). Through insurance data, damage ratio (the ratio of the financial loss over the total value of insured property), and damage state definition, the study defines 4 vulnerability curves (Figure A.50) by the *maximum likelihood estimation method*. The study does not concern a specific building typology and aggregates results for residential, industrial and commercial buildings. Furthermore, it does not address explicitly the uncertainty.

- Source: reference tag for this study is **Yum_2020**.
- Year: although the year of the study is 2020, the authors deal with an event of **2003**.
- Region: **South Korea**.
- Event type: **typhoon** Maemi.
- Curve typology: **vulnerability curves**.
- Approach: **past-loss data**, i.e. based on the insurance companies data.
- Wind pressure model: -
- Direction of wind: -
- Terrain roughness: -
- Terrain category: -
- Terrain category reference code: -
- Surrounding condition: -

- Exposure category: -
- Exposure category reference code: -
- Date of building construction or retrofit: -
- Reference building code: -
- Structure technology: -
- Type of use: vulnerability curves refers to **aggregated** lines of business, i.e. groupings of buildings, of **industrial, commercial and residential buildings**.
- Geometry in plan: -
- Number of storey: -
- Enclosure classification: -
- Criteria for enclosure classification: -
- Curve or data level: **whole building**.
- Level specification: **building**.
- Amount of damage corresponding to Damage State DS: the authors define 4 damage states corresponding to the following damage ratio thresholds (lower limits): **0** (damage state I), **0.003** (damage state II), **0.006** (damage state III) and **0.01** (damage state IV).
- Corresponding Hazus-type Damage State (HDS): -
- Corresponding HDS upper level: -
- Roof typology: -
- Roof technology: -
- Roof slope: -

- Roof overhang: -
- Roof height definition: -
- Roof height: -
- Roof-to-wall connection: -
- Covering typology: -
- Covering technology: -
- Covering size: -
- Covering connection: -
- Envelope walls typology: -
- Envelope walls technology: -
- Envelope percentage of openings: -
- Openings typology: -
- Openings technology: -
- IM reference height: -.
- IM reference time: 10-min..
- IM typology: **sustained wind speed** (i.e. mean).
- IM unit of measurements: **m/s**.
- Values model: vulnerability curves are **parametric** log-normal distribution. However, due to the lack of distribution parameters in the study, it is imported into the database by **discrete values**.
- Values unit of measurements: the authors provides vulnerability curves in terms of **probability of exceedence a given damage state** (Figure A.50).

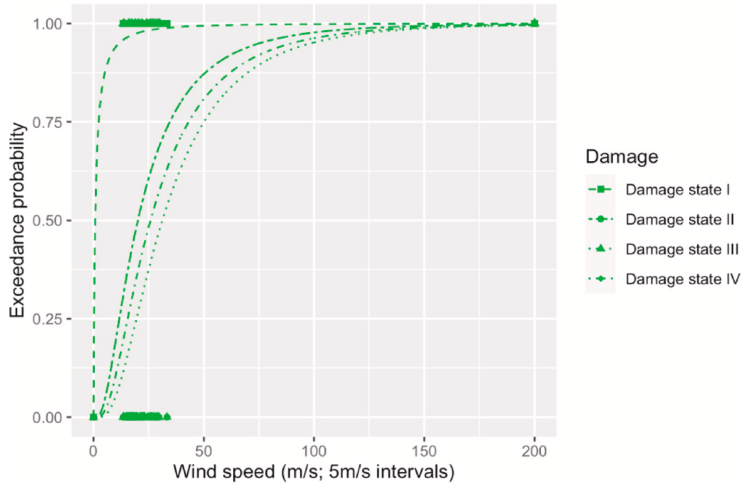


Figure A.50: Vulnerability curves (adapted from [100])

- Debris: -
- Debris model: -
- Shielding: -
- Shielding model: -
- Water penetration damage: -
- Water penetration damage model: -
- Secondary damage to people: -
- Secondary damage to people model: -
- Uncertainty: uncertainties were **taken into account**.
- Tag: **33-36** of vulnerability database.

A.3.2 Component vulnerability curves

Sparks, Schiff, and Reinhold (1994), “Wind damage to envelopes of houses and consequent insurance losses.” [78]

See section A.3.1 for details.

Zhang, Nishijima, and Maruyama (2014), “Reliability-based modeling of typhoon induced wind vulnerability for residential buildings in Japan.” [102]

See section A.2.2 for details.

Bibliography

- [1] A. U. Abdelhady. “Resilience of Residential Wooden Structures against Wind Hazards.” Ph.D. dissertation. PhD thesis. University of Michigan, 2021. DOI: <https://dx.doi.org/10.7302/1401>.
- [2] A. U. Abdelhady, S. M. J. Spence, and J. McCormick. “Risk and fragility assessment of residential wooden buildings subject to hurricane winds.” In: *Structural Safety* 94 (2022), p. 102137. ISSN: 0167-4730. DOI: <https://doi.org/10.1016/j.strusafe.2021.102137>. URL: <https://www.sciencedirect.com/science/article/pii/S0167473021000606>.
- [3] Academy of Disaster Reduction and Emergency Management - Ministry of Emergency Management and Ministry of Education National Disaster Reduction Center of China - Ministry of Emergency Management Information institute of the Ministry of Emergency Management. *2019 Global Natural Disaster Assessment Report*. Report. 2020. URL: <https://www.preventionweb.net/go/73363>.
- [4] T. S. Acosta. “Risk assessment of low-rise educational buildings with wooden roof structures against severe wind loadings”. In: *Journal of Asian Architecture and Building Engineering* (2021), pp. 1–13. DOI: 10.1080/13467581.2021.1909596. eprint: <https://doi.org/10>

.1080/13467581.2021.1909596. URL: <https://doi.org/10.1080/13467581.2021.1909596>.

- [5] C. Amante and B. Eakins. “ETOPO1 1 Arc-Minute Global Relief Model: procedures, data sources and analysis.” In: *NOAA Technical Memorandum NESDIS NGDC-24* (Mar. 2009). DOI: 10.7289/V5C8276M.
- [6] Architectural Institute of Japan. *Recommendations for Loads on Buildings*. Japan, 2004.
- [7] ASCE. *Minimum design loads for buildings and other structures, Standard ASCE 7-02*. Ed. by S. E. I. of the American Society of Civil Engineers. Reston, VA, 2002.
- [8] S. Ascolese. “Analisi di rischio da vento estremo per portafogli di edifici, basata su fragilità di componenti.” Thesis. Dipartimento di Strutture per l’Ingegneria e l’Architettura, Naples, Italy, 2022.
- [9] P. Bicheron, M. Leroy, C. Brockmann, U. Krämer, B. Miras, M. Huc, F. Niño, P. Defourny, C. Vancutsem, O. Arino, F. Ranera, D. Petit, V. Amberg, B. Berthelot, and D. Gross. “Globcover: a 300 m global land cover product for 2005 using ENVISAT MERIS time series.” In: *Proceeding of the Second International Symposium on Recent Advances in Quantitative Remote Sensing* (Jan. 2006), pp. 538–542.
- [10] N. E. Busch and H. A. Panofsky. “Recent spectra of atmospheric turbulence.” In: *Quarterly journal of the Royal Meteorological Society* 94 (1968), pp. 132–148. DOI: <https://doi.org/10.1002/qj.49709440003>.
- [11] O.-D. Cardona, M. G. Ordaz, M. G. Mora, M. A. Salgado-Gálvez, G. A. Bernal, D. Zuloaga-Romero, M. Cristina, L. Yamín, and D. González. “Global risk assessment: A fully probabilistic seismic and tropical cyclone wind risk assessment.” In: *International Journal of Disaster Risk Reduction* 10 (2014). Global probabilistic assessment of risk from natural hazards for the Global Assessment Report 2013 (GAR13), pp. 461–476. ISSN: 2212-4209. DOI: <https://doi.org/10.1080/13467581.2021.1909596>.

- .1016/j.ijdrr.2014.05.006. URL: <https://www.sciencedirect.com/science/article/pii/S2212420914000454>.
- [12] M. Ciampoli, F. Petrini, and G. Augusti. “Performance-Based Wind Engineering: Towards a general procedure.” In: *Structural Safety* 33.6 (2011), pp. 367–378. ISSN: 0167-4730. DOI: <https://doi.org/10.1016/j.strusafe.2011.07.001>. URL: <https://www.sciencedirect.com/science/article/pii/S0167473011000579>.
 - [13] I. L. CIMNE ITEC S.A.S. and E. S.A. “Background Paper prepared for the Global Assessment Report on Disaster Risk Reduction 2013.” In: *Probabilistic Modelling of Natural Risks at the Global Level: Global Risk Model* (2013).
 - [14] K. M. Clark. “A Formal Approach to Catastrophe Risk Assessment and Management.” In: *Proceedings of the Casualty Actuarial Society* 73 - part 2 (1986).
 - [15] Consiglio Nazionale delle Ricerche (CNR). *Istruzioni per la valutazione delle azioni e degli effetti del vento sulle costruzioni*. 2009.
 - [16] D. M. Deaves and R. I. Harris. “A mathematical model of the structure of strong winds.” In: *C.R.I.A. Report 76* (1981).
 - [17] G. G. Deierlein, H. Krawinkler, and C. A. Cornell. “A framework for performance-based earthquake engineering.” In: *Conference: 2003 Pacific Conference on Earthquake Engineering, Christchurch, New Zealand* (2003).
 - [18] Department of Homeland Security Federal Emergency Management Agency Mitigation Division. *Hazus-MH 2.1 - Technical Manual*. Washington, D.C.
 - [19] I. Depina, V. Divic, A. Munjiza, and B. Peroš. “Perfomance-based wind engineering assessment of critical telecommunication infrastructure subjected to bora wind.” In: *Engineering Structures* 236 (June 2021), p. 112083. DOI: <10.1016/j.engstruct.2021.112083>.
 - [20] G. S. Durst. “Wind speed over short periods of time.” In: *The meteorological Magazine* (1960).

- [21] B. Ellingwood, J. van de Lindt, D. Gromala, D. Rosowsky, R. Gupta, and S. Pryor. “Performance-Based Engineering for Light-Frame Wood Construction in the United States: Status and Challenges.” In: *Proc. 2006 World Conf. on Timber Engineering* ().
- [22] B. Ellingwood, D. Rosowsky, Y. Li, and J. Kim. “Fragility Assessment of Light-Frame Wood Construction Subjected to Wind and Earthquake Hazards.” In: *Journal of Structural Engineering-asce - J STRUCT ENG-ASCE* 130 (Dec. 2004). doi: 10.1061/(ASCE)0733-9445(2004)130:12(1921).
- [23] F. Fan and W. Pang. “Tornado Hazard Analysis and Effect of Structure Size.” In: *13th International Conference on Applications of Statistics and Probability in Civil Engineering (ICASP13)* (2019). doi: <https://doi.org/10.22725/ICASP13.409>.
- [24] J. Filliben, K. Gurley, J.-P. Pinelli, E. Simiu, and C. Subramanian. “Fragility curves, damage matrices, and wind induced loss estimation.” In: *Management Information Systems* (Jan. 2002), pp. 119–126.
- [25] J. L. Franklin, M. Black, and K. Valde. “GPS Dropwindsonde Wind Profiles in Hurricanes and Their Operational Implications.” In: *Weather and Forecasting* 18 (2003), pp. 32–44. doi: [http://dx.doi.org/10.1175/1520-0434\(2003\)018<0032:GDWPIH>2.0.CO;2](http://dx.doi.org/10.1175/1520-0434(2003)018<0032:GDWPIH>2.0.CO;2).
- [26] D. G. Friedman. “Computer simulation in natural hazard assessment.” eng. In: University of Colorado. Program on Technology, Environment and Man. Monograph (1975).
- [27] D. G. Friedman. “Natural Hazard Risk Assessment for an Insurance Program.” In: *The Geneva Papers on Risk and Insurance* 9.30 (1984), pp. 57–128. ISSN: 02521148, 23110112. URL: <http://www.jstor.org/stable/41950111>.
- [28] T. T. Fujita. “Proposed Characterization of Tornadoes and Hurricanes by Area and Intensity.” In: *SMRP Research Paper Number 91* (1970). URL: <https://swco-ir.tdl.org/handle/10605/261875>.

- [29] W. C. Gangloff. “Common mode failure analysis.” In: *IEEE PES Summer Meeting Energy Resources Conf.* (1974), pp. 27–30.
- [30] A. M. Goliger and R. V. Milford. “A review of worldwide occurrence of tornadoes.” In: *Journal of Wind Engineering and Industrial Aerodynamics* 74–76 (1998), pp. 111–121. ISSN: 0167-6105. DOI: [https://doi.org/10.1016/S0167-6105\(98\)00009-9](https://doi.org/10.1016/S0167-6105(98)00009-9). URL: <https://www.sciencedirect.com/science/article/pii/S0167610598000099>.
- [31] Government Printer. *Queensland Home Building Code. Appendix 4 to the Standard Building By-Laws 1975 Under the Building Act 1975-1981*. Queensland, Australia, 1981.
- [32] M. Grayson, W. Pang, and S. Schiff. “Three-dimensional probabilistic wind-borne debris trajectory model for building envelope impact risk assessment.” In: *Journal of Wind Engineering and Industrial Aerodynamics* 102 (2012), pp. 22–35. ISSN: 0167-6105. DOI: <https://doi.org/10.1016/j.jweia.2012.01.002>. URL: <https://www.sciencedirect.com/science/article/pii/S0167610512000037>.
- [33] L. Griffis, V. Patel, S. Muthukumar, and S. Baldava. “A Framework for Performance-Based Wind Engineering.” In: *Advances in Hurricane Engineering*, pp. 1205–1216. DOI: 10.1061/9780784412626.105. eprint: <https://ascelibrary.org/doi/pdf/10.1061/9780784412626.105>. URL: <https://ascelibrary.org/doi/abs/10.1061/9780784412626.105>.
- [34] J. J. C. Gumaro, T. J. S. Acosta, L. R. E. Tan, J. C. Agar, E. A. J. Tingatinga, J. K. B. Musico, D. A. D. Plamenco, M. N. C. Ereño, J. S. Pacer, I. B. O. Villalba, and J. Y. J. Hernandez. “Identification of key components for developing building types for risk assessment against wind loadings: The case of Cebu Province, Philippines”. In: *International Journal of Disaster Risk Reduction* 67 (2022), p. 102686. ISSN: 2212-4209. DOI: <https://doi.org/10.1016/j.ijdrr.2021.102686>. URL: <https://www.sciencedirect.com/science/article/pii/S2212420921006476>.

- [35] E. J. Gumbel. “The Return Period of Flood Flows.” In: *The Annals of Mathematical Statistics* 12.2 (1941), pp. 163–190. ISSN: 00034851. URL: <http://www.jstor.org/stable/2235766>.
- [36] S. Gunay and K. Mosalam. “PEER Performance-Based Earthquake Engineering Methodology, Revisited.” In: *Journal of Earthquake Engineering* 17 (Aug. 2013). DOI: 10.1080/13632469.2013.787377.
- [37] Halpern and Glick Pty.Ltd. *Investigation of the performance of industrialised residential buildings*. Report on Cyclone Tracy. Aust. Dept. of Housing and Construction, 1975.
- [38] B. A. Harper, J. D. Kepert, and J. D. Ginger. *Guidelines for converting between various wind averaging periods in tropical cyclone conditions*. 2010.
- [39] R. I. Harris. “On the spectrum and auto-correlation function of gustiness in high winds.” In: *Report 5273* (1968).
- [40] G. C. Hart. “Estimation of structural damage due to tornadoes.” In: *Proceedings of the Symposium on Tornadoes: Assessment of Knowledge and Implications for Man* (1976), pp. 645–665.
- [41] D. J. Henderson and J. D. Ginger. “Vulnerability model of an Australian high-set house subjected to cyclonic wind loading.” In: *Wind and Structures* 10.3 (2007), pp. 269–285. DOI: <https://doi.org/10.12989/WAS.2007.10.3.269>.
- [42] R. L. Hendrick, D. G. Friedman, and W. Sewell. “Potential impacts of storm modification on the insurance industry.” In: *Human Dimensions of Weather Modification*, ed. by WRD Sewell, Department of Geography Research Paper 105 (1966), p. 229.
- [43] J. D. Holmes. *Wind loading of structures*. Spon Press, 2003. ISBN: 0-203-34234-8.
- [44] J. D. Holmes, A. C. Allsop, and J. D. Ginger. “Gust durations, gust factors and gust response factors in wind codes and standards.” In: *Wind and Structures* 19.3 (2014), pp. 339–352. DOI: 10.12989/WAS.2014.19.3.339.

- [45] R. A. Howard, J. E. Matheson, and D. W. North. “The Decision to Seed Hurricanes.” In: *Science* 176.4040 (1972), pp. 1191–1202. DOI: 10.1126/science.176.4040.1191. eprint: <https://www.science.org/doi/pdf/10.1126/science.176.4040.1191>. URL: <https://www.science.org/doi/abs/10.1126/science.176.4040.1191>.
- [46] I. Iervolino. *Dinamica delle strutture e ingegneria sismica. Principi e applicazioni*. Italy: Hoepli, 2021.
- [47] IF Scale Steering Group. “The International Fujita (IF) Scale Tornado and Wind Damage Assessment Guide.” In: *Draft document* (2018). URL: https://www.essl.org/media/publications/IF-scale_v0.10.pdf.
- [48] Japan Meteorological Agency. “Guidelines for the Japanese Enhanced Fujita Scale.” In: *Draft document* (2015). URL: https://www.data.jma.go.jp/obd/stats/data/bosai/tornado/kaisetsu/guideline_en.pdf.
- [49] T. von Karman. “Progress in the Statistical Theory of Turbulence.” In: *Proceedings of the National Academy of Sciences* 34.11 (1948), pp. 530–539. ISSN: 0027-8424. DOI: 10.1073/pnas.34.11.530. eprint: <https://www.pnas.org/content/34/11/530.full.pdf>. URL: <https://www.pnas.org/content/34/11/530>.
- [50] A. C. Khanduri and G. C. Morrow. “Vulnerability of buildings to windstorms and insurance loss estimation.” In: *Journal of Wind Engineering and Industrial Aerodynamics* 91.4 (2003), pp. 455–467. ISSN: 0167-6105. DOI: [https://doi.org/10.1016/S0167-6105\(02\)00408-7](https://doi.org/10.1016/S0167-6105(02)00408-7). URL: <https://www.sciencedirect.com/science/article/pii/S0167610502004087>.
- [51] K. R. Knapp, M. C. Kruk, D. H. Levinson, H. J. Diamond, and C. J. Neumann. “The International Best Track Archive for Climate Stewardship (IBTrACS): Unifying tropical cyclone data.” In: *B. Am. Meteorol. Soc.* 91 (2010), pp. 363–376. DOI: <https://doi.org/10.1175/2009BAMS2755.1>.

- [52] C. Konthesingha, M. Stewart, P. Ryan, J. Ginger, and D. Henderson. “Reliability based vulnerability modelling of metal-clad industrial buildings to extreme wind loading for cyclonic regions.” In: *Journal of Wind Engineering and Industrial Aerodynamics* 147 (Dec. 2015), pp. 176–185. DOI: 10.1016/j.jweia.2015.10.002.
- [53] V. Le and L. Caracoglia. “Life-cycle cost assessment of vertical structures under nonstationary winds: Downburst vs. tornado loads.” In: *Engineering Structures* 243 (2021), p. 112515. ISSN: 0141-0296. DOI: <https://doi.org/10.1016/j.engstruct.2021.112515>. URL: <https://www.sciencedirect.com/science/article/pii/S0141029621006659>.
- [54] K. Lee. “Site-specific hazards and load models for probability-based design.” PhD thesis. Department of Civil, Construction, and Environmental Engineering, Oregon State University, Corvallis, OR., 2004.
- [55] K. H. Lee and D. V. Rosowsky. “Fragility assessment for roof sheathing failure in high wind regions.” In: *Engineering Structures* 27.6 (2005), pp. 857–868. ISSN: 0141-0296. DOI: <https://doi.org/10.1016/j.engstruct.2004.12.017>. URL: <https://www.sciencedirect.com/science/article/pii/S0141029605000477>.
- [56] R. H. Leicester and G. F. Reardon. “Statistical Analysis of the Structural Damage by Cyclone Tracy.” In: *The Institution of Engineers* (1976). URL: https://www.researchgate.net/publication/279581243_A_statistical_analysis_of_the_structural_damage_by_Cyclone_Tracy.
- [57] Y. Li and B. R. Ellingwood. “Hurricane damage to residential construction in the US: Importance of uncertainty modeling in risk assessment.” In: *Engineering Structures* 28.7 (2006), pp. 1009–1018. ISSN: 0141-0296. DOI: <https://doi.org/10.1016/j.engstruct.2005.11.005>. URL: <https://www.sciencedirect.com/science/article/pii/S0141029605004335>.

- [58] J. W. van de Lindt and T. N. Dao. “Performance-Based Wind Engineering for Wood-Frame Buildings.” In: *Journal of Structural Engineering* 135.2 (2009), pp. 169–177. DOI: 10.1061/(ASCE)0733-9445(2009)135:2(169).
- [59] M. S. Mason and K. I. Parackal. “Vulnerability of buildings and civil infrastructure to tropical cyclones: A preliminary review of modelling approaches and literature.” In: *Bushfire and Natural Hazards* (Feb. 2017). URL: https://www.bnhcrc.com.au/sites/default/files/managed/downloads/vulnerability_of_buildings_and_civil_infrastructure_to_tropical_cyclones.pdf.
- [60] H. Masoomi and J. van de Lindt. “Tornado fragility and risk assessment of an archetype masonry school building.” In: *Engineering Structures* 128 (Dec. 2016). DOI: 10.1016/j.engstruct.2016.09.030.
- [61] MATLAB. *Version 9.8.0. 1417392 (R2020a Update 4)*. Natick, Massachusetts: The MathWorks Inc., 2020.
- [62] R. M. Osegueda and R. L. Bowles. “A simple, analytic 3-dimensional downburst model based on boundary layer stagnation flow.” In: *NASA Technical Memorandum* (1988). URL: <https://ntrs.nasa.gov/citations/19880018674>.
- [63] Z. Ouyang and S. M. J. Spence. “A Performance-Based Wind Engineering Framework for Envelope Systems of Engineered Buildings Subject to Directional Wind and Rain Hazards.” In: *Journal of Structural Engineering* 146.5 (2020), p. 04020049. DOI: 10.1061/(ASCE)ST.1943-541X.0002568. eprint: <https://ascelibrary.org/doi/pdf/10.1061/%28ASCE%29ST.1943-541X.0002568>. URL: <https://ascelibrary.org/doi/abs/10.1061/%5C%28ASCE%5C%29ST.1943-541X.000256>.
- [64] Z. Ouyang and S. M. J. Spence. “Performance-based wind-induced structural and envelope damage assessment of engineered buildings through nonlinear dynamic analysis.” In: *Journal of Wind Engineering and Industrial Aerodynamics* 208 (2021), p. 104452. ISSN: 0167-

6105. DOI: <https://doi.org/10.1016/j.jweia.2020.104452>. URL: <https://www.sciencedirect.com/science/article/pii/S0167610520303627>.
- [65] Z. Ouyang and S. M. Spence. “A performance-based damage estimation framework for the building envelope of wind-excited engineered structures.” In: *Journal of Wind Engineering and Industrial Aerodynamics* 186 (2019), pp. 139–154. ISSN: 0167-6105. DOI: <https://doi.org/10.1016/j.jweia.2019.01.001>. URL: <https://www.sciencedirect.com/science/article/pii/S0167610518302629>.
- [66] J. P. Palutikof, B. B. Brabson, D. H. Lister, and S. T. Adcock. “A review of methods to calculate extreme wind speeds.” In: *Meteorological Applications* 6.2 (1999), pp. 119–132. DOI: <https://doi.org/10.1017/S1350482799001103>.
- [67] C. Paulotto, M. Ciampoli, and G. Augusti. “Some proposals for a first step towards a Performance Based Wind Engineering.” In: *Proceedings of the IFED - international forum in engineering decision making; First Forum* (2004).
- [68] F. Petruzzelli and I. Iervolino. “FRAME V.1.0: A rapid fragility-based seismic risk assessment tool.” In: *Proc. of Second European Conference on Earthquake Engineering and Seismology, 2ECEES* (2014), pp. 24–29.
- [69] J.-P. Pinelli, E. Simiu, K. Gurley, C. Subramanian, L. Zhang, A. Cope, J. J. Filliben, and S. Hamid. “Hurricane Damage Prediction Model for Residential Structures.” In: *Journal of Structural Engineering* 130.11 (2004), pp. 1685–1691. DOI: 10.1061/(ASCE)0733-9445(2004)130:11(1685). eprint: <https://ascelibrary.org/doi/pdf/10.1061/\%28ASCE\%290733-9445\%282004\%29130\%3A11\%281685\%29>. URL: <https://ascelibrary.org/doi/abs/10.1061/\%28ASCE\%290733-9445\%282004\%29130\%5C3A11\%281685\%29>.

- [70] G. L. Pita. “Review of CAPRA Vulnerability Module (Hurricane Suite).” In: *Advances in Probabilistic Flood Hazard Assessment (CAPRA) technical notes* (2015). URL: <https://openknowledge.worldbank.org/handle/10986/22981>.
- [71] G. L. Pita. *Review of CAPRA Vulnerability Module (Hurricane suite)*. World bank group, 2015. URL: <https://openknowledge.worldbank.org/handle/10986/22981>.
- [72] G. L. Pita, J.-P. Pinelli, K. Gurley, and J. Mitrani-Reiser. “State of the Art of Hurricane Vulnerability Estimation Methods: A Review.” In: *Natural Hazards Review* 16 (Sept. 2014), p. 04014022. DOI: 10.1061/(ASCE)NH.1527-6996.0000153.
- [73] M. D. Powell, P. J. Vickery, and T. A. Reinhold. “Reduced drag coefficient for high wind speeds in tropical cyclones.” In: *Nature* 422 (), pp. 279–283.
- [74] H. Qin and M. G. Stewart. “System fragility analysis of roof cladding and trusses for Australian contemporary housing subjected to wind uplift.” In: *Structural Safety* 79 (2019), pp. 80–93. ISSN: 0167-4730. DOI: <https://doi.org/10.1016/j.strusafe.2019.03.005>. URL: <https://www.sciencedirect.com/science/article/pii/S0167473018303618>.
- [75] J. C. Sciaudone, D. Feuerborn, G. N. Rao, and S. Daneshvaran. “Development of objective wind damage functions to predict wind damage to low-rise structures.” In: *Proceedings of the 8th US Conference on Wind Engineering, American Association of wind Engineering* (1997).
- [76] G. Solari. “Wind Loading of Structures: Framework, Phenomena, Tools and Codification.” In: *Structures* 12 (2017), pp. 265–285. ISSN: 2352-0124. DOI: <https://doi.org/10.1016/j.istruc.2017.09.008>. URL: <https://www.sciencedirect.com/science/article/pii/S2352012417300632>.

- [77] G. Solari, M. Burlando, and M. P. Repetto. “Detection, simulation, modelling and loading of thunderstorm outflows to design wind-safer and cost-efficient structures.” In: *Journal of Wind Engineering and Industrial Aerodynamics* 200 (2020), p. 104142. ISSN: 0167-6105. DOI: <https://doi.org/10.1016/j.jweia.2020.104142>. URL: <https://www.sciencedirect.com/science/article/pii/S0167610520300520>.
- [78] P. R. Sparks, S. D. Schiff, and T. A. Reinhold. “Wind damage to envelopes of houses and consequent insurance losses.” In: *Journal of Wind Engineering and Industrial Aerodynamics* 53 (1-2 1994), pp. 145–155. ISSN: 0167-6105. DOI: [https://doi.org/10.1016/0167-6105\(94\)90023-X](https://doi.org/10.1016/0167-6105(94)90023-X). URL: <https://www.sciencedirect.com/science/article/abs/pii/016761059490023X>.
- [79] P. R. Sparks and S. A. Bhinderwala. “Relationship Between Residential Insurance Losses and Wind Conditions in Hurricane Andrew.” In: *Proceedings of Hurricanes of 1992: Lessons Learned and Implications for the Future* (1992).
- [80] Standard association of Australia. *AS1170-1973, SAA Loading Code, Part 2 - Wind Forces (Metric Units)*. Ed. by S. A. of Aust. Sydney, 1975.
- [81] Standard association of Australia. *Structural design actions – Part 2: Wind actions, AS/NZS 1170.2:2002*. Sydney, Australia, 2002.
- [82] C. D. Standohar-Alfano and J. W. van de Lindt. “Empirically Based Probabilistic Tornado Hazard Analysis of the United States Using 1973–2011 Data.” In: *Natural Hazards Review* 16.1 (2015), p. 04014013. DOI: 10.1061/(ASCE)NH.1527-6996.0000138. eprint: <https://ascelibrary.org/doi/pdf/10.1061/\%28ASCE\%29NH.1527-6996.0000138>. URL: <https://ascelibrary.org/doi/abs/10.1061/\%28ASCE\%29NH.1527-6996.0000138>.
- [83] Y. Tamura and A. Kareem. *Advanced Structural Wind Engineering*. Vol. Sundararajan C. (eds) Probabilistic Structural Mechanics Handbook. Japan: Springer, 2013. ISBN: 978-4-431-54719-8.

- [84] C. Tan and W. Fang. “Mapping the Wind Hazard of Global Tropical Cyclones with Parametric Wind Field Models by Considering the Effects of Local Factors.” In: *Int J Disaster Risk Sci* 9 (2018), pp. 86–99. DOI: <https://doi.org/10.1007/s13753-018-0161-1>.
- [85] Tokyo Polytechnic University. *Aerodynamic database of non-isolated low-rise buildings*. Tokyo, Japan, 2007. URL: http://www.wind.arch.t-kougei.ac.jp/info_center/windpressure/grouplowrise/mainpage.html.
- [86] L. A. Twisdale and P. J. Vickery. *Extreme-Wind Risk Assessment*. Vol. Sundararajan C. (eds) Probabilistic Structural Mechanics Handbook. Boston, MA: Springer, 1995. ISBN: 978-1-4613-5713-1.
- [87] C. O. Unanwa, J. R. McDonald, K. C. Mehta, and D. A. Smith. “The development of wind damage bands for buildings.” In: *Journal of Wind Engineering and Industrial Aerodynamics* 84.1 (2000), pp. 119–149. ISSN: 0167-6105. DOI: [https://doi.org/10.1016/S0167-6105\(99\)00047-1](https://doi.org/10.1016/S0167-6105(99)00047-1). URL: <https://www.sciencedirect.com/science/article/pii/S0167610599000471>.
- [88] UNISDR. *Global Assessment Report on Disaster Risk Reduction*. Report. 2013.
- [89] UNISDR. *Global Assessment Report on Disaster Risk Reduction*. Report. 2015.
- [90] P. J. Vickery, J. Lin, P. F. Skerlj, L. Twisdale, and K. Huang. “HAZUS-MH Hurricane Model Methodology. I: Hurricane Hazard, Terrain, and Wind Load Modeling.” In: *Natural Hazards Review* 7 (2006), pp. 82–93.
- [91] P. J. Vickery, P. F. Skerlj, J. Lin, L. Twisdale, M. A. Young, and F. Lavelle. “HAZUS-MH Hurricane Model Methodology. II: Damage and Loss Estimation.” In: *Natural Hazards Review* 7 (2006), pp. 94–103.

- [92] P. J. Vickery and P. F. Skerlj. "Hurricane Gust Factors Revisited." In: *Journal of Structural Engineering* 131.5 (2005), pp. 825–832. DOI: 10.1061/(ASCE)0733-9445(2005)131:5(825). eprint: [https://ascelibrary.org/doi/pdf/10.1061/\(ASCE\)0733-9445\(2005\)131:5\(825\)](https://ascelibrary.org/doi/pdf/10.1061/(ASCE)0733-9445(2005)131:5(825)). URL: [https://ascelibrary.org/doi/abs/10.1061/\(ASCE\)0733-9445\(2005\)131:5\(825\)](https://ascelibrary.org/doi/abs/10.1061/(ASCE)0733-9445(2005)131:5(825)).
- [93] G. R. Walker. *Effect on building*. Report on Cyclone Tracy. Aust. Dept. of Housing and Construction, 1975.
- [94] G. R. Walker. "Modelling the vulnerability of buildings to wind - a review." In: *Canadian Journal of Civil Engineering* (2011). DOI: <https://doi.org/10.1139/L11-047>.
- [95] R. J. Walker G. R. e Roy. "Wind loads on houses in an urban environment." In: *Proceedings, 1st Asia Pacific Symposium on Wind Engineering* (1985).
- [96] P. J. Ward, V. Blauthut, N. Bloemendaal, J. E. Daniell, M. C. de Ruiter, M. J. Duncan, R. Emberson, S. F. Jenkins, D. Kirschbaum, M. Kunz, S. Mohr, S. Muis, G. A. Riddell, A. Schäfer, T. Stanley, T. I. E. Veldkamp, and H. C. Winsemius. "Review article: Natural hazard risk assessments at the global scale." In: *Natural Hazards and Earth System Sciences* 20 (2020), pp. 1069–1096. DOI: <https://doi.org/10.5194/nhess-20-1069-2020>.
- [97] M. Wehner, J. Ginger, J. Holmes, C. Sandland, and M. Edwards. "Development of methods for assessing the vulnerability of Australian residential building stock to severe wind." In: *IOP Conference Series: Earth and Environmental Science* 11 (2010), p. 012017. DOI: 10.1088/1755-1315/11/1/012017. URL: <https://doi.org/10.1088/1755-1315/11/1/012017>.
- [98] Wind science and engineering center. *A Recommendation for an Enhanced Fujita scale (EF-Scale)*. Lubbock, Texas: Texas Tech University, 2004.

- [99] L. E. Yamin, A. I. Hurtado, A. H. Barbat, and O. D. Cardona. “Seismic and wind vulnerability assessment for the GAR-13 global risk assessment”. In: *International Journal of Disaster Risk Reduction* 10 (2014). Global probabilistic assessment of risk from natural hazards for the Global Assessment Report 2013 (GAR13), pp. 452–460. ISSN: 2212-4209. DOI: <https://doi.org/10.1016/j.ijdrr.2014.05.007>. URL: <https://www.sciencedirect.com/science/article/pii/S2212420914000466>.
- [100] S.-G. Yum, J.-M. Kim, and H.-H. Wei. “Development of vulnerability curves of buildings to windstorms using insurance data: An empirical study in South Korea.” In: *Journal of Building Engineering* 34 (Nov. 2020), p. 101932. DOI: 10.1016/j.jobe.2020.101932.
- [101] D. Zeng, H. Zhang, and C. Wang. “Modelling correlated damage of spatially distributed building portfolios under scenario tropical cyclones.” In: *Structural Safety* 87 (2020), p. 101978. ISSN: 0167-4730. DOI: <https://doi.org/10.1016/j.strusafe.2020.101978>. URL: <https://www.sciencedirect.com/science/article/pii/S0167473020300576>.
- [102] S. Zhang, K. Nishijima, and T. Maruyama. “Reliability-based modeling of typhoon induced wind vulnerability for residential buildings in Japan.” In: *Journal of Wind Engineering and Industrial Aerodynamics* 124 (2014), pp. 68–81. ISSN: 0167-6105. DOI: <https://doi.org/10.1016/j.jweia.2013.11.004>. URL: <https://www.sciencedirect.com/science/article/pii/S016761051300250X>.